Unterschrift des Betreuers

TECHNISCHE UNIVERSITÄT WIEN
Vienna University of Technology

D I P L O M A R B E I T

Implementation, improvement and comparison of different calibration methods of high purity germanium detectors for gamma-ray spectrometry and exemplary application in radionuclide metrology

Ausgeführt am

Atominstitut der Technischen Universität Wien,
im
Labor Radioaktivität des Bundesamts für Eich- und Vermessungswesen
und im
Low-Level Counting Laboratory Arsenal der Universität für Bodenkultur Wien

unter der Anleitung von Univ. Prof. DI Dr. techn. Franz Josef Maringer

durch

Hannah Moser, BSc
0726598

Datum

Unterschrift (Student)

Erklärung zur Verfassung der Arbeit

Hiermit erkläre ich, dass ich diese Arbeit selbständig verfasst habe, dass ich die verwendeten Quellen und Hilfsmittel vollständig angegeben habe und dass ich die Stellen der Arbeit, einschließlich Tabellen, Karten und Abbildungen, die anderen Werken oder dem Internet im Wortlaut oder dem Sinn nach entnommen sind, auf jeden Fall unter Angabe der Quelle als Entlehnung kenntlich gemacht habe.

I declare that I have authored this thesis independently, that I have not used other than the declared sources/resources and that I have explicitly marked all material which has been quoted either literally or by content from the used sources.

Wien, am

(Hannah Moser)

Abstract

γ-ray spectrometry is a highly sophisticated process of measuring and evaluating sample activity. The results of this technique are only as good as the procedures applied. In order to obtain significant data, it is necessary to use a detector properly calibrated according to its application and use the correct reference materials and standards. The Joint Research Project MetroMETAL Ionising Radiation Metrology for the Metallurgical Industry (European Metrology Research Programme EMRP) has the goal to create "reference standards for composite steel, cast steel, slag and fume dust containing a known activity of some radionuclides (^{60}Co, ^{137}Cs, ^{192}Ir, ^{226}Ra and ^{241}Am) considered as potential contaminants" that are "prepared in geometries/matrices that match the industrial environments for which they are designed". [1]
Prototypes of those standards are sent to the participating partners for evaluation. Part of the tasks of this project is the comparison of Monte Carlo codes for efficiency and activity simulation in order to gain insight into their respective strengths and weaknesses. In that respect it is necessary to design a detector image for the use of Monte Carlo codes in radiation transport.

In the course of this work a functioning and validated detector model has been created and tested by comparing simulated peak efficiencies to the experimentally found values of the participating laboratories. The results of the intercomparisons are presented in this work. The goal of MetroMETAL is to provide recommendations on future measurement protocols, standards and methods in the metallurgical industry.

Another application, where a properly calibrated detector is necessary, is the monitoring of environmental radiation levels. In that respect sediment samples taken at two hydroelectric power plants located on the Danube river are evaluated. Ongoing measurements establish a baseline for present and future reference. This is particularly relevant for assessment of radiation levels after accidents and understanding of environmental transport and distribution of radioactive material.

Zusammenfassung

Gammaspektrometrie ist ein hochspezialisierter Prozess der Aktivitätsbestimmung einer Probe über die Messung der Anzahl und Energie der von der Probe emittierten Photonen. Die Resultate sind jedoch nur so gut, wie die angewandten Methoden. Die korrekte und sorgfältige Kalibrierung der Messgeräte - in diesem Fall ein hochreiner Germaniumdetektor - ist daher von besonderer Bedeutung. Im Zuge dieser Arbeit werden Methoden zur Kalibrierung aufgezeigt.

Des Weiteren wurde im Rahmen des European Metrology Research Programme (EMRP) MetroMETAL ein Detektormodell erstellt, validiert und getestet. Ziel von MetroMETAL ist unter anderem die Entwicklung von Referenzstandards für die in der Metallindustrie anfallenden Materialien wie Metall, Schlacke und Asche, die mit bekannten Aktivitäten üblicher Verunreinigungen wie ^{60}Co, ^{137}Cs, ^{192}Ir, ^{226}Ra und ^{241}Am versetzt sind sowie die Evaluierung von Stärken und Schwächen unterschiedlicher Monte Carlo Codes. Prototypen der entwickelten Standards werden in den teilnehmenden Laboratorien vermessen und evaluiert. Die Resultate dieses Vergleichs finden sich im hinteren Teil dieser Arbeit. [1]

Eine besonders wichtige Anwendung für Gammaspektrometrie ist die Vermessung und Überwachung der natürlichen Strahlenbelastung in der Umwelt. Gerade bei der Vermessung von schwach aktiven Umweltproben ist die Verwendung gut kalibrierter Messgeräte essentiell. Im Zuge dieser Diplomarbeit wurden Donausedimentproben zweier österreichischer Wasserkraftwerke ausgewertet. Die laufende Ermittlung der Aktivität der Umwelt liefert notwendige Daten für das Verständnis natürlicher Transportprozesse und die Verteilung radioaktiven Materials und kann auch als Nulllinie im Katastrophenfall dienen.

Acknowledgements

I would like to express my gratitude to my supervisor Univ.Prof. Dipl.-Ing. Dr. Franz Josef Maringer for the useful comments, remarks and engagement through the learning process and writing of this master thesis. Furthermore, I would like to thank the employees of Bundesamt für Eich- und Vermessungswesen (BEV) and Low-level Counting Laboratory Arsenal (BOKU/TU) for the use of their facilities and their professional help. Last but not least, I would like to thank my loved ones, who have supported me throughout the entire process, financially and emotionally. I will be grateful forever for your love and support.

Contents

IV. Appendix

List of Figures

List of Tables

List of commonly used terms, abbreviations and symbols

SEGe	Standard electrode coaxial germanium (detector)
FWHM	Full width at half maximum
FWTM	Full width at tenth maximum
Z	Number of protons
N	Number of neutrons
$t_{1/2}$	Half-life
A	Activity
eV	Electron Volt
P	Probability
E	Energy
t	Time
r	Count rate
f_{corr}	Coincidence summing correction factor
σ^2	Variance
σ	Standard deviation
ϵ_T	Total efficiency
ϵ_P	Peak efficiency
relative efficiency	Efficiency relative to a 3 x 3 inch NaI scintillation detector
ν	Frequency
ps	Point source

Table 1.: Commonly used abbreviations and symbols

Part I.

Fundamentals

1. Introduction

This work focuses on the use of the Monte Carlo code PENELOPE 2011 used for the simulation of radiation transport in radionuclide metrology. In the course of Bundesamt für Eich- und Vermessungswesen's participation in the European Metrology Research Programme IND04 MetroMetal, a virtual detector image of a high-purity germanium detector had to be devised and calibrated as a basis for the code. One of the objectives of the project is to devise reference materials spiked with a known activity of radionuclides typically found in metallurgical industry. Prototypes of those newly devised standards were then used to partake in intercomparisons of the involved laboratories in order to test some of the most commonly used Monte Carlo codes for their applicability in that area. This work shows the results of the analysis of these samples conducted using PENELOPE 2011.

Additionally, sediment samples of two Austrian hydro-electric power plants located on the Danube were taken and analysed using Canberra Industries Genie 2000 software. The objective of the project is to monitor the radioactivity of the Danube river over the course of years. Samples from November 2013 to August 2014 were analysed and evaluated.

2. Structure of the atom

An atom is a small unit of matter composed of neutrons, protons and electrons. According to Niels Bohr, the neutrons and protons form the nucleus of the atom where most of its mass is located with the electrons revolving around the nucleus on predefined closed orbits. Bohr assumed that electrons only emit electromagnetic radiation when jumping between those orbits. The orbit nearest the nucleus is called K-shell, the one next to it L-shell and so on. According to this nomenclature, radiation emitted by an electron jumping to the K-shell is called a K-line, radiation by an electron jumping to the L-shell is called L-line etc.pp. The radiation emitted when an electron fills a vacancy in a lower energy state is characteristic for a particular atom. The electrons on the orbit farthest away from the nucleus are called valence electrons.
Even though Bohr's model is not accurate and a very simplified version of the actual structure of an atom it is sufficient for the purpose of explaining the basic physical effects relevant to gamma ray spectrometry.

The number of protons Z and number of neutrons N make up the mass number A.

$$\mathrm{A} = \mathrm{Z} + \mathrm{N} \tag{2.1}$$

A common way to write the properties of an atom is

$$^{\mathrm{A}}_{\mathrm{Z}}\mathrm{X}_{\mathrm{N}} \tag{2.2}$$

where X is a place holder for an elemental symbol (e.g. H for hydrogen, Na for sodium, etc.).

3. Radioactivity

3.1. Activity

Radioactivity is the process in which an unstable nucleus spontaneously transforms into a stable nucleus by emitting particles and/or radiation. Such unstable nuclei exist in nature but can also be man-made through nuclear fission and nuclear reactions.

Such transformations - also called radioactive decay - are only possible when the bond energy of the initial state is higher than the bond energy of the final state. It can be achieved by a variety of processes described in the following subsection.

Radioactivity is a statistical process that can be described by a Poisson distribution. The resulting decays per second in a sample - the expected value of the distribution - is called *activity* A. It's unit is s^{-1} specifically called *Becquerel* Bq

$$[A] = 1\,\mathrm{s}^{-1} \mathrel{\widehat{=}} 1\,\mathrm{Bq} \tag{3.1}$$

The *massic activity* a - the activity in reference to the sample's mass - therefore is measured in Bq/kg.

For all nuclei of the same kind the probability for decay is the same. It is important to note that all decay events are spontaneous and independent of each other. It is impossible to tell which nuclei will decay, only that by a certain time a certain number of nuclei will have decayed. The probability for decay is defined by the decay constant λ

$$\lambda = \frac{\mathrm{d}P}{\mathrm{d}t} = \frac{\ln(2)}{t_{1/2}} \tag{3.2}$$

where $t_{1/2}$ is the half life that defines the time after which only half of the original nuclei N_0 still exist or - in other words - half of the nuclei have transformed. The half life depends on the nuclide in question [2, p. 39].

The activity can then be determined by the number of transformed particles (expected value dN*) per time

$$A = -\frac{\mathrm{d}N^*}{\mathrm{d}t} = \lambda \cdot N \tag{3.3}$$

where N is the number of nuclei of one kind at a given moment. Integration leads to the law of decay

$$N = N_0 \cdot \mathrm{e}^{-\lambda \cdot t} \tag{3.4}$$

or

$$A = A_0 \cdot \mathrm{e}^{-\lambda \cdot t} \tag{3.5}$$

Activity can be measured by detecting the particles released in the process of decay or de-excitation of a nucleus. The number of released particles is an indicator for the activity of the sample. Since there are different ways for a nucleus to obtain stability, the emitted particles and their number vary from element to element. One way is to measure the number and energy of emitted γ-rays. This method is called γ-ray spectrometry.

3.2. Forms of radioactivity

The stability of a nucleus is defined by the ratio of protons to neutrons. In light-weight atoms the ratio is about 1:1. As the atom gets heavier the number of protons rises, causing the Coulomb repulsion to become stronger. More neutrons are needed in order to compensate the repulsion and create stability, amounting to about 50 % more neutrons than protons in atoms with an atomic number of about 200 [3, p. 80]. Therefore, in unstable nuclei reactions occur that change the ratio of protons to neutrons in order to obtain a stable state. In addition to that, the nucleus wants to reach the lowest possible energy state, therefore emitting energy if possible. It is important to note that the atom before and after the decay are not necessarily of the same element.

3.2.1. α-decay

α-decay is a form of radioactive decay where the parent nucleus emits a ${}^4_2\mathrm{He}$ nucleus - also called α-particle.

$$ {}^{\mathrm{A}}_{\mathrm{Z}}\mathrm{X} \longrightarrow {}^{\mathrm{A}-4}_{\mathrm{Z}-2}\mathrm{X} + {}^4_2\mathrm{He} \tag{3.6}$$

The daughter nucleus remains with a reduced number of protons and electrons. The potential energy is converted to kinetic energy and divided between the α-particle and the daughter nucleus according to their masses. Since four elemental components of the nucleus are involved in an α-decay this form of decay occurs primarily in heavy nuclei where the number of particles in the nucleus is high and therefore the probability to create an α-particle is higher than in lighter nuclei. Figure 3.1 shows the process.

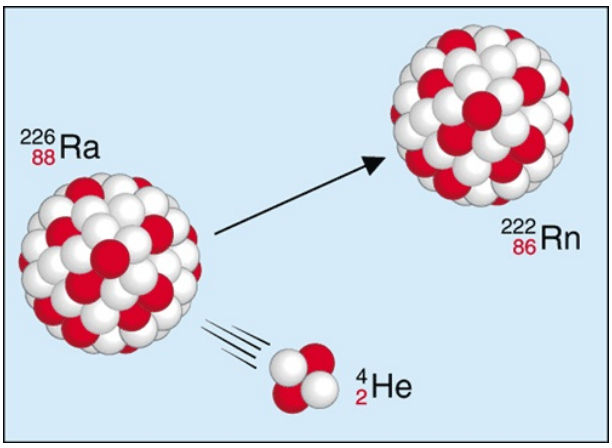

Figure 3.1.: Alpha decay example [4]

3.2.2. β-decay

β^--decay

Using the mechanism of the β^--decay, an excess neutron can transform into a proton, thus shifting the balance in favour of the protons. This process is only possible if the neutron can occupy a vacant proton level lower than the one it was occupying before (Pauli exclusion principle), hence minimising the overall energy of the nucleus. Figure 3.2 shows that principle schematically.

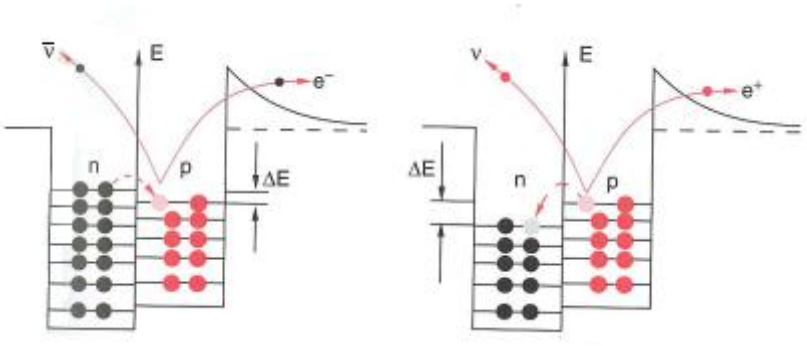

Figure 3.2.: Depiction of β-transition. Lower and vacant energy levels are occupied by transformation of a) a neutron into a proton (β^--decay) and b) vice versa (β^+-decay). In order to maintain charge a charged particle (e^+ or e^-) leaves the nucleus [2, p. 49]

As charge and angular momentum have to be conserved an electron and an electron antineutrino leave the nucleus additionally.

$$n \longrightarrow p + e^- + \bar{\nu}_e \tag{3.7}$$

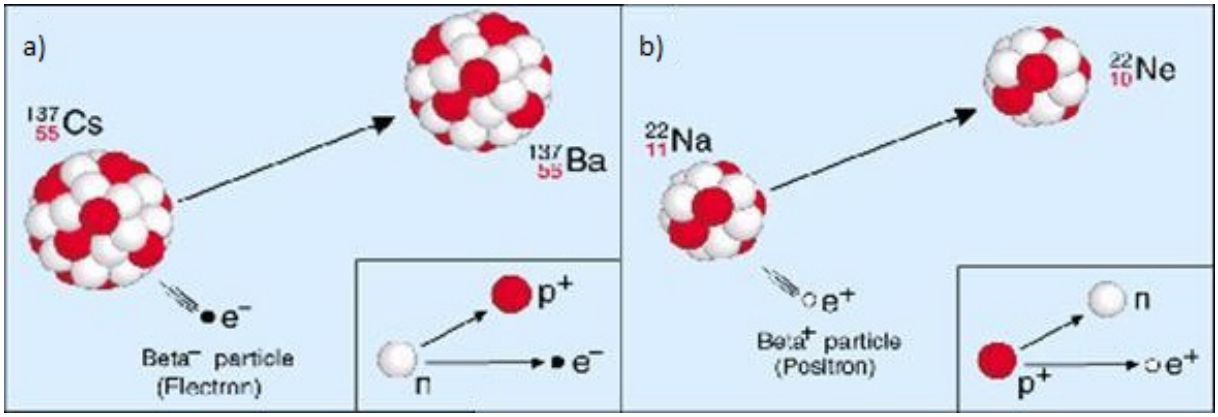

Figure 3.3.: Examples of β-decay, a) β^--decay, b) β^+-decay [5]

$$^{A}_{Z}\mathrm{X} \longrightarrow ^{A}_{Z+1}\mathrm{X} + \mathrm{e}^- + \bar{\nu}_\mathrm{e} \tag{3.8}$$

Figure 3.3a shows the process.

β^+-decay

β^+-decay follows the same principle as β^--decay, but a proton is converted into a neutron instead. Therefore, a positron and an electron neutrino are emitted from the nucleus. Figure 3.3b shows the process.

$$\mathrm{p} \longrightarrow \mathrm{n} + \mathrm{e}^+ + \nu_\mathrm{e} \tag{3.9}$$

$$^{A}_{Z}\mathrm{X} \longrightarrow ^{A}_{Z-1}\mathrm{X} + \mathrm{e}^+ + \nu_\mathrm{e} \tag{3.10}$$

3.2.3. Electron capture

Electrons occupying an atom's 1s orbital (K-shell) have the highest probability density $\mid \psi(r) \mid^2$ in the centre of the nucleus (r=0). During the electron's presence in the nucleus it can be "captured" by a proton, thereby transforming into a neutron. Again, since the angular momentum is conserved, an electron neutrino also leaves the nucleus.

$$\mathrm{e}^- + \mathrm{p} \longrightarrow \mathrm{n} + \nu_\mathrm{e} \tag{3.11}$$

The thereby fulminating vacancy in the K-shell is filled by an electron of a higher energy

level whose excess energy is released as characteristic x-ray radiation of the energy hν.

Electron capture is sometimes also called ϵ-decay or EC. It is in direct competition with β^+-decay. The energy freed by the conversion is 1022 keV ($\hat{=}$ 2 $m_e c^2$), thus making EC more attractive than β^+-decay. The energy can either be transferred to the electron neutrino as kinetic energy, or transformed into excitation energy of the nucleus. Figure 3.4 shows the process.

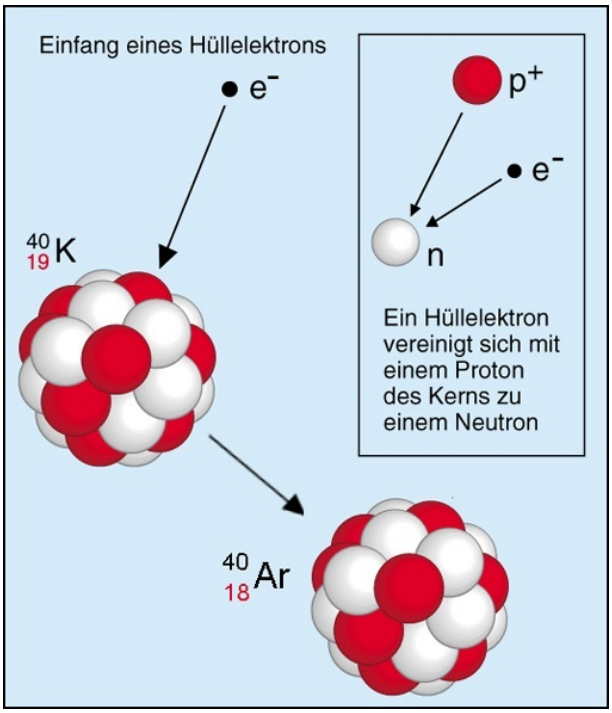

Figure 3.4.: Electron capture example [6]

3.2.4. γ-radiation

A preceding α- or β-decay leaves the daughter nucleus in an excited state. Such a nucleus can emit its excitation energy by releasing it as electromagnetic radiation

$$ {}^{A}_{Z}\mathrm{X}^{*} \longrightarrow {}^{A}_{Z}\mathrm{X} + \gamma \tag{3.12} $$

The de-excitation of the nucleus works completely analogous to the de-excitation of electrons. The energy released by that process is

$$ \mathrm{h} \cdot \nu = E_i - E_k \tag{3.13} $$

where E_k is the energy of the excited state and E_i the energy of the final state. Figure 3.5 shows the process.

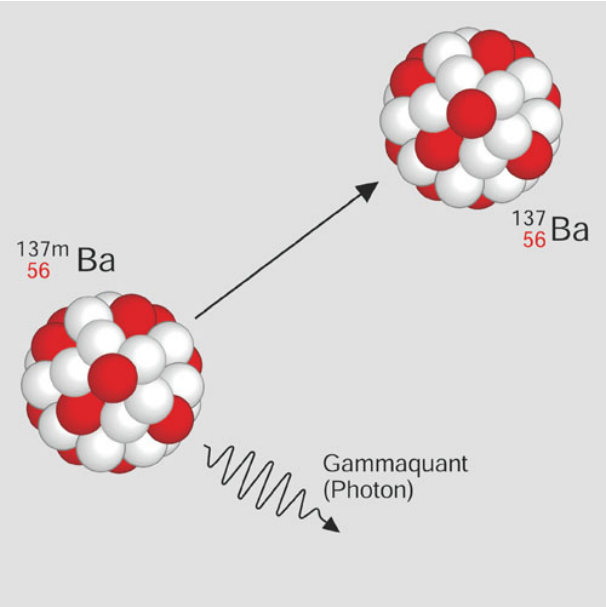

Figure 3.5.: De-excitation of a nucleus by emitting a γ-quantum [7]

3.2.5. Inner conversion

In addition to γ-ray emission, a nucleus can de-excite by transferring its excitation energy directly to an electron:

$$ {}^{A}_{Z}X^{*} \longrightarrow {}^{A}_{Z}X^{+} + e^{-} \tag{3.14} $$

The electron in question is usually of the 1s orbital, since the wave functions of 1s electrons and the nucleus overlap significantly. The excited electron can now leave the compound, leaving a positively charged atom behind. Inner conversion is sometimes referred to as inner photoelectric effect.

Often more than one transition is necessary for the nucleus to reach a stable state. A series of decays and transitions takes place before the final state is obtained. This process is called a decay chain. Figure 3.6 shows the natural uranium-radium decay chain.

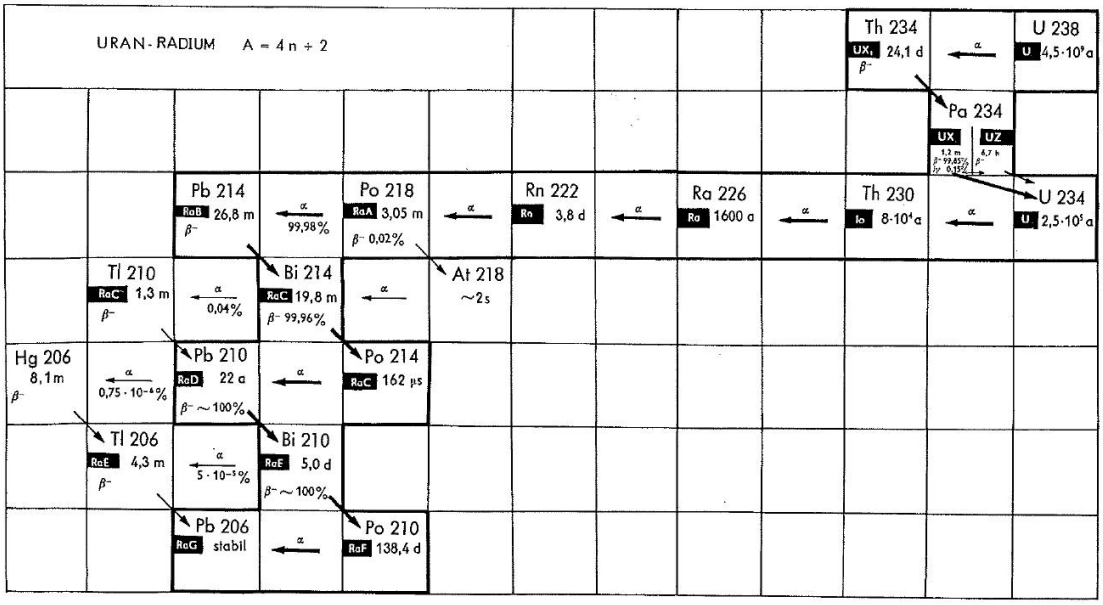

Figure 3.6.: Uranium radium decay chain [8, p. 24]

4. X- and γ-rays

X- and γ-rays are defined as highly penetrating electromagnetic radiation of wave lengths in the range of 10^{-7} to 10^{-11} cm and, therefore, frequencies of 10^{17} to 10^{21} s^{-1}. X-rays are stated between 10^{19} and 10^{21} s^{-1} (10^{-9} to 10^{-11} cm) while γ-rays are stated between 10^{17} and 10^{19} s^{-1} (or 10^{-7} to 10^{-9} cm), thus only representing a small part of the electromagnetic spectrum [9, p. 2].

Phenomena like discrete atomic spectra, photoelectric emission and wavelength shift of radiation scattered by electrons cannot be explained assuming a wave nature of the radiation. As a solution, Max Planck suggested that a body cannot absorb or emit energy in a continuous way, but only as whole-number multiples of a given energy - a quantum [9, p. 2].

Around 1914 James Franck and Gustav Hertz proved the postulated existence of discrete energy levels in atoms. In 1927 Arthur Compton received the Nobel Prize for observing a wavelength shift and unexpected distribution of scattering angles in x-rays scattered by free electrons that could not be explained by classical electromagnetism. He demonstrated that the wavelength shift was similar to the shift observed in elastic collisions of particles [10, p. 82]. Thus, emission and scattering could be explained by assuming that radiation propagates through space as discrete quanta, or photons. Each photon is a charge-free and massless particle whose energy is given by

$$E = \mathrm{h}\nu = \frac{\mathrm{hc}}{\lambda} \tag{4.1}$$

where h is the Planck constant, c the velocity of light, ν the frequency and λ the wavelength of the radiation. Photon energies are usually measured in electron volts (eV). 1 eV is the equivalent of an electron (i.e. a particle of e_0 elementary charge) being accelerated by a potential of 1 V, therefore

$$1\,\mathrm{eV} = 1.602 \cdot 10^{-19}\ \frac{\mathrm{kg} \cdot \mathrm{m}^2}{\mathrm{s}^2} \tag{4.2}$$

Following this definition, radiation up to approximately 40 keV is considered x-rays and radiation between 40 keV and 4 MeV are γ-rays. [9, p. 2]

The above mentioned definition of x- and γ-rays by range of wavelength or frequency is very general. Therefore, x- and γ-rays are often differentiated by their point of origin. X-rays are electromagnetic radiation that is emitted when an atomic electron transitions between different states of the atom, whereas γ-rays are emitted when the nucleus transitions from

an excited state to a lower state. This leads to an overlap in energy range where γ-rays as low as a few keV, as well as x-rays from transuranium elements with energies as high as 140 keV have been reported. [9, p. 2ff]

5. Interaction of photons with matter

There are various different ways for photons to interact with matter. The most important effects for radiation measurements being photoelectric absorption, Compton scattering and pair production. In all three processes photon energy is partially or completely transferred to electrons. The photon is either absorbed completely or scattered from its path. Electrons are freed from their respective atomic compounds and subsequently interact with matter, creating electron-ion or electron-hole pairs. [11, p. 29f] [12, p. 50]

Figure 5.1 shows the main interaction processes of photons in matter according to energy.

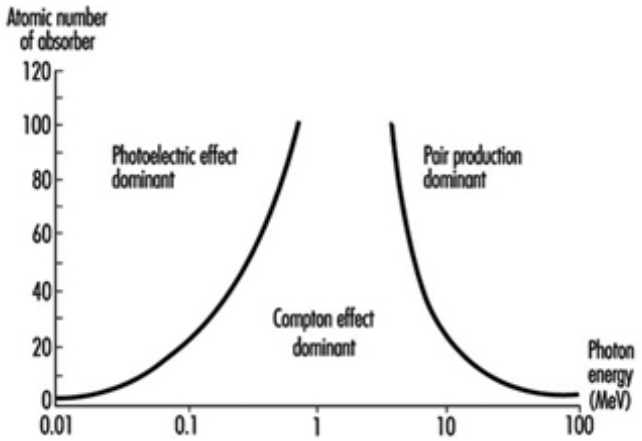

Figure 5.1.: Photon interaction processes [13]

5.1. Photoelectric absorption

Photoelectric absorption is the process where a photon interacts with, and is completely absorbed by, an absorber atom. As a result, an energetic photoelectron is ejected from the compound. Since momentum and energy need to be conserved, the interaction has to take place with the atom as a whole and is not possible with free electrons. Photoelectric absorption is most likely with a K-shell electron if the incident photon has enough energy to free it. The kinetic energy of the photoelectron is given by

$$E_{e^-} = \mathrm{h}\nu - E_b \tag{5.1}$$

where hν is the energy of the photon and E_b the energy of the electron's bond.

The ejected electron leaves a vacancy in the atom's shell that is quickly filled by either an electron from one of the other shells, or capture of an electron from the medium. Therefore, characteristic x-ray photons may follow the interaction. In some cases the release of an Auger electron can substitute the characteristic radiation. The ejected particles' energy will be absorbed in the neighbouring material and trigger interactions there.

The interaction cross section for photoelectric absorption is a complicated function of photon energy E_γ and atomic number Z of the absorber material and can be depicted in a simplified way by

$$\tau = \text{constant} \cdot \frac{Z^n}{E_\gamma^s} \tag{5.2}$$

where n varies between 4 and 5 and s varies between -4 and -3 depending on the energy [14, p. 76]. That strong dependence on Z and E_γ is the reason why photoelectric absorption takes place mainly in high-Z materials at low photon energies and becomes negligible at higher energies (see figure 5.1). Furthermore, the equation shows that high-Z materials are very effective in absorbing photons, which makes them very popular materials for shielding purposes (e.g. lead). [12, p. 50f] [11, p. 31]

5.2. Compton scattering

Compton scattering is the predominant interaction process for energies common in γ-ray spectrometry. The incoming photon is scattered on an electron of the absorber material and deflected at an angle Θ in respect to its original direction (see figure 5.2). In that process a part of its energy is passed on to the electron. The portion of energy that is transferred depends strongly on the scattering angle and can vary from zero to very large portions but never all energy is transferred. The distribution of scattering angles can be predicted by the Klein-Nishina formula

$$\frac{\mathrm{d}\sigma}{\mathrm{d}\Omega} = Z\, r_0^2 \left(\frac{1}{1+\alpha(1-\cos\Theta)}\right)^2 \left(\frac{1+\cos^2\Theta}{2}\right) \left(1 + \frac{\alpha^2(1-\cos\Theta)^2}{(1+\cos^2\Theta)[1+\alpha(1-\cos\Theta)]}\right) \tag{5.3}$$

where

$$\alpha = \frac{\mathrm{h}\cdot\nu}{\mathrm{m}_o\cdot\mathrm{c}^2} \tag{5.4}$$

and r_0 is the classical electron radius [12, p. 53].

High-energy photons undergo a series of such scattering events, distributing their energies over a large volume before their energies are low enough for photoelectric absorption.

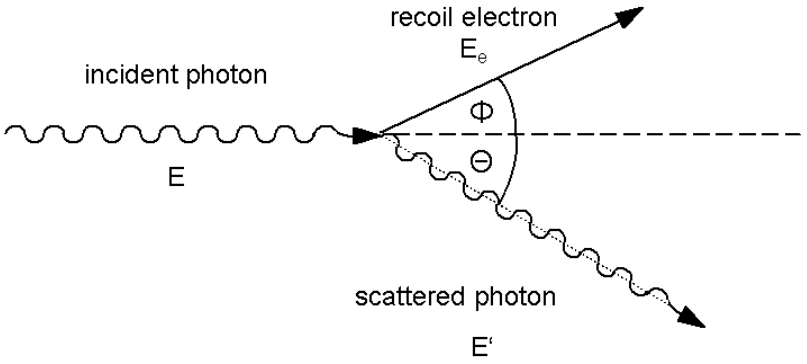

Figure 5.2.: Compton scattering of photons

The Compton cross section is approximately

$$\eta = \text{constant} \cdot E^t \tag{5.5}$$

where t varies between -0.5 and -1 [14, p. 76]. At about 150 keV the cross sections for photoelectric absorption and Compton scattering become comparable but Compton scattering quickly predominates with increasing photon energies [11, p. 35].

5.3. Pair production

Pair production is the primary interaction process for high-energy photons of a few MeV. It becomes possible when a photon's energy exceeds twice the rest-mass energy of an electron (1022 keV) although the possibility for this kind of interaction remains very low until energies of several MeV are reached [12, p. 53f].

In the nuclear Coulomb field the energy of such photons is used to generate an electron-positron pair (therefore $2m_ec^2$). The rest of the energy goes into kinetic energy of the newly formed particles. Both will be slowed down in the neighbouring medium and eventually the positron with nearly zero energy will annihilate with an electron, generating two photons of slightly less than 511 keV each that are emitted in nearly opposite directions in order to conserve momentum. The rest of the energy and momentum goes to the atom in which the electron was bound. The two resulting photons will carry their energy away from their point of origin and interact with matter by Compton scattering and photoelectric absorption.

The cross section for pair production is very complicated but as an approximation

$$\kappa \sim Z \cdot log(E) \tag{5.6}$$

can be given. [11, p. 36] [14, p. 76]

5.4. Attenuation of γ-rays

When a monoenergetic collimated beam of photons is incident on a layer of absorber material each of the aforementioned interaction processes removes photons from the incident beam, either by absorption or scattering away from the detector direction. If the absorber material is thin enough for the photons to pass through, a number of photons and electrons of different energies will emerge on the other side of the layer. The attenuation is a simple exponential function given by

$$N = N_0 \cdot \mathrm{e}^{-\mu_l \cdot d} \tag{5.7}$$

where N is the number of transmitted photons, N_0 the original number of photons incident on the absorber, d the thickness of the absorber material and μ_l the linear attenuation coefficient [11, p. 37].

The probability of occurrence of either of the interaction processes can be given per unit path length and depends on the density of the material. The total linear attenuation coefficient is the sum of the partial attenuation coefficients of the main interaction for each interaction process:

$$\mu_l = \mu_\tau + \mu_\eta + \mu_\kappa \tag{5.8}$$

The partial attenuation coefficients can be obtained by multiplying the interaction cross section of the process by $\rho \cdot N_A/M$, where ρ is the density of the material, N_A the Avogadro constant and M the molar mass. Since the linear attenuation coefficient varies proportionally with the density of the absorber, the mass attenuation coefficient

$$\mu_m = \frac{\mu_l}{\rho} \tag{5.9}$$

is more widely used. It is independent of the specific material and the state the material is in (e.g. solid or liquid) [12, p. 55].

When using voluminous sources for γ-ray spectrometry the same principle applies, since the radiation can originate at any possible point inside the source. Therefore, attenuation of the photons by the source material itself has to be considered.

6. Monte Carlo simulation

Monte Carlo simulation is a stochastic method for simulating the behaviour of mathematical and physical systems using random numbers. Statistical sampling has been known for a long time but only with the introduction of the first electronic digital computers (around 1948) it became an easily applied tool [15]. Nowadays, with the availability of fast and affordable (desktop) computers and memory, Monte Carlo simulation has become an integral tool in radiation physics. Especially where numerical methods fail or become too complex Monte Carlo simulation is a useful option. [16]

In Monte Carlo simulation, the same experiment is repeated very often under identical circumstances using pseudo-random numbers. Applied to radiation transport physics that means that a computer creates and tracks millions of particle histories. Those histories can be viewed as a random sequence of free flights that end with an interaction event in which the particle loses energy and changes its direction of movement. Sometimes secundary particles are generated and eventually the original particle is absorbed. In order to simulate those histories, an interaction model is needed. It consists of a set of differential cross sections for the relevant interaction mechanisms that are used to determine the probability distribution functions of the random variables used to characterise the track. The path of a particle depends on the variables for free path between interaction points, the kind of interaction taking place, energy loss and angular deflection [17]. This large number of random particles is then used to estimate average particle behaviour. Parameters such as scattering cross section, emission probability, absorption energies, etc. stay the same for every generated particle of the same energy. Also this method allows to predict the statistical uncertainty of the averaged result. Due to the easily available computing power, it is often very low and becomes negligible in comparison to the uncertainties of the used input data, source definition, etc. [18]

For the application in radiation transport physics many different codes exist. Some of the most widely used codes for efficiency and activity calculations in radionuclide metrology are MCNP, GEANT, GESPECOR and PENELOPE. The simulations shown in this work were performed using PENELOPE 2011. More information on this code will be provided in the "Materials & Methods" section.

7. Statistics

In order to process and interpret the collected data correctly it is necessary to work with statistics. Since radioactivity is a random process, the measured data is subject to some degree of statistical fluctuation [12, p. 65]. Since the quantities of interest in γ-ray spectrometry can usually not be measured directly, it is necessary to engage some kind of statistical interpretation of the data in order to assess the significance of a quantity and make predictions about the outcome. The true value of quantities, such as activity of a source and energy of a γ-ray, cannot possibly be known and has to be calculated. Therefore, the significance and uncertainty of all involved quantities have to be assessed in order to derive the true value of the quantity in question. [11, p.39]

7.1. The binomial distribution

The binomial distribution is a discrete probability distribution. It is used to describe the number of successes in a series of n identical but independent experiments. The only statement that can be made is "did a certain event take place", yes or no. The probability of a success is p. Therefore the predicted probability of counting x successes can be given by

$$P(x) = \frac{n!}{(n-x)!\,x!}\,p^x\,(1-p)^{n-x} \tag{7.1}$$

where n and x can only assume integer values.

The binomial distribution is a normalized distribution

$$\sum_{x=0}^{n} P(x) = 1 \tag{7.2}$$

with a mean value of

$$\bar{x} = \sum_{x=0}^{n} xP(x) \tag{7.3}$$

Application of 7.1 and 7.2 and carrying out the summation leads to

$$\bar{x} = p\,n \tag{7.4}$$

giving the mean value of the distribution as the number of trials multiplied by the probability of one trial being a success. The mean value is used as an estimate of the unknown true value of the quantity in question.

In order to make an assessment of the significance of a quantity, it is necessary to assign a standard deviation σ to it. The standard deviation signifies the spread of the individual data points around the mean value and therefore is a means to describe the fluctuation predicted by a given distribution. It can be read by the width of the distribution and is also sometimes called an uncertainty.

For any set of data the predicted variance σ^2 can be given as

$$\sigma^2 = \sum_{x=0}^{n} (x - \bar{x})^2 \, P(x) \tag{7.5}$$

Since 7.1 and 7.7 apply, the variance σ^2 and standard deviation σ of the binomial distribution can be given by

$$\sigma^2 = \bar{x}(1-p) \tag{7.6}$$

$$\sigma = \sqrt{\bar{x}(1-p)} \tag{7.7}$$

7.2. Transition to Poisson distribution

In case of a large number of trials ($n \to \infty$) and a small chance for success ($p \to 0$) the binomial distribution gives way to the Poisson distribution. This is the case for radioactive samples, where in respect to the total number of atoms in the sample only relatively few nuclei decay.

In other words, only relatively few counts are recorded in comparison to the total number of radionuclides. This especially applies, if the half-life is long in respect to the total measuring time and the probability of a success reduces to

$$P(x) = \frac{(pn)^x \mathrm{e}^{-pn}}{x!} \quad \text{or} \quad P(x) = \frac{(\bar{x})^x \mathrm{e}^{-\bar{x}}}{x!} \tag{7.8}$$

The main simplification achieved through the application of the Poisson distribution is the fact that now neither the individual success probability p nor the number of trials n has to be known individually but only their product pn. Therefore, the only significant parameter for the Poisson distribution is the mean value $\bar{x}$. Using 7.5 and 7.8, the variance and standard deviation of the Poisson distribution can be given by

$$\sigma^2 = \bar{x} \quad \longrightarrow \quad \sigma = \sqrt{\bar{x}} \tag{7.9}$$

The following example shows the influence the size of pn has on the standard deviation and therefore the importance of a long measuring time. Assuming the same measurement is checked twice: once after 100 counts have been recorded and once after 1000 counts have been recorded, the product pn varies only with n, since the probability for decay stays the same.

If, for example, n=100 counts have been recorded in a full energy peak, the relative statistical uncertainty is

$$\frac{\sigma(n)}{n} = \frac{\sqrt{100}}{100} = 10\ \% \tag{7.10}$$

With 1000 recorded counts it is only

$$\frac{\sigma(n)}{n} = \frac{\sqrt{1000}}{1000} = 3.2\ \% \tag{7.11}$$

This shows that the more pulses are recorded, the smaller the statistical uncertainty and, therefore, the better the significance of the obtained quantity.

7.3. Approximation by Gaussian distribution

If now, in addition to a large number of trials and low chance for success, the mean value $\bar{x}$ of the distribution is large, the Poisson distribution can be approximated by the Gaussian distribution [19, p. 190]. It is also a normalised distribution with

$$P(x) = \frac{1}{\sqrt{2\pi\bar{x}}} \exp\left(-\frac{(x-\bar{x})^2}{2\bar{x}}\right) \tag{7.12}$$

With those assumptions, the predicted variance σ^2 and standard deviation σ are equal to those of the Poisson distribution shown in 7.9.

Since the standard deviation is only known by measurement of a finite number of events, instead of the full population, deviations from the Gaussian distribution (a continuous distribution) still occur. These depend largely on the number of events measured and, therefore, the measuring time. Deviations from the Gaussian distribution are taken into account by introducing the so-called Student factor

$$t = \frac{\text{deviation of the mean value from the expected value}}{\text{flactuation of the mean value}} \tag{7.13}$$

in order to define the confidence interval [20, p. 4 - 16]. The confidence interval is an interval used to determine the range in which a certain parameter moves when conducting an experiment infinitely often. It is used to measure the reliability of an estimated value.

The Student distribution is very similar to the Gaussian distribution and transitions into the Gaussian distribution for n $\rightarrow \infty$.

7.4. Propagation of uncertainties

In γ-ray spectrometry the quantities of interest are usually not measured directly but determined indirectly through the measurement of other quantities and more or less complicated calculation of the quantity of interest through addition, multiplication, etc. When there are two or more quantities involved in the calculation, each of them with their own standard deviation and probably with different influence on the outcome, their uncertainties do not propagate linearly. Therefore, a propagation of uncertainty has to be conducted in order to obtain a realistic uncertainty value.

In case of Y, a function of unrelated and normally distributed quantities X_1, X_2, X_3 ,...

$$Y = f(X_1, X_2, X_3, ...) \tag{7.14}$$

propagation of uncertainties can be conducted as

$$\sigma^2(\bar{Y}) = \sum_i \left(\frac{\partial f(\bar{X_1}, \bar{X_2}, \bar{X_3}, ...)}{X_i} \right)^2 \cdot \sigma^2(\bar{X_i}) \tag{7.15}$$

The resultant quantity Y is also normally distributed. [12, p. 87f]

Part II.

Materials & Methods

8. Metrological dictionary

Metrology and the associated vocabulary play a major role when conducting γ-ray spectrometry. Therfore, it makes sense to define a few commonly used terms.

The publication "International Vocabulary of Metrology - Basic and General Concepts and Associated Terms" compiled by the Joint Committee for Guides in Metrology defines **calibration** as an "operation that, under specified conditions, in a first step, establishes a relation between the quantity values with measurement uncertainties provided by measurement standards and corresponding indications with associated measurement uncertainties and, in a second step, uses this information to establish a relation for obtaining a measurement result from an indication". It also states that the "calibration may be expressed by a statement, calibration function, calibration diagram, calibration curve, or calibration table" [21].

That means, that basically a calibration is a comparison between measurements - one made with a device that is known to be showing the "correct" or agreed upon values and one that was obtained with another device in the same manner. That first device is called a **standard**. A calibration function is then generated and applied to make the results of the tested device match the standard.

In order to make measurements comparable, **traceability** must be ensured. This means that the measurement result can be "related to a reference through a documented unbroken chain of calibrations, each contributing to the measurement uncertainty" [21]. Those references are national or international standards - so-called etalons - held by the national metrology institutes.

In this work certified standard point sources were used as calibration sources. Those point sources were tested against a national primary standard and issued with a certificate stating the activity and standard uncertainty at the production time. That makes them traceable and certified secondary standards.

9. γ-ray spectrometry

9.1. Detector development

Studies in the field of radiation began around 1900 when Wilhelm Conrad Röntgen first observed that radiation from his gas-discharge tubes produced fluorescence on a paper screen coated with platinum barium cyanide (1895) [22] and Antoine Henri Becquerel discovered natural radioactivity using uranium salts and photographic plates (1896). In 1900 Paul Ulrich Villard discovered that in addition to α- and β-particles discovered by Ernest Rutherford in 1899, natural radiation contains a third kind of "particles" which cannot easily be stopped and whose paths cannot be averted by magnetic fields. He named those particles γ-rays [11, p. 8]

Those first methods only provided the possibility to prove the existence of x- and γ-rays but no way to *count* or otherwise analyse the observed radiation.

Advances in radiation dosimetry were made with the development of proportional counters that allowed for a better quantitative measurement of radiation, as well as instantaneous detection. Proportional counters produce a signal proportional to the radiation energy if the particles deposit their full energy in the gas. As this works only for x- and γ-rays with energies low enough to interact primarily by photoelectric effect (approximately 100 keV or less), these counters are generally only used to measure the number of events, not the energy of the photons involved. [11, p. 8]

A major improvement to measurement instrumentation was made with the invention of the NaI(Tl) scintillation detectors. These detectors make use of the fact that scintillating materials emit photons in response to incident radiaton. Those photons can be converted into an electric signal using a photomultiplier. After some developing it became possible to produce scintillation crystals large enough to allow a high absorption rate of photons up to, and above, 1 MeV with relatively good resolution (7.5-8.5 % for the 662 keV γ-ray from ^{137}Cs in a crystal with 3 inches in diameter and length) and efficiency due to the high atomic number of iodine and good chemical stability. [11, p. 9]

The improvement of the ionisation chamber with higher density materials finally lead to the development of semiconductor detectors in 1962. Semiconductor detectors provide excellent

resolution of less than 2 keV at 1332 keV, which is an improvement of more than a factor 10 over the resolution of NaI(Tl) detectors. [11, p. 10f]

Semiconductor detector take advantage of the p-n-junction and the resultant electrical field also used in diodes [23]. As there are many different designs for semiconductor detectors with different areas of application. This description focuses on the detector type used in this work - the Standard Electrode Coaxial Germanium Detector (SEGe). See figures 9.1 and 9.2 for different detector types. SEGe are often referred to as Pure Ge, HPGe, Intrinsic Ge or Hyperpure Ge Detectors. In contrast to the earlier lithium drifted germanium detectors (Ge(Li)) where lithium acts as an interstitial donor impurity compensating acceptor impurities with three valence electrons, such as boron, aluminium, gallium or indium and, therefore, creating an intrinsic region. The intrinsic region in a high purity germanium detector can be accomplished directly without compensation by creating a diode structure [11, p. 76] (see figure 9.3). Figure 9.4 shows the difference in the histogram of a Ge(Li) and a HPGe detector. The term relative efficiency refers to the detector efficiency relative to a 3 x 3 inch NaI scintillation detector. It can be seen that the HPGe detector offers much better resolution.

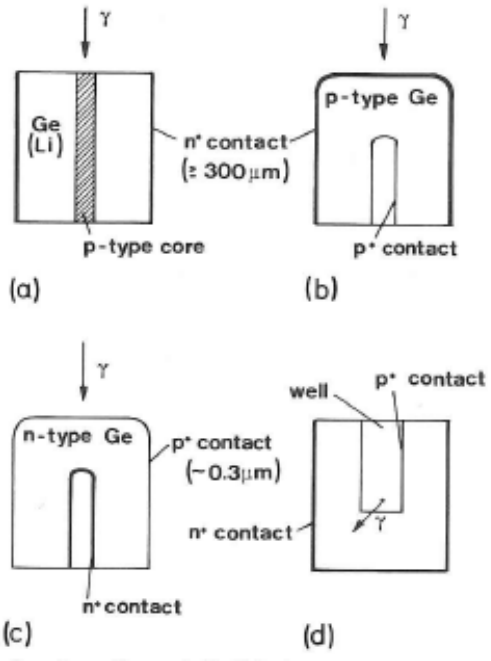

Figure 9.1.: Differnt detector geometries: a) open-end coaxial Ge(Li), b) closed-end coaxial of p-type material, c) closed-end coaxial of n-type material, d) well detector [11, p. 81]

Basically, the SEGe detector is a cylindrical high-purity semiconductor crystal with an axial hole at the bottom (closed-ended coaxial detector). The electrodes are diffused lithium (n-type contact) on the exterior and implanted boron on the surface of the well (p-type contact). Impurities of only 10^{10} atoms/cm^3 allow for a depletion of the entire volume, using

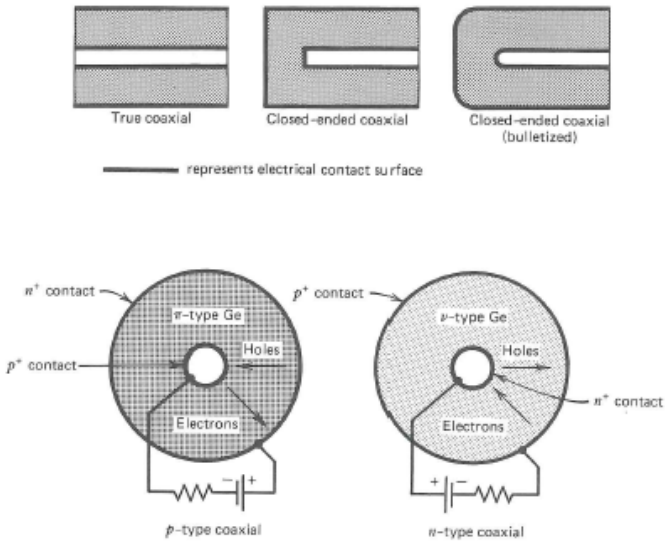

Figure 9.2.: Cross sections of most common detector types [12, p. 391]

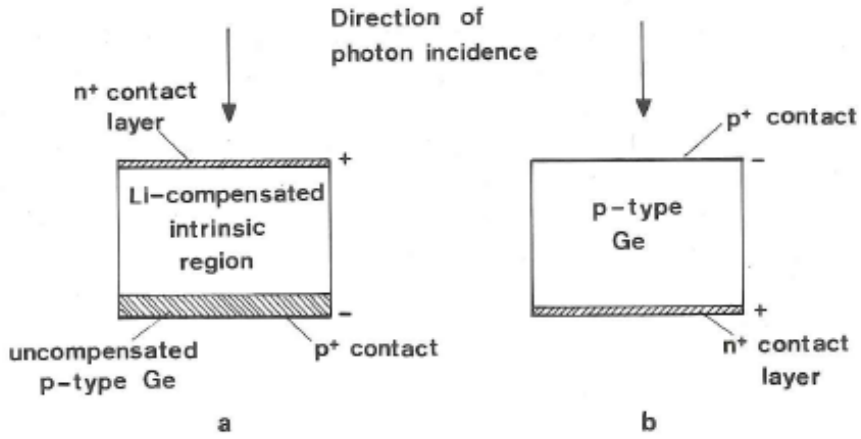

Figure 9.3.: a) Ge(Li) detector (planar), b) p-type high purity Ge detector (planar) [11, p. 77]

only a moderate reverse bias and causing an electric field across the active region. Photon interaction within the depleted region leads to freeing of charge carriers that migrate to their respective collecting electrodes. The resultant charge is converted to a voltage pulse proportional to the energy deposited by the incident photon by a preamplifier. To efficiently collect the secondary charge (secondary electrons) all semiconductor detectors have to be made of a single crystal. [25]

The main problem of the earlier Ge(Li) detectors was that they had to be cooled all the time to avoid destruction of the intrinsic region due to significant lithium diffusion at room temperature. The great advantage of high-purity Ge detectors in respect to other detectors is, that they only have to be kept cold while in operation. This reduces thermal charge generation which makes an impact on the recorded spectra [11, p. 11], [25]. A standard

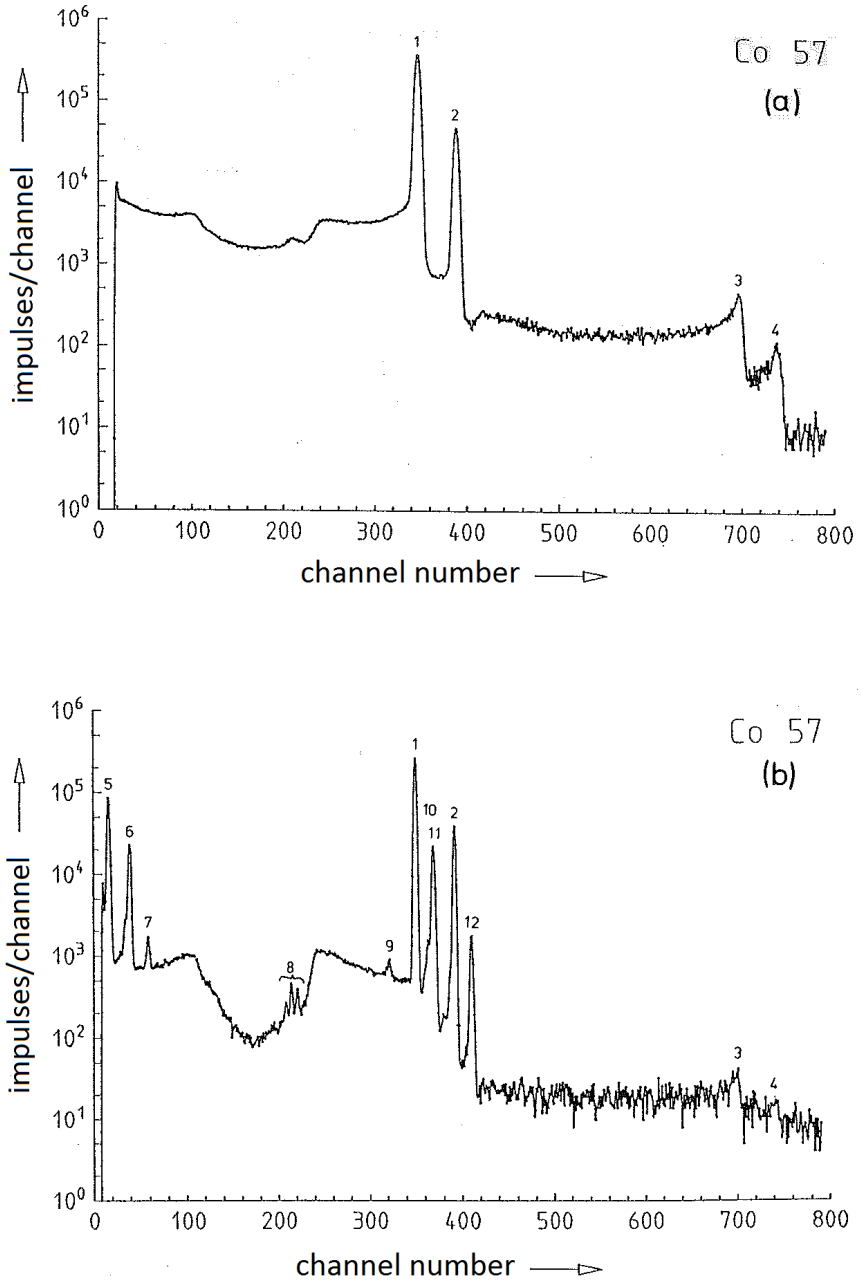

Figure 9.4.: Spectrum of ^{57}Co taken with a) a Ge(Li) detector (12.5 % relative efficiency), b) an n-type high-purity germanium detector (25 % relative efficiency) 1 cm above the end cap [24, p. 57]

medium for cooling is liquid nitrogen as it is low in cost and boils at 77 K, which is sufficient to suppresses thermal noise in the detector. Tough many different semiconductor materials have been tested only silicon and germanium are used at the moment since the difficult manufacturing process of relatively large high-purity crystals is very well established in these materials. Whilst germanium detectors can be used over a wide range of energy, silicon

detectors can only be used for photons of low energy because of silicon's low atomic number.

9.2. Full energy peak and total efficiency

9.2.1. Full energy peak,

The full energy peak is the peak in a γ-spectrum in which photons of a certain energy E that deposit their whole energy in the detector material, are counted. It is sometimes also called total absorption peak or photo peak. It is used for activity calculations.

9.2.2. Total efficiency

The total efficiency is defined as the ratio of the number of pulses recorded in the spectrum to the number of photons emitted from the source

$$\epsilon_T = \frac{\text{number of pulses recorded}}{\text{number of photons emitted from the source}} \tag{9.1}$$

In other words: The total efficiency is the probability of a γ-ray being recorded anywhere in the spectrum [26]. It is important for the calculation of coincidence summing correction factors, since the loss of counts in one full energy peak is proportional to the total efficiencies of the coincident photon line. The total efficiency can be obtained either by solving a numerical integral or experimentally. Since the total efficiency is not only a function of the detector itself, but of the measurement geometry as a whole, the experimentally obtained total efficiency is more precise as the mathematical approach has to neglect effects like photons scattered into the detector by surrounding materials. [11, p. 245f]

For an experimental determination of the total efficiency single-line photon emitters are used. Most radionuclides emit more than one γ-ray or additionally emit x-rays but a small number of single-line emitters exists. Some nuclides have a contribution of low-energy particles to a distinct line. Usually it can be subtracted quite easily, making ^{241}Am, ^{109}Cd, ^{139}Ce, ^{51}Cr, ^{85}Sr, ^{137}Cs, ^{54}Mn suitable calibration nuclides. The total efficiency ϵ_T can then be obtained by

$$\epsilon_T = \frac{N_t}{A \cdot p} \tag{9.2}$$

where N_t is the total count rate, A the activity of the sample and p the γ-ray emission probability. It is recommended to record a pulse height spectrum with more than one calibration source in order to safely be able to extrapolate to zero pulse height as well as verify that only photons of one energy are detected. The efficiency-function is generated by least-squares

approximation using the measurement points [27, p. 19]. Figure 9.5 shows such an efficiency curve.

The ratio of full energy peak to total efficiency is referred to as peak-to-total ratio r. It is used to correct for losses from peak areas due to coincidence summing.

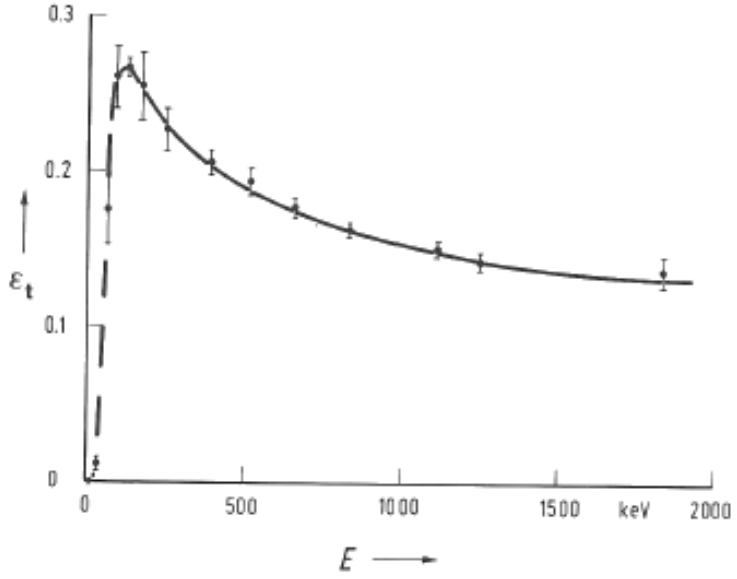

Figure 9.5.: Total efficiency curve taken with a Ge(Li) detector (12.5 % relative efficiency) with the source mounted directly on the detector window [11, p. 247]

9.3. The pulse height spectrum

As mentioned above, every photon that interacts with the semiconductor detector material inside the intrinsic zone will generate charge carriers that are moved to their respective electrodes by the electric field. The number of liberated particles depends on the energy of the incident photon. Software manages the translation of the number of particles into a count in the associated energy bin of the γ-spectrum. If the photon deposits all of its energy inside the detector material, it is added as a count in the full energy peak (e.g. 661.7 keV for ^{137}Cs or either 1173.2 keV or 1332.5 keV for ^{60}Co). If the photon only deposits a fraction of its energy and then leaves the detector, it will show as a count in a lower energy bin in the spectrum and add to the Compton continuum. The maximum energy transferred to the electron by Compton scattering E_e can be calculated using

$$E_e = E \cdot \left(1 - \frac{1}{1 + \alpha(1 - \cos\Theta)}\right) \tag{9.3}$$

The residual energy of the photon is given by

$$E' = E \cdot [1 + \alpha(1 - \cos\Theta)] \tag{9.4}$$

As can be deduced from formula 9.4, the highest energy is transferred at an angle of 180° (head-on collision), determining an upper energy limit for the Compton continuum and resulting in the so-called Compton edge. In addition, a photon can also be Compton scattered before it enters the detector material, for example on the shielding or container material. It can be shown that scattering angles of over 110-120° result in backscattered photons of nearly the same energy (see figure 9.6) In the spectrum this results in a backscatter peak at 0.2-0.25 MeV [12, p. 301].

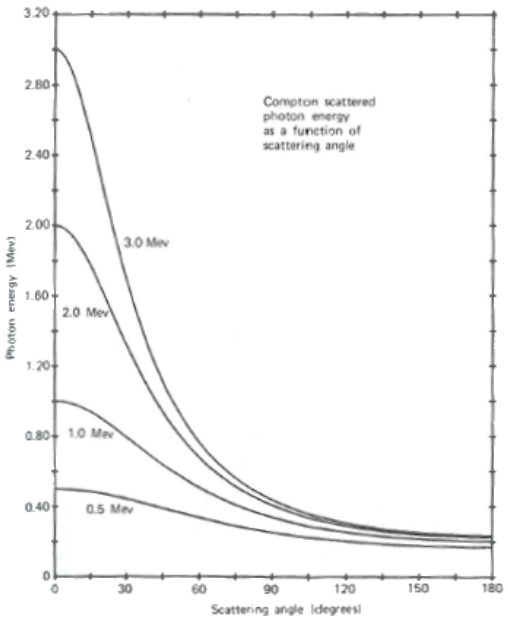

Figure 9.6.: Variation of scattered γ-ray energy with scattering angle [12, p. 301]

Other effects are sum peaks and escape peaks. The sum peak develops if more than one photon deposits its energy at the "same time" i.e. in the same resolution window of the detector. Basically, the detector cannot differentiate between the particles and perceives them as one particle of the totalled energy of the individual particles. That leads to a count in a higher energy bin. Since these photons are not counted into their according full energy peak bins, that effect falsifies the measured efficiencies and in the following any activity calculation, which makes the use of correction factors necessary. This effect will be explained in more detail in the section dealing with coincidence summing correction.

Escape peaks develop when one of the photons created in electron positron annihilation escapes from the detector material with all of its energy. That leads to a count in an energy bin that is reduced by 511 keV (single escape peak). The escape of both photons without

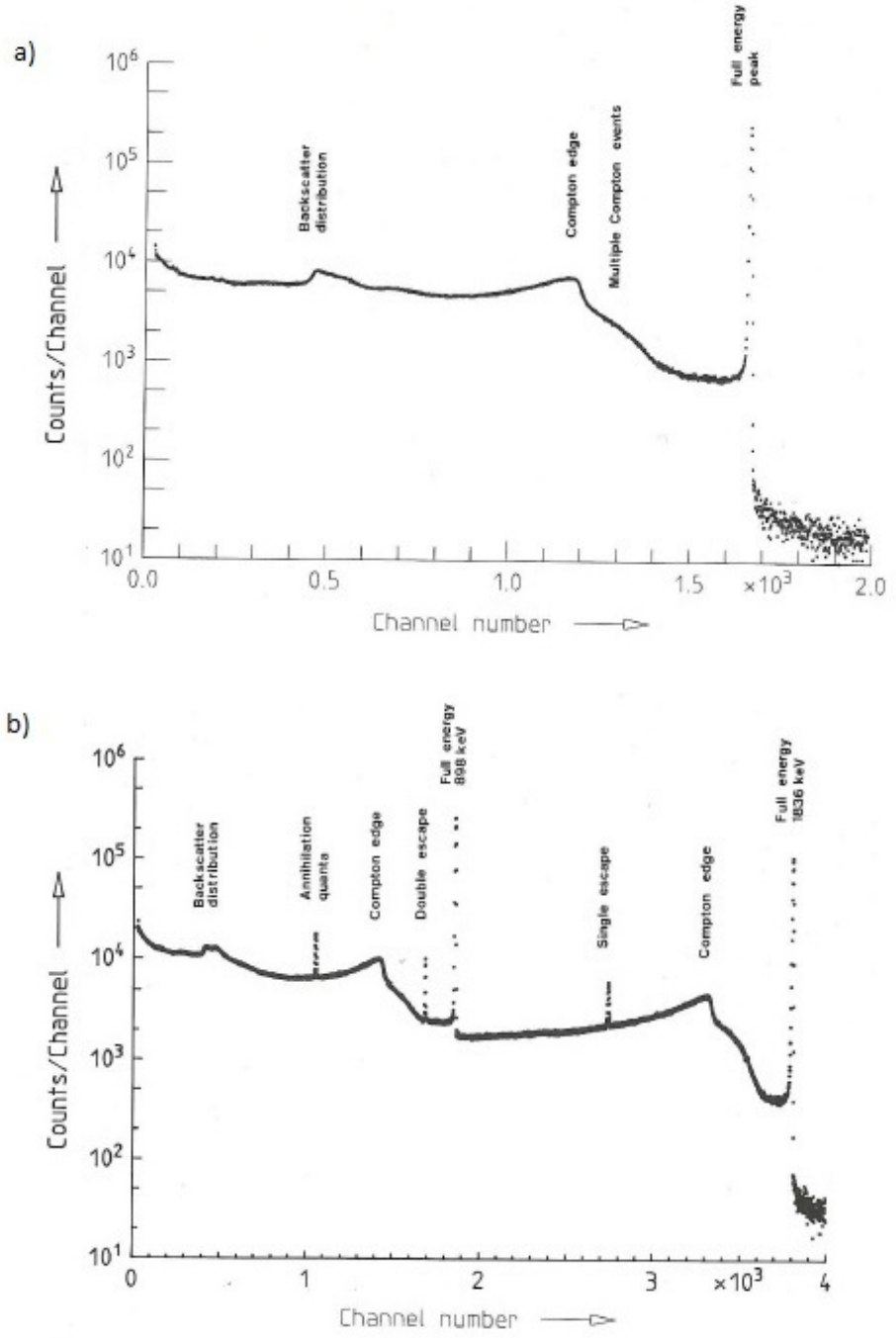

Figure 9.7.: Pulse height spectrum of a) ^{137}Cs and b) ^{88}Y [11, p. 153]

depositing their energy leads to a reduction of 1022 keV in respect to the original photon energy and, therefore, to a count in an energy bin reduced by that number (double escape peak). Since this effect occurs particularly with higher photon energies of several MeV it can be disregarded when working with environmental samples.

Figure 9.7 shows two spectra taken with a 12 % Ge(Li) detector denominating the above mentioned effects.

9.4. Activity calculation

The activity of a nuclide can be calculated using the formula

$$A = \frac{N(E) \cdot f_{corr}}{t \cdot \epsilon(E) \cdot p(E)} = \frac{r \cdot f_{corr}}{\epsilon(E) \cdot p(E)} \tag{9.5}$$

where N(E) is the number of net counts in a photo peak corresponding to the energy E, t the measurement time, $r = \frac{N(E)}{t}$ the count rate, ϵ(E) the peak efficiency of the γ-ray spectrometer, p the emission probability of a γ-ray of energy E and f_{corr} a coincidence summing correction factor that will be commented on in the next section. Self attenuation of the γ-rays can either be considered by means of an additional correction factor or in the simulation of the spectrometer efficiency. [28]

The emission probabilities of nuclei have been studied intensively and can be looked up in various tables, e.g. the Decay Data Evaluation Project [29].

9.5. Coincidence summing correction

After a radioactive decay, the daughter nuclide usually runs through many energy levels of the decay scheme. Since the life-time of the intermediate states is generally very short, the emitted photons are emitted in coincidence (in a matter of picoseconds). Figure 9.8 illustrates the process. Depending on the measurement geometry, there is a chance that some of those particles interact with the detector material at the same time. Since the resolution time of a standard germanium detector is in the range of microseconds, those photons cannot be distinguished and are perceived as one particle of the total energy of all the incident photons. A new photo peak with the totalled energy appears in the spectrum, while the other photo peaks are missing counts. That leads to a wrong calculation of the overall activity of a sample.

For example, ^{60}Co emits two photons in one decay, one of 1332.5 keV and one of 1173.2 keV. When those two photons interact with the detector material in the same resolution window and both of them deposit all of their energy, they are perceived by the detector as one particle of 2505.7 keV. This adds one count to the 2505.7 keV photo peak while the 1332.5 keV and 1173.2 keV photo peak are each missing one count. The same principle applies when one or both photons only deposit part of their energies.

The chance for coincidence summing depends highly on the distance between sample and detector, the geometry and material of sample, detector and shielding and the resolution time of the detector [27, p. 22]. For typical measurement geometries and energies of environmental

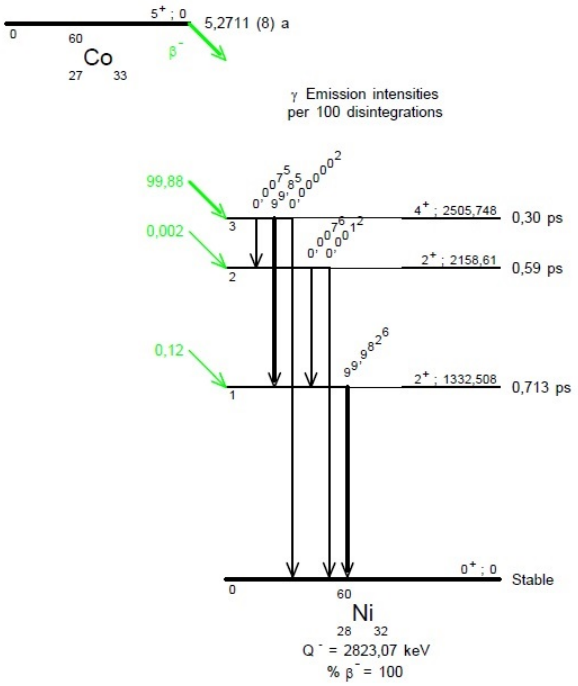

Figure 9.8.: Decay scheme of ^{60}Co [29]

samples necessary corrections can be in the range of 10 % - 50 % ($f_{corr} = 1.1 - 1.5$) [24, p. 37 - 52].

Since the physical parameters of sample and detector are usually a given that cannot be changed, the most effective way to prevent coincidence summing is the source-detector geometry that can be altered by the user. Figure 9.9 shows the histogram of two measurements of ^{60}Co taken at different distances from the detector end cap. The height of the sum-peak at 2505.7 keV changes significantly with the sample-detector-distance.

Every line emitted by a nuclide has to be corrected separately. For ^{60}Co - a nuclide that decays emitting only two lines - the coincidence summing correction is relatively simple and can be given by

$$f_{corr,1173} = \frac{1}{1 - \epsilon_{T,1332}} \quad \text{and} \quad f_{corr,1332} = \frac{1}{1 - \epsilon_{T,1173}} \tag{9.6}$$

where $\epsilon_{T,E}$ is the total efficiency of the denoted line. [24, p. 11]

Correction factors have been widely studied and can be looked up in tables. For example in [30].

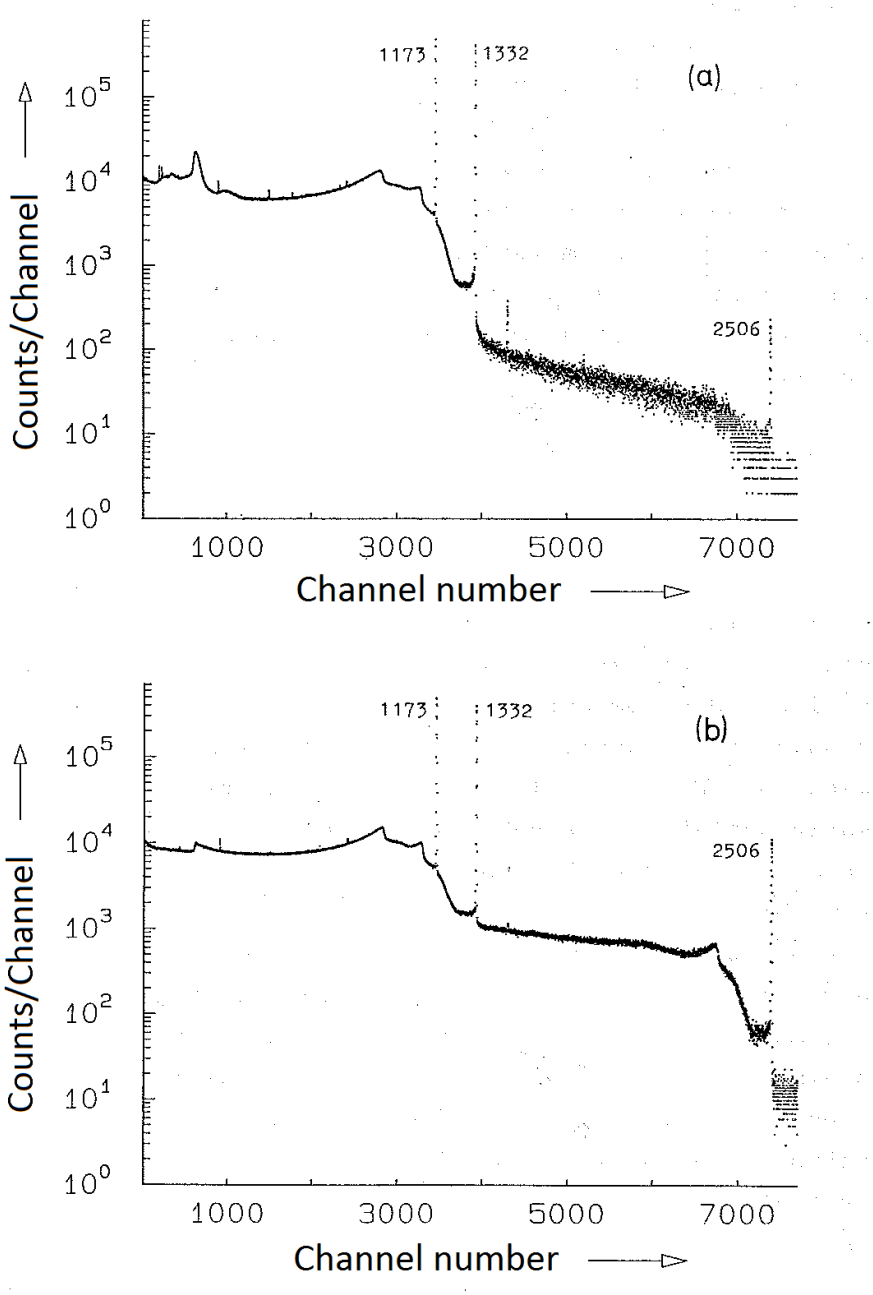

Figure 9.9.: Spectrum of ^{60}Co taken with an n-type HPGe detector (25 % relative efficiency) at a) 20 cm, b) 1 cm above the detector end cap [24, p. 8]

The chance for a summation of photons not originating from the same decay process (e.g. from different nuclides or the decay of different nuclei) is only relevant with very high count rates of more than 1000 counts per second. That resulting effect is called random coincidence summing while the previously mentioned effect is called true coincidence summing. As an example, it becomes possible that two 661.7 keV photons from two different ^{137}Cs nuclei (^{137}Cs is a single-line emitter!) deposit their energy within the same resolution window of

the detector, creating a sum peak 1323.4 keV. The only relevant parameters for random coincidence summing are count rate and resolution time. [27, p. 23], [12, p. 304]

Figure 9.10 shows the difference between true and random coincidence summing.

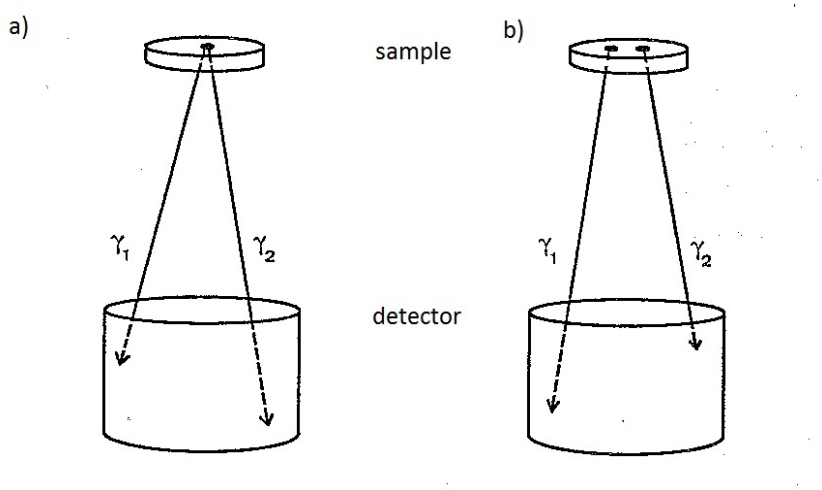

Figure 9.10.: Difference between a) true and b) random coincidence summing [24, p. 6]

10. Laboratory equipment

10.1. Detector

10.1.1. BEV activity laboratory Seibersdorf

One of the detectors used in this diploma thesis is a Canberra Industries standard electrode coaxial germanium detector (SEGe) with an automated liquid nitrogen cooling system. It will be referred to as the Seibersdorf detector owing to its location. Figure 10.1 shows photographs of the detector assembly.

The Seibersdorf detector has been repaired in 2007 due to increased crystal leakage current. Canberra Industries stated that the "crystal has been re-implanted, re-etched and remounted. Vacuum has been reconditioned and checked after a cycle" [31].

The specifications taken from the original detector data sheet compiled by Canberra Industries in 1995 and the Canberra Industries information sheet on SEGe detectors [25], as well as the informations provided by the manufacturer after repair are shown in table 10.1. Originally, the detector also had a thin beryllium window that was removed while at repair. The data sheets can be looked up in the annex.

The term dead layer refers to a layer of inactive germanium on the surface of the germanium crystal that does not add to the active detector volume [32]. It acts as an attenuating layer and especially low-energy photons are affected by it. For higher-energy photons, like those emitted by a ^{60}Co nucleus, the effect is almost negligible.

In addition to the dead layer, a so-called transition zone exists. It is only a partially active layer with low collection efficiency. Photons counted in that zone only contribute to the Compton continuum but not to the full energy peak. Therefore, it can be viewed as an attenuation layer in respect to the detector efficiency. Since it is difficult to estimate the thickness of the transition zone, the effective thickness of the inactive germanium layer is not well known. [32], [33].

The size of the inactive germanium layer affects the size of the active volume of the detector. The larger it gets, the smaller the active volume gets, resulting in a reduction of the detector

Figure 10.1.: Detector assembly of the Seibersdorf detector with liquid nitrogen container, dewar and timer for the automated cooling system

efficiency. The size of the effective dead layer depends on the manufacturing process, the age of the detector and, foremost, on the temperature at which the detector is kept. If the detector is kept warm most of the time, the outer dead layer growth causes the efficiency for low energies (e.g. photons emitted by ^{241}Am at 59.54 keV) to drop by 10 % every 6-9 months. For medium-high energies the efficiency reduction amounts to 2-3 % per year [34]. Low-energy photons are much more affected by the size of the dead layer, as their energy is not high

	1995 (new detector)	2007 (after repair)
Model	GC3020	GC3020
Relative efficiency	30.2	25.6 %
FWHM at 122 keV (^{57}Co)	0.931 keV	0.867 keV
FWHM 1332 keV (^{60}Co)	1.78 keV	1.77 keV
FWTM at 1.332 MeV (^{60}Co)	3.35 keV	3.28 keV
Peak to Compton ratio (P/C)	60.8:1	60.8:1
Peak shape	2.00	2.00
Crystal diameter	56.5 mm *	56.5 mm *
Crystal Length	55 mm *	55 mm *
Endcap diameter	76 mm *	76 mm *
Crystal to endcap distance	5 mm *	5 mm *
Cryostat model	7935SL-7	7935SL-7
Preamplifier model	2001CSL	2001CSL
Outer dead layer	0.5 mm *	1 mm *
Dead layer hole	0.3 μm *	0.3 μm *

Table 10.1.: Detector dimensions provided by the manufacturer in 1995 and 2007. *nominal value specified by manufacturer. No further measurements were conducted to obtain those values

enough to penetrate a thick attenuating layers. In most cases the thickness and sensitivity of the dead layer is not homogeneous over the detector surface, adding another challenge [35], [36]. In the course of this work it is assumed that the dead layer is a homogeneous layer of fixed thickness in order to simplify the already very complex simulation and reduce simulation time.

10.1.2. BOKU/TU Low-level Counting Laboratory Arsenal

The second detector used to make measurements will be referred to as the Arsenal detector. It is a Baltic Scientific Instruments automated low-background gamma-ray spectrometry system based on a high-purity germanium detector. Table 10.2 shows the relevant detector information.

Model	GCD-50195X
relative efficiency	> 50 %
FWHM at 122 keV (^{57}Co)	< 750 eV
FWHM 1332 keV (^{60}Co)	< 1950 eV
FWTM/FWHM	< 1.9
Peak to Compton ratio (P/C)	60:1
Crystal diameter	80 mm *
Crystal Length	40 mm *
Thickness of carbon epoxy input window	0.8 mm *
Front dead layer	0.3 μm *

Table 10.2.: Detector dimensions provided by the manufacturer in 2007. *nominal value specified by manufacturer

10.2. Shielding

In order to minimize signals generated by photons not emitted from the source a shield is used. Mostly those, for the purposes of γ-ray spectrometry, unwanted photons come from decay processes in surrounding material and air as well as cosmic radiation. Usually, lead is used due to its very high density and the resultant compactness of the shielding. The higher the density of the material the greater its stopping power for photons. Other materials such as concrete could be used but thicker shieldings would be needed.

The shield used for the experiments in with the Seibersdorf detector is made from a 10 cm thick lead cylinder put around the detector. The lower part has a hole in it to connect the detector to the rest of the hardware. The upper part is rotatable in order to allow comfortable source positioning. To minimize the effect of x-rays generated by photon scattering in the lead the inside of the shielding is lined with 1 mm cadmium and 1 mm copper on top of that. The inside diameter of the shielding is 28 cm in order to reduce backscattering of photons from the source. Figure 10.2 shows photographs of the opened and closed detector shield and an inside view of the inner copper lining and stainless steel end cap. The source is positioned centred on top of the end cap.

The shielding of the Arsenal detector is of similar design. It consists of 10 cm thick lead with a 1.25 mm thick stainless steel lining on the outside. On the inside another 2 cm of very pure lead are attached. On top of that is 1 mm of tin lining. The inside surface is made of 1.5 mm thick electrolytic copper. The inside diameter of the shielding is 17.5 cm. Figure 10.3 shows the schematics of the Arsenal shielding. In addition, the Arsenal detector is located in a room shielded by 1.6 m of concrete lined with 3 cm of lead and 0.6 cm of steel. Combined

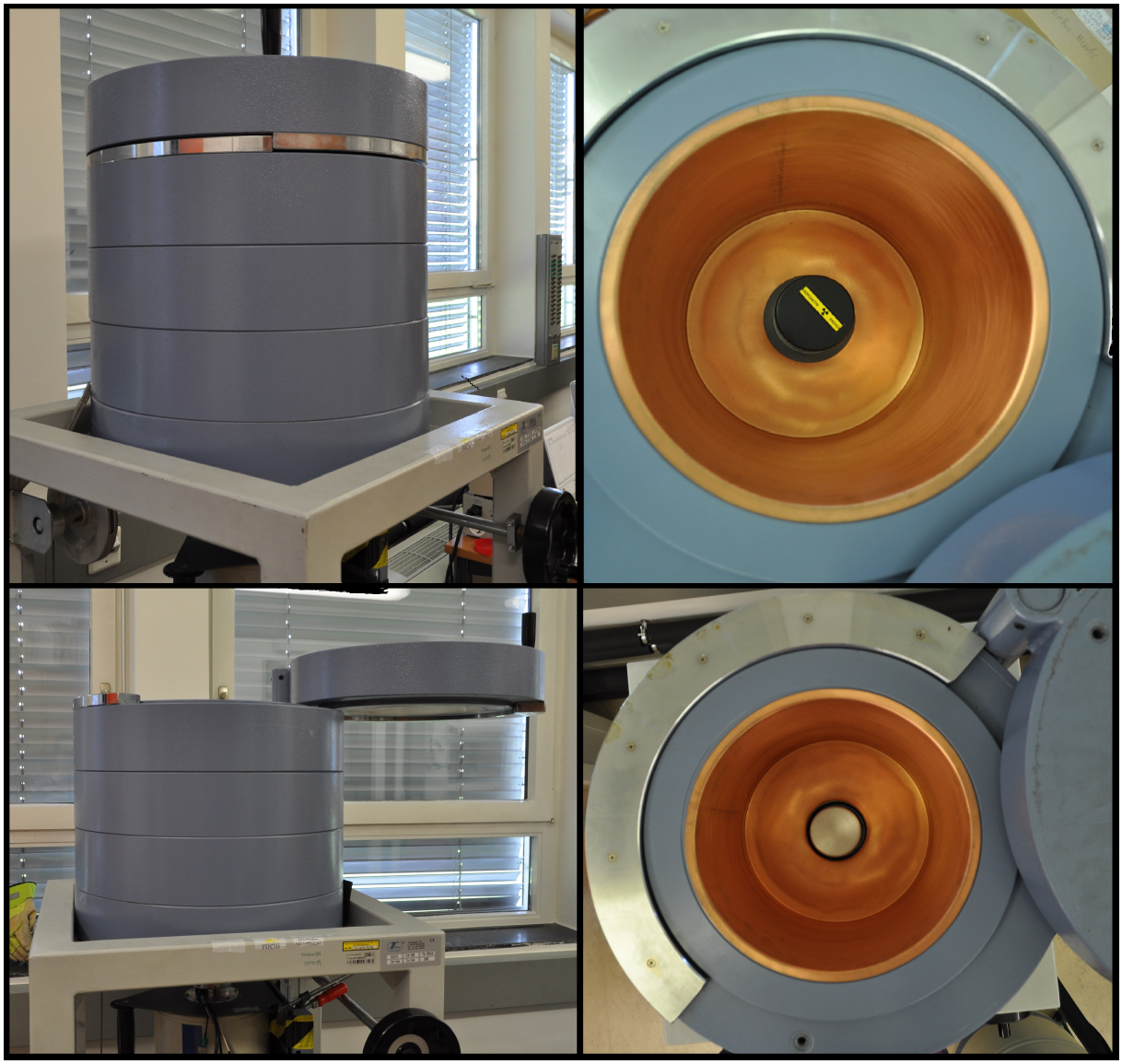

Figure 10.2.: Seibersdorf detector shield

with a specialised air filtering system that reduces the amount of radon the laboratory design leads to very low background count rates that is especially beneficial when dealing with low-activity environmental samples. [37] Unfortunately, due to necessary repairs on the detector the Arsenal detector could not be used for more than a few preliminary measurements.

10.3. Genie^{TM}2000 γ-ray spectrometry software

Genie 2000 is the γ-ray spectrometry software used in this work. It is developed and sold by detector manufacturer Canberra Industries Inc. Genie 2000 or sometimes Genie2k is a very commonly used tool in radiation physics due to its versatility. It collects data and displays it

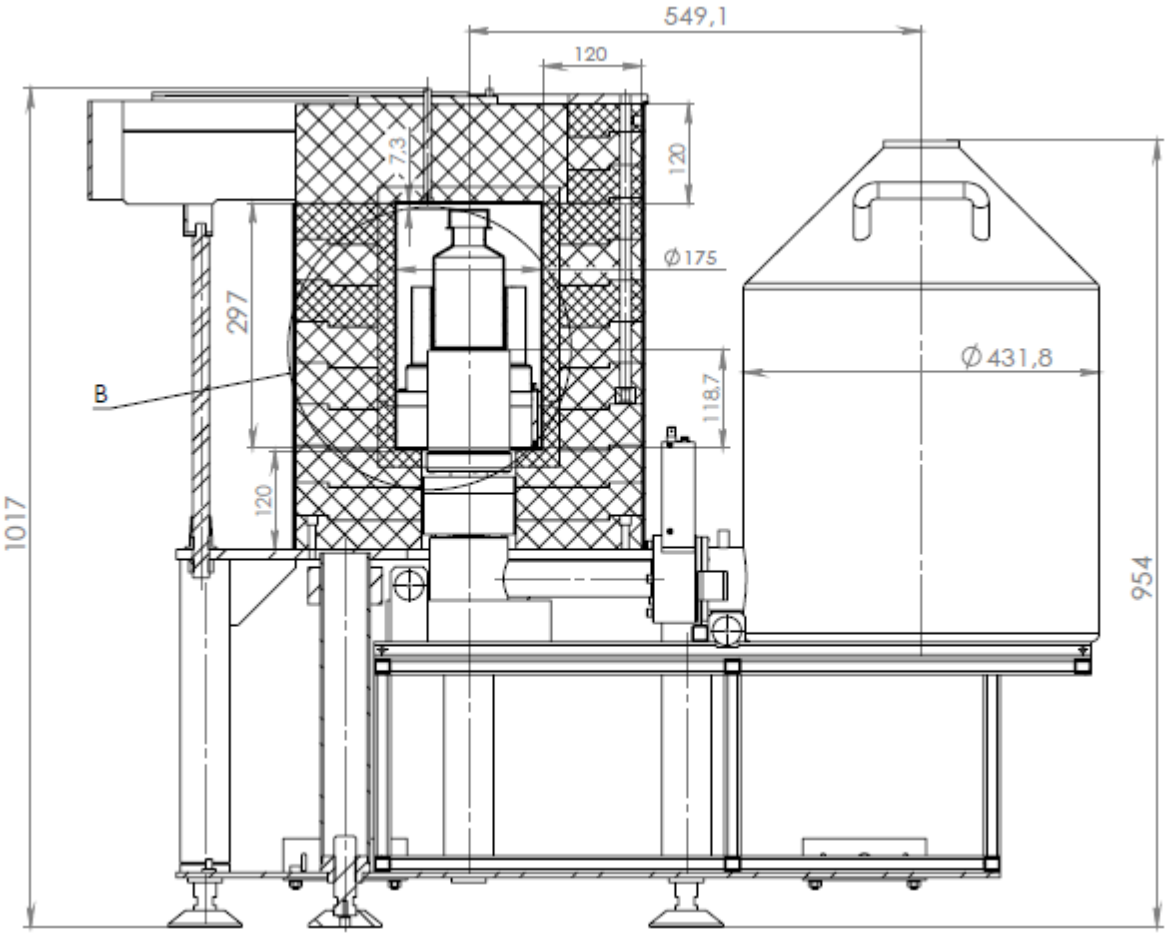

Figure 10.3.: Schematics of Arsenal shield [38]

in near real-time on the computer screen. The so gained spectrum can be analysed directly by the software.

A user programming environment for custom development exists but there are many predefined analysis routines. The user can define analysis sequences using these packages and insert sample information. Among other things it is possible to identify the peak areas of the measured full energy peaks and match them and their energies to the respective nuclide, perform background subtraction, etc. To gain proper data energy, efficiency and peak-to-total calibrations have to be performed in order to generate the necessary connections between the detector channel and the software as well as allow for corrections of the measured spectrum due to the imperfections of the detector crystal and setup (e.g. see coincidence summing correction).

With the additional package of ISOCS^{TM}/LabSOCS^{TM} it becomes possible to define source geometries and use them as a virtual efficiency calibration. The virtual efficiency calibration replaces the real efficiency calibration. This is very useful since a real efficiency calibration

has to be done using the exact same geometry and material as the unknown sample. Especially when measuring many different sample types this procedure becomes tedious and calibration standards are expensive and often not available in the necessary geometries. The built-in geometry composer allows to generate many different sample types and geometries. The program then calculates efficiency data points with which the calibration file can be written. Genie 2000 can then correct the measured spectrum and efficiencies considering self-attenuation effects of the source and calculate the activity of the sample. Together with a detector characterisation performed by Canberra Industries that takes into account the detector specific characteristics like distances between the components, attenuating layers, etc. it becomes possible to use the virtual efficiency calibration to calculate the activity of the sample.

10.3.1. Energy calibration

The energy calibration is not a real calibration in the metrological sense but in the colloquial sense of the word. It establishes a connection between the channels of the spectrum and their corresponding energies. First, the spectrum of a nuclide is being recorded. Then the user inserts the energies of the known photo peaks of the nuclide in question. This can either be done manually or using a predefined calibration file. Genie 2000 then calculates a curve of the form

$$E = \mathrm{A} + \mathrm{B} * ch + \mathrm{C} * ch^2 + ... \tag{10.1}$$

between the peaks (ch gives the channel number) that is used to match each channel to an energy [39, p. 24].

To include changes in the crystal stemming from temperature changes and dead layer growth the energy calibration should be repeated routinely.

For the energy calibration done in this work ^{152}Eu was used. The energies for the peaks used for the manual input where delivered with the sample by the manufacturer (see Appendix). Due to its many peaks over the whole energy range usually used in γ-ray spectrometry ^{152}Eu is a commonly used nuclide for energy calibration.

10.3.2. Efficiency calibration

The efficiency calibration is used in order to determine the activity of a sample and correct for material specific properties of sample and detector as well as taking source-detector-distance into account. The efficiency of a detection system depends on many factors including

- the energy of the incident γ-ray,
- the purity and alignment of the molecules in the crystal,
- the material surrounding the crystal,
- sample-detector geometry,
- self-attenuation in the sample matrix.

In order to correct for effects caused by either of those points it is necessary to conduct an efficiency calibration. It can be determined by experimentally measuring calibrations standards with a known activity. Since it is necessary to calibrate for each sample form, sample-detector geometry and nuclide individually this process becomes very costly and time consuming if one wants or needs to use many different sample geometries. Therefore, systems like the Genie 2000 add-on ISOCS/LabSOCS are very interesting for those users.

10.3.3. Peak-to-Total calibration

In order to calculate coincidence summing corrections via Genie 2000 the peak-to-total ratio (P/T ratio) at all energies has to be known. That is the ratio of peak efficiency to total efficiency of a certain energy or the number of observed counts in a full energy peak over the counts generated by that energy over the whole spectrum. Canberra Industries recommends to take measurements of six "single"-line nuclides, ^{109}Cd, ^{57}Co, ^{113}Sn, ^{137}Cs, ^{54}Mn and ^{65}Zn for the generation of the peak-to-total calibration curve. If it is available, ^{241}Am is also a viable addition. After running a peak analysis a chi-squared minimization technique is applied to fit the main energies of the nuclides by a logarithmic function

$$\ln(P/T) = \mathrm{a} \cdot \ln E_\gamma + \mathrm{c} \cdot (\ln E_\gamma)^2 + \frac{\mathrm{d}}{E_g^n} \tag{10.2}$$

gaining the total efficiency of the detector as a funciton of γ-ray energy.

Since ^{57}Co, ^{113}Sn, and ^{65}Zn are not really single-line nuclides and the full energy peaks of their main energy are surrounded by (much smaller) satellite peaks an iterative process is applied to reduce the influence of the satellite peaks in those spectra. The peak-to-total ratio at a satellite peak energy is used to calculate how many of the counts in the continuum stem from that satellite peak energy. That number of counts is then subtracted from the number of total counts in the spectrum.

$$N_{continuum} = N_{satellite} \cdot \left[\frac{1}{P/T} - 1\right] \tag{10.3}$$

Using the corrected total number of counts a new P/T ratio for the main energy peak can be calculated and the curve can be fitted again. Each new iteration improves the correction. Canberra Industries recommends using 10 iterations in order to ensure convergence for all cases. Using the values calculated in the final iteration step the calibration curve can be calculated and extrapolated to channel 0. A polynomial of the second order is used for the fit of the higher energies in order to provide a linear extrapolation in the log-log scale. The cross-over energy of the curve can be set by the user but is 122 keV by default (^{57}Co). [40, p. 268f]

10.3.4. ISOCS^{TM}/LabSOCS^{TM}

ISOCS/LabSOCS is a mathematical calibration software and an add-on for Genie 2000. The abbreviations stand for In-Situ Object Calibration Software/Laboratory Sourceless Calibration Software. As mentioned before it can be used to eliminate all traditional calibration sources from the analysis and calibration process. In place of the measurement with an actual calibration source to calibrate and perform an efficiency correction the user only has to define a few properties of the source and the source-detector geometry. Pre-defined templates can be chosen that match the source geometry - e.g. Marinelli beaker, point source, cylindrical source, etc.

The parameters the user has to specify are:

- geometrical information and material of various parts of the sample and sample holder, e.g. thickness and material of bottom/side wall, sample diameter/height/etc, sample composition, etc. The amount of information necessary depends on the chosen template and therefore on the complexity of the sample design,
- source-detector distance (end cap to underside of the source),
- thickness and material of any attenuating layers between the end cap and the source (e.g. air/acrylic glass when using a sample holder),
- the detector characterisation of the detector used for the measurement.

In order to specify the above mentioned parameters a program called "Geometry Composer" comes with ISOCS/LabSOCS. It provides a graphical user interface in which the user can input the necessary data. To define the materials a library of pre-defined common substances which the user can modify and add to is incorporated into the program.

Opposed to other mathematical calibration software the user using ISOCS/LabSOCS can not specify any detector information. This information can be incorporated into the calculation by selecting the detector characterisation of the detector the measurement was done with from a drop-down list. The characterisation has been done by the manufacturer before shipping. In the process traceable standard sources and the Monte Carlo code MCNP are used to create a radiation response profile of the actual crystal built into the system in question. [41]

10.4. PENELOPE 2011

Although many different Monte Carlo codes exist and many of those are specifically designed for the use in radiation physics this work concentrates on the use of the code PENELOPE. The version used is PENELOPE 2011.

PENELOPE was devised at the university of Barcelona with the first version published in 1996. PENELOPE is an acronym that stands for "penetration and energy loss of positrons and electrons". It was initially designed to describe the energy loss of electrons and positrons following interaction events in matter. The part dealing with photon interaction was added at a later point.

PENELOPE 2011 is able to simulate and evaluate electron and photon transport and calculate all kinds of interactions in the energy range of 50 keV to 1 GeV. No specific knowledge of the underlying scattering and transport mechanisms have to be known to the user. One thing PENELOPE assumes is that the mass of the atom is concentrated in the nucleus. Since it is much larger than the electron mass the nucleus is regarded as having infinite mass. This validates the assumption that the nucleus can absorb any amount of recoil momentum without absorbing energy. Excitation and de-excitation of the nuclear energy levels can be disregarded, simplifying the calculation of cross sections and therefore reducing the time required for the simulation. [16]

The user gets a package with the Fortran source code. First the various subroutines have to be linked. After that the user gets a main program which performs the actual calculations and a material library that includes all the chemical elements as well as some commonly used materials (e.g. glass, water, etc.). The material library can also be used to build any material of a specific composition. That can either be done by input of the stoichiometric formula or fraction of weight percentage. The program then calculates the material-specific parameters such as mean excitation energy, cross sections, relaxation time, etc. Those materials can then be used to build an image of the actual detector and source used in the experiment. This should be done as detailed as possible as every difference in geometry results in a difference in efficiency. The geometry of the image is defined by homogeneous bodies that are limited

by quadric surfaces. This allows for many different shapes and forms.

In order to check the geometry the source code package comes with two programs - gview2d.exe and gview3d.exe - that visualise the coded geometry on the computer screen.

To provide the parameters of the simulation a steering program (hereafter called an input file or in-file) has to be written. It assigns the necessary variables like primary particle, what part(s) of the detector and source image emits radiation, energy, source position, energy bin width, material files used, simulation time, cut-off energies, etc. to the main program.

The most basic options for a voluminous sample in a container on a holder 4.55 cm above the detector end cap can be seen in the code listing below (Figure 10.4).

The first part defines the source parameters: type of primary particle, photon energy, source position, active body and direction of radiation.

The second part defines material data and simulation parameters, it states the material files used and links them to the material data used in the geometry file and the respective electron and photon cut-off energies.

The third part lists the geometry file containing the detector and source image.

The fourth part is used to define the detector properties such as simulated energy range, energy bin width, name of the output file and the bodies used for detection.

The fifth part defines job properties such as dump-files that allow to continue the simulation in case it is interrupted, the interval in which information is written into the dump file and the number of simulated particle histories. Additionally or instead a simulation time can be defined. The simulation stops whenever the first of the two parameters is reached.

After the simulation has successfully run PENELOPE generates several output files that contain the information to calculate full energy peak and total efficiencies. Additionally, the user receives information about absorption efficiencies and absorbed energy in the surrounding bodies, number of histories as well as some general information about the simulation.

```
TITLE  MetroMETAL slag sample, 226Ra HSlag13, 186 keV, Seibersdorf
.
>>>>>>>> Source definition.
SKPAR  2                          [Primary particles: 1=electron, 2=photon, 3=positron]
SPECTR 1.86211e5  1                             [E bin: lower-end and total probability]
SPECTR 1.86211e5 -1.0e0                         [E bin: lower-end and total probability]
SPOSIT 0 0 6.3185
SBOX   7.2 7.2 1.805
SBODY  19
SCONE  0 0 180
.
>>>>>>>> Material data and simulation parameters.
MFNAME Ge.mat                                          [Material file, up to 20 chars]
MSIMPA 1.9E3 1.9E2  1.9E3 0.1 0.1 1.9E3  1.9E2         [M,EABS,C1,C2,WCC,WCR]
MFNAME GeINAC.mat                                      [Material file, up to 20 chars]
MSIMPA 1.9E3 1.9E2  1.9E3 0.1 0.1 1.9E3  1.9E2                  [M,EABS,C1,C2,WCC,WCR]
MFNAME POLYSTYRENE.mat                                 [Material file, up to 20 chars]
MSIMPA 1.9E3 1.9E2  1.9E3 0.1 0.1 1.9E3  1.9E2                  [M,EABS,C1,C2,WCC,WCR]
MFNAME Cu.mat                                          [Material file, up to 20 chars]
MSIMPA 1.9E3 1.9E2  1.9E3 0.1 0.1 1.9E3  1.9E2                  [M,EABS,C1,C2,WCC,WCR]
MFNAME Be.mat                                          [Material file, up to 20 chars]
MSIMPA 1.9E3 1.9E2  1.9E3 0.1 0.1 1.9E3  1.9E2                  [M,EABS,C1,C2,WCC,WCR]
MFNAME Al.mat                                          [Material file, up to 20 chars]
MSIMPA 1.9E3 1.9E2  1.9E3 0.1 0.1 1.9E3  1.9E2                  [M,EABS,C1,C2,WCC,WCR]
MFNAME Cd.mat                                          [Material file, up to 20 chars]
MSIMPA 1.9E3 1.9E2  1.9E3 0.1 0.1 1.9E3  1.9E2                  [M,EABS,C1,C2,WCC,WCR]
MFNAME Air.mat                                         [Material file, up to 20 chars]
MSIMPA 1.9E3 1.9E2  1.9E3 0.1 0.1 1.9E3  1.9E2                  [M,EABS,C1,C2,WCC,WCR]
MFNAME Pb.mat                                          [Material file, up to 20 chars]
MSIMPA 1.9E3 1.9E2  1.9E3 0.1 0.1 1.9E3  1.9E2                  [M,EABS,C1,C2,WCC,WCR]
MFNAME slag.mat                                        [Material file, up to 20 chars]
MSIMPA 1.9E3 1.9E2  1.9E3 0.1 0.1 1.9E3  1.9E2                  [M,EABS,C1,C2,WCC,WCR]
.
>>>>>>>> Geometry definition file.
GEOMFN PQneu100.geo                                    [Geometry file, up to 20 chars]
.
>>>>>>>> Energy deposition detectors (up to 25).
ENDETC 0 1.86211e5 124                          [Energy window and number of bins]
EDSPC  spc-enddet-001.dat
EDBODY 2                                      [Active body; one line for each body]
EDBODY 3
.
>>>>>>>> Job properties
RESUME dump0.dmp                             [Resume from this dump file, 20 chars]
DUMPTO dump0.dmp                               [Generate this dump file, 20 chars]
DUMPP  60                                                  [Dumping period, in sec]
.
NSIMSH 1.0e9                                  [Desired number of simulated showers]
TIME 10000                                       [Allotted simulation time, in sec]
.
END                                                 [Ends the reading of input data]
```

Figure 10.4.: In-file listing of MetroMETAL ^{226}Ra_HSlag13 sample

11. Monte Carlo simulation using PENELOPE 2011

In order to simulate the efficiency of samples a detector model has to be created first. This was done using the Monte Carlo code PENELOPE 2011. The aim is to obtain less than 5 % deviation from the efficiency calculated by LabSOCS or using a physical calibration source. In the course of this work it emerged that the nominal values provided by the detector manufacturer are insufficient for a precise simulation. The consultation of papers issued in the field of efficiency calibration using Monte Carlo simulation like Hurtado et al. [42], Padilla Cabal et al. [43] and Hardy et al. [44] has lead to the belief that strong deviations between the real physical parameters of the detector and the parameters provided by the manufacturer of up to a few mm are the norm.

Therefore, a method similar to the one described by J. C. Helmer et al. [44] has been used to obtain a more precise model.

Firstly, ^{241}Am,^{57}Co and ^{109}Cd point sources were measured at 0 and 4.55 mm distance from the detector end cap. The ratios of the full energy peak areas at different distances of each nuclide where used to determine the distance of the detector crystal from the end cap.

Secondly, the comparison of the simulated peak efficiencies at 4.55 cm of both point sources was used to determine the front and side dead layer of the crystal surface.

A measurement of ^{137}Cs was used to determine the length and radius of the hole. A measurement of ^{60}Co was used to determine the length of the crystal.

Lastly, a comparison of the efficiencies of ^{137}Cs and ^{60}Co was used to determine the size of the dead layer on the hole.

It is important to note that the size of the dead layer in the simulation does not necessarily reflect its real size. Due to the aforementioned transition zone beneath the dead layer whose thickness is unknown it is impossible to separate the two of them. Additionally, the simulated dead layer also compensates for the impurities, defects and imperfect charge collection of the real crystal. [44]

Figures 11.1 and 11.2 show 2d detector images of the Seibersdorf and Arsenal detectors.

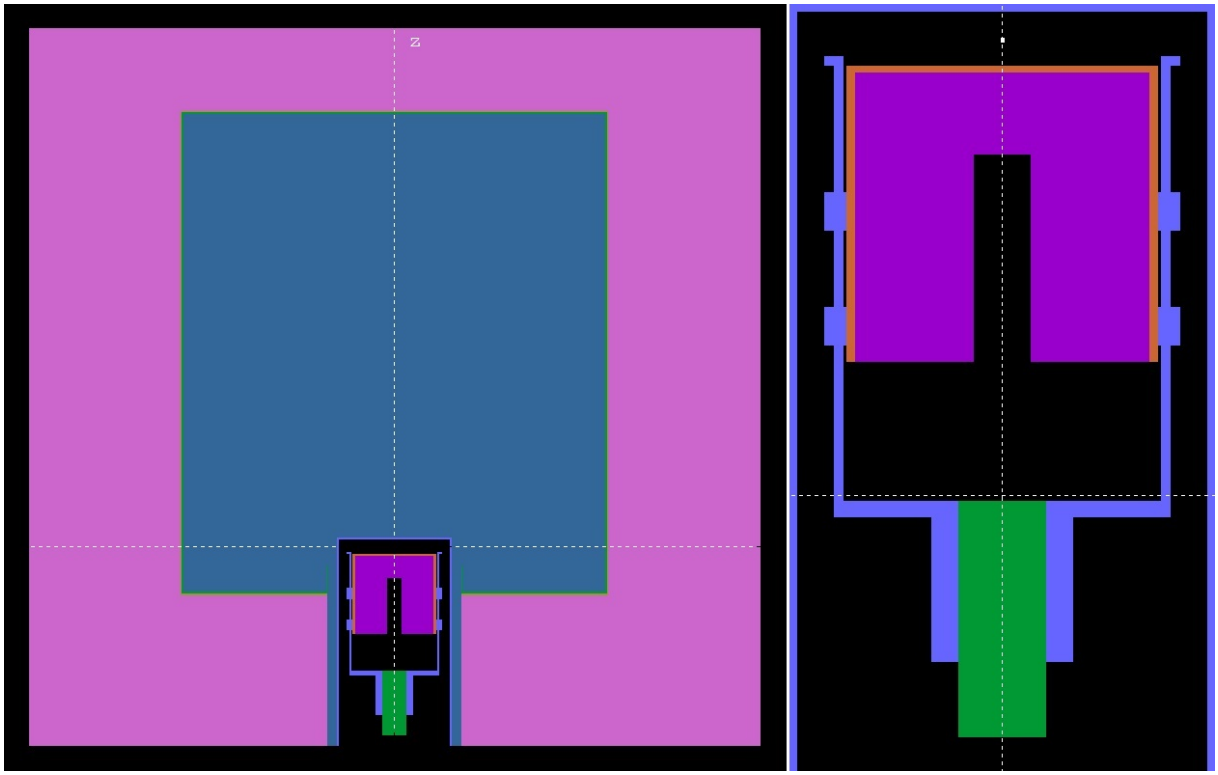

Figure 11.1.: Detector image of Seibersdorf detector

Figure 11.3 shows 3d images.

The listing below (Figure 11.4) shows a typical PENELOPE 2011 output file. It is taken from the simulation of a ^{241}Am point source positioned 4.55 cm above the detector end cap. 10^5 particle histories were tracked. It can be used to calculate the detector efficiency. Those efficiencies can then be compared to the efficiency computed by LabSOCS or - when no coincidence summing occurs - hand. Together with each lines yield, the measured count rate of the full energy peak and computed coincidence correction factors it is possible to calculate the activity of the sample. The exact energies of the photons and their yield involved in each simulation and calculation where taken from Monographie BIPM-5 - "Table of Radionuclides" [45]. This monograph is issued by the Bureau International des Poids et Mesures and contains the findings of the Decay Data Evaluation Project [29].

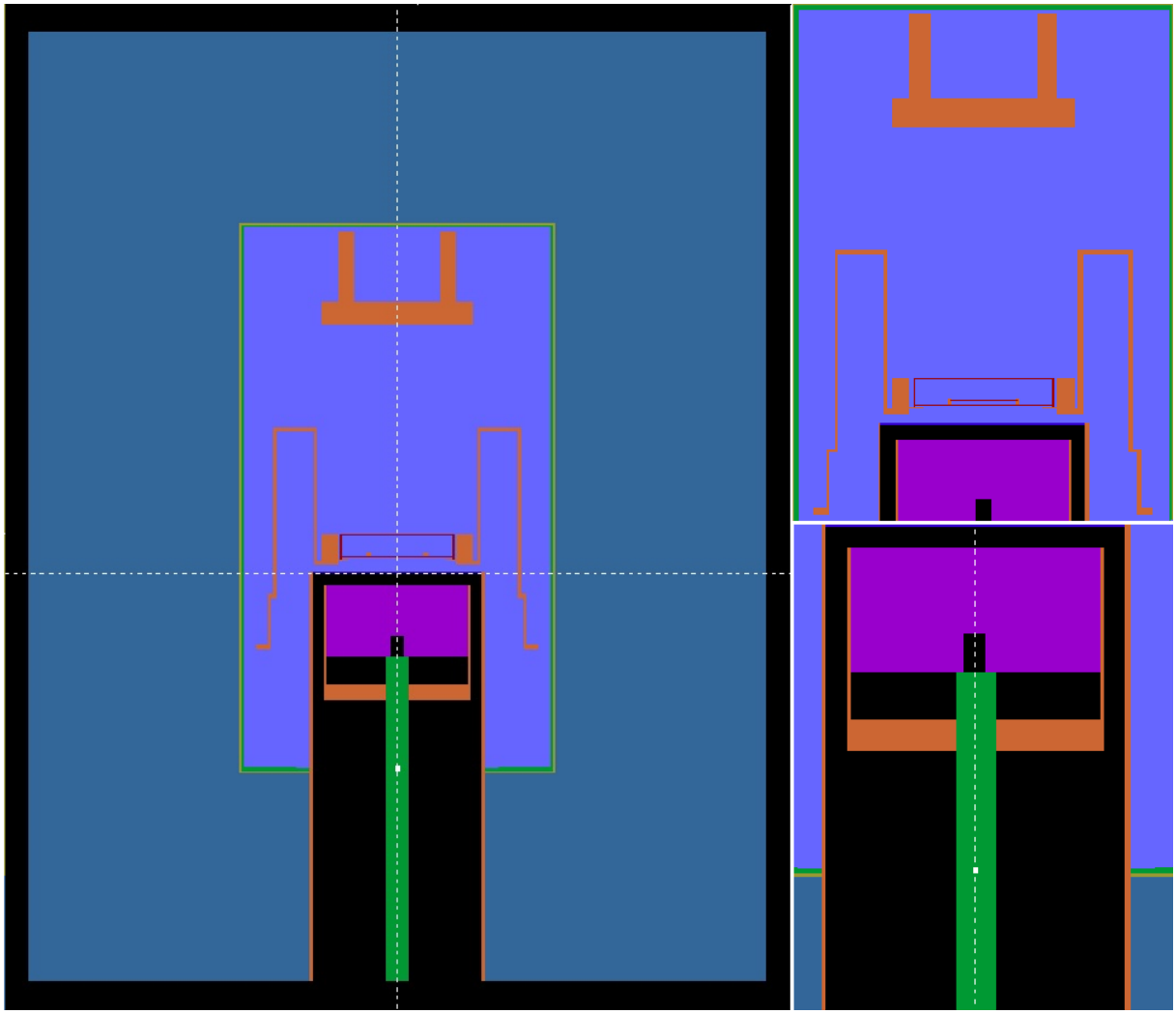

Figure 11.2.: Detector image of Arsenal detector including sample holder and point source in a PS3 container

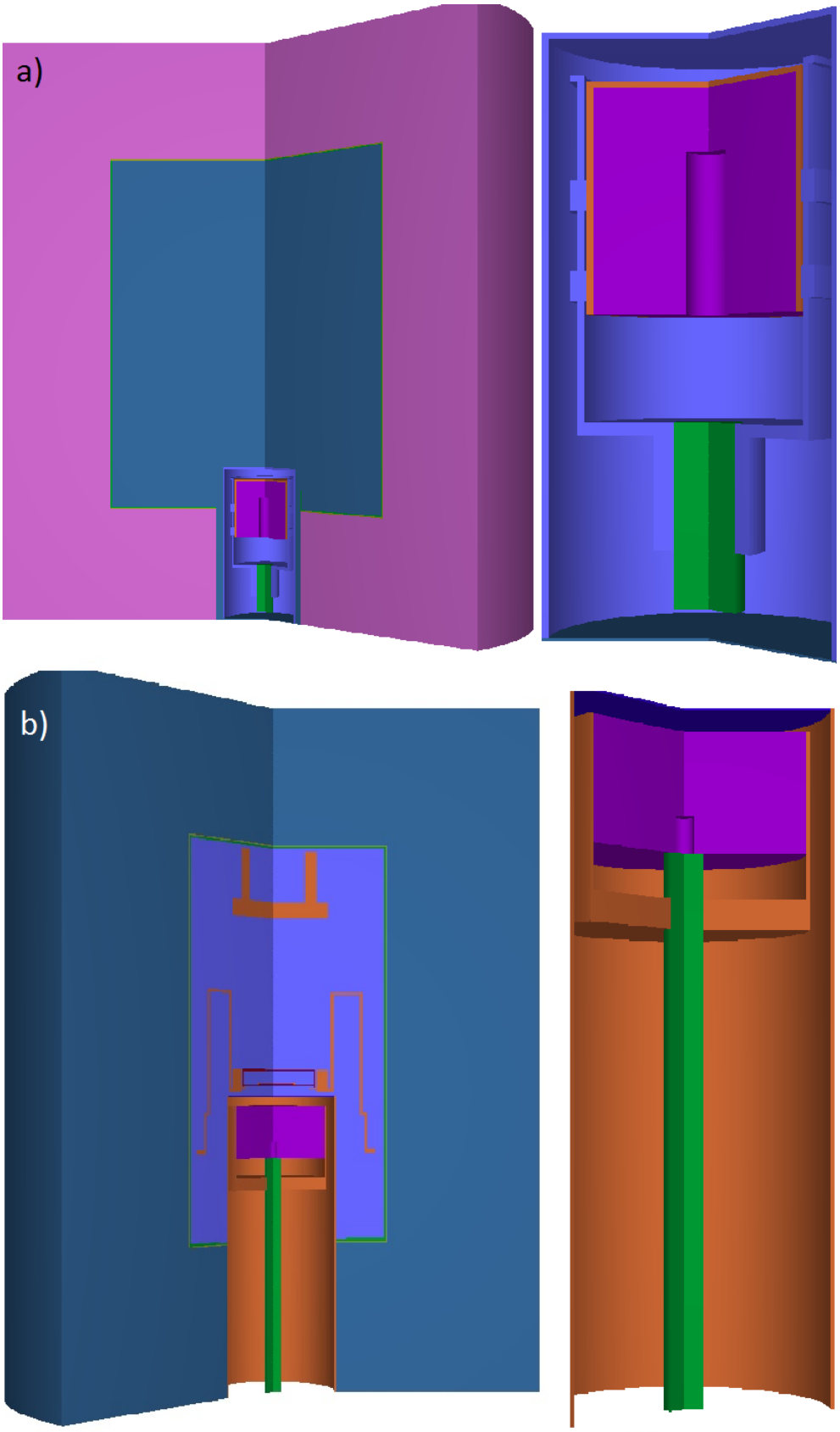

Figure 11.3.: 3d detector image of a) Seibersdorf, b) Arsenal detector

As can be seen PENELOPE 2011 lists the energy bins and the according probability density and uncertainty. It is necessary to note that the uncertainty PENELOPE computes is a merely statistical uncertainty that does not take any uncertainties in the knowledge of the physical parameters into account. In order to calculate peak and total efficiencies those probabilities and uncertainties have to be multiplied by the bin width.

```
#  Results from PENMAIN. Output from energy-deposition detector #  1
#  Deposited energy spectrum.
#  WARNING: May be strongly biased if interaction forcing is used!
#  1st column: deposited energy (eV).
#  2nd column: probability density (1/(eV*particle)).
#  3rd column: statistical uncertainty (3 sigma).

  7.442613E+02  1.000000E-35  1.000000E-35
  2.232784E+03  1.000000E-35  1.000000E-35
  3.721306E+03  1.343614E-08  2.850208E-08
  5.209829E+03  1.000000E-35  1.000000E-35
  6.698351E+03  6.718071E-09  2.015411E-08
  8.186874E+03  1.000000E-35  1.000000E-35
  9.675396E+03  5.374457E-08  5.700244E-08
  1.116392E+04  2.687228E-08  4.030762E-08
  1.265244E+04  1.343614E-08  2.850208E-08
  1.414096E+04  1.000000E-35  1.000000E-35
  1.562949E+04  6.718071E-09  2.015411E-08
  1.711801E+04  1.000000E-35  1.000000E-35
  1.860653E+04  1.000000E-35  1.000000E-35
  2.009505E+04  6.718071E-09  2.015411E-08
  2.158358E+04  1.000000E-35  1.000000E-35
  2.307210E+04  1.000000E-35  1.000000E-35
  2.456062E+04  1.000000E-35  1.000000E-35
  2.604914E+04  1.000000E-35  1.000000E-35
  2.753767E+04  1.000000E-35  1.000000E-35
  2.902619E+04  1.000000E-35  1.000000E-35
  3.051471E+04  1.000000E-35  1.000000E-35
  3.200323E+04  1.000000E-35  1.000000E-35
  3.349176E+04  1.000000E-35  1.000000E-35
  3.498028E+04  1.000000E-35  1.000000E-35
  3.646880E+04  1.000000E-35  1.000000E-35
  3.795732E+04  1.000000E-35  1.000000E-35
  3.944585E+04  1.000000E-35  1.000000E-35
  4.093437E+04  1.000000E-35  1.000000E-35
  4.242289E+04  1.000000E-35  1.000000E-35
  4.391141E+04  1.000000E-35  1.000000E-35
  4.539994E+04  1.000000E-35  1.000000E-35
  4.688846E+04  1.343614E-08  2.850208E-08
  4.837698E+04  1.000000E-35  1.000000E-35
  4.986550E+04  2.015421E-08  3.490760E-08
  5.135403E+04  1.343614E-08  2.850208E-08
  5.284255E+04  1.343614E-08  2.850208E-08
  5.433107E+04  2.687228E-08  4.030762E-08
  5.581959E+04  6.046264E-08  6.045992E-08
  5.730812E+04  2.687228E-08  4.030762E-08
  5.879664E+04  6.852433E-06  6.403828E-07
```

Figure 11.4.: Output file listing of a simulation of an ^{241}Am point source

12. Radioactive sources

12.1. Activity reference sources

The point source used for energy calibration is a ^{152}Eu point source. It was manufactured by Physikalisch-Technische Prüfanstalt (PTB) in Germany. It is a traceable secondary standard. The sources used for establishing the detector parameters are also calibrated and traceable secondary standards manufactured by PTB. The certificates are shown in the annex. Figure 12.1 shows a photograph of some of the used point sources.

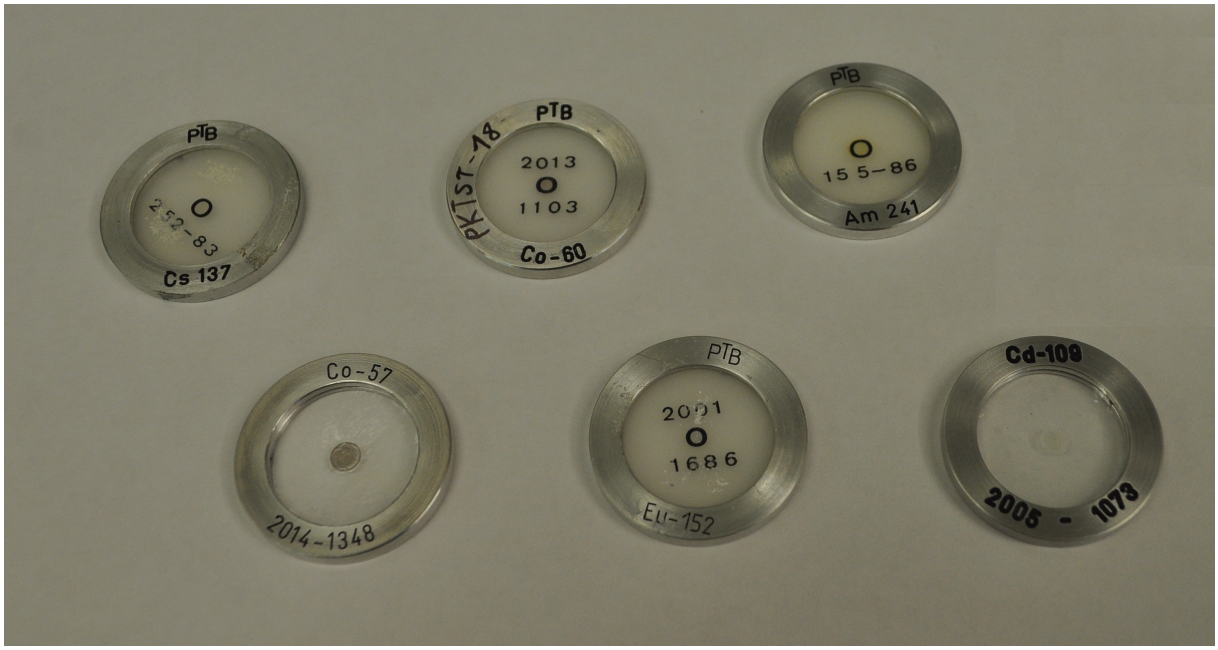

Figure 12.1.: Point sources used for energy calibration and establishing the detector parameters

For the peak-to-total calibration a peak-to-total calibration source set was purchased from Canberra Industries. It contains ^{109}Cd, ^{57}Co, ^{113}Sn, ^{137}Cs, ^{54}Mn and ^{65}Zn point sources. It was manufactured by Spectrum Techniques. Figure 12.2 shows a photograph of the used peak-to-total calibration sources. For these sources, traceability is not necessary as they are only used to perform relative measurements.

For the efficiency calibrations the virtual calibration software ISOCS/LabSOCS was used.

Figure 12.2.: Peak-to-total calibration source set

Geometry composer reports are given in the annex.

12.2. EMRP MetroMETAL Sources

12.2.1. VUHZ No. 002

The sample VUHZ No. 002 is a homogeneous cast steel cylinder without cover or container. Figure 12.3 shows a photograph of the sample. The elemental composition of VUHZ No. 002 is shown in table 12.1.

Source parameters:

- mass 75.25 g
- radius 1.743 cm
- height 1.003 cm
- density 7.745 g/cm^3

Element	Weight fraction (%)	Element	Weight fraction (%)
Al	0.04	Mn	0.30
C	0.16	Ni	0.16
Cr	0.20	Mo	0.03
Cu	0.20	P	0.02
Co	0.01	S	0.05
Fe	98.62	Si	0.21

Table 12.1.: Elemental composition of stainless steel used in VUHZ Nr. 002 [46]

Figure 12.3.: VUHZ No. 002 sample

12.2.2. SK hFD ID03

The sample SK hFD ID03 is made from a homogeneous cylinder of pressed fume dust inside a container. Figure 12.4 shows a photograph of the sample. The elemental composition of the fume dust sample is shown in table 12.2.

Source parameters:

- mass 50.20 g
- height in the container 1.872 cm
- density 0.707 g/cm^3

Container parameters:

- outer radius 3.575 cm
- side wall thickness 0.100 cm
- total outer height 4.650 cm
- bottom thickness 0.100 cm
- top thickness 0.100 cm
- container material polypropylene (C_3H_{6x})
- density container material 0.90 g/cm^3

Element	Weight fraction (%)	Element	Weight fraction (%)
Al	0.05	Ni	0.0083
Br	0.33	O	22.587
C	1.52	P	0.0043
Ca	0.013	Pb	0.6
Cd	0.027	Sb	0.053
Cl	0.2	Si	0.083
Fe	1.5	Zn	73
Mn	0.024		

Table 12.2.: Elemental composition of fume dust used in SK hFD ID03 [46]

12.2.3. ^{226}Ra_HSlag13

The sample ^{226}Ra_HSlag13 is made from a homogeneous cylinder of pressed slag inside a container. Figure 12.5 shows a photograph of the sample. The elemental composition of the fume dust sample is shown in table 12.3.

Source parameters:

- mass 160.60 g
- height in the container 1.805 cm

Figure 12.4.: Fume dust sample SK hFD ID03

- density 2.185 g/cm^3

Container parameters:

- outer radius 3.770 cm
- side wall thickness 0.170 cm
- total outer height 3.000 cm
- bottom thickness 0.116 cm
- top thickness 0.116 cm
- container material polypropylene (C_3H_{6x})
- density container material 0.90 g/cm^3

Element	Weight fraction (%)	Element	Weight fraction (%)
Al	3.15	Mn	5.62
C	0.34	Mg	0.97
Ca	12.75	O	37.28
Cr	1.94	Ti	0.75
H	0.52	Si	6.90
Fe	29.78		

Table 12.3.: Elemental composition of slag used in ^{226}Ra_HSlag13 [46]

Figure 12.5.: Slag sample ^{226}Ra_HSlag13

12.3. Environmental Samples

Ongoing measurements of environmental samples are necessary in order to establish a baseline of typical radionuclide concentration. This baseline can be used to compare results to after a radiation accident, understand natural processes, etc. The concentration values may still vary depending on rainfall, flooding or drought but usually only within a certain range.

In the period of November 2013 to August 2014 sediment samples were taken from the hydroelectric power plants Wallsee-Mitterkirchen (located on the border between Upper and Lower Austria) and Ottensheim-Wilhering (Upper Austria). Figure 12.6 shows both places on the map. Both power plants are located on the Danube river and provide part of Austria's electricity. The sediments were collected from the filtering reservoir located upstream of the turbines. Figures 12.7 and 12.8 show schematic views of the power plants.

Figure 12.6.: Positions of hydroelectric power plants Wallsee-Mitterkirchen (left) and Ottensheim-Wilhering (right) [47]

Table 12.4 shows the calculation of the elemental composition of the sediment determined using composition data provided by Kralik and Augustin-Gyurits [48] and information on the geological structures collected by the RRUFF project [49]. Kralik and Augustin-Gyurits mention a fraction of 3.4 % organic material. This share was included using the composition of the IAEA ICRU sphere.

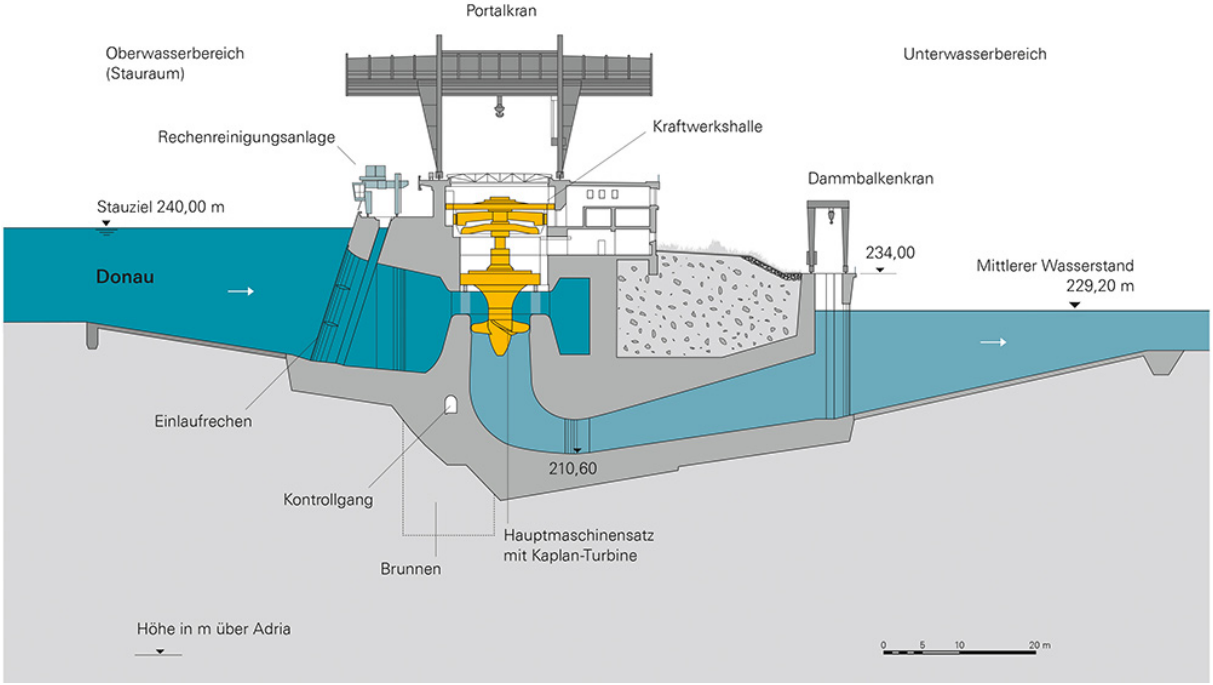

Figure 12.7.: Schematic view of hydroelectric powerplant Wallsee-Mitterkirchen [50]

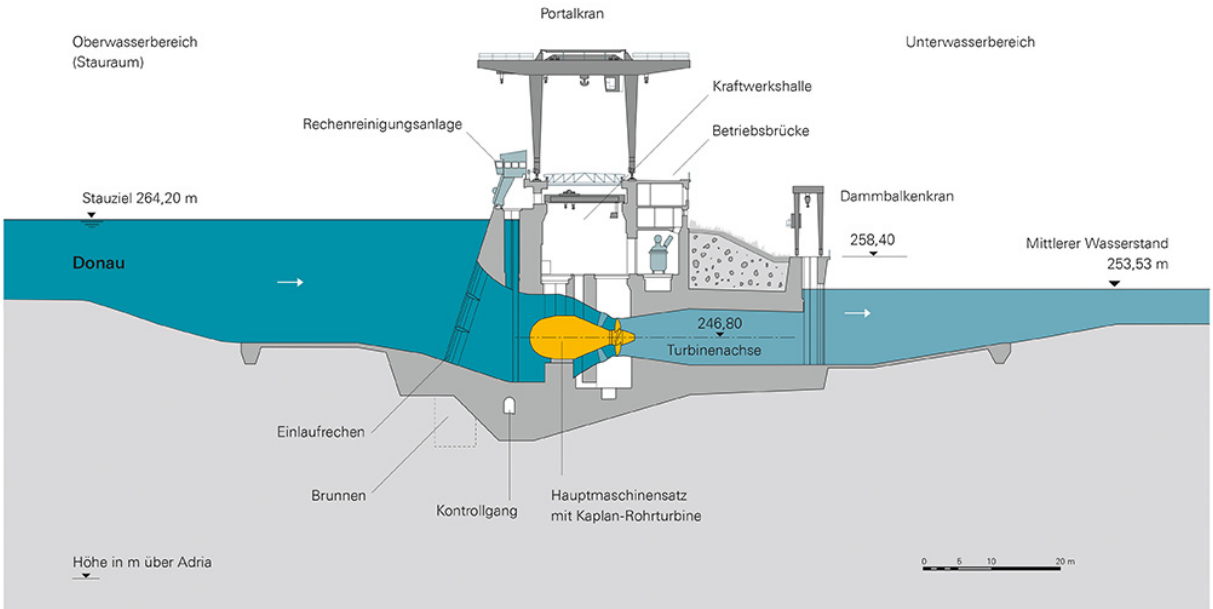

Figure 12.8.: Schematic view of hydroelectric powerplant Ottensheim-Wilhering [51]

Element	Weight fraction (%)	Element	Weight fraction (%)
O	46.75	Ba	2.38
Si	19.02	Mg	2.56
Ca	7.70	Sr	1.63
Al	7.24	H	0.88
Fe	4.93	Na	0.43
C	3.13	N	0.35
K	2.79	B	0.20

Table 12.4.: Calculated average elemental composition of Danube sediments in Austria

Part III.

Results & discussion

13. Detector calibration

This section shows the results of the detector calibration as described above.

Energy calibration was performed measuring a ^{152}Eu point source positioned in the centre of the end cap. The resulting energy calibration curve is shown in figure 13.1.

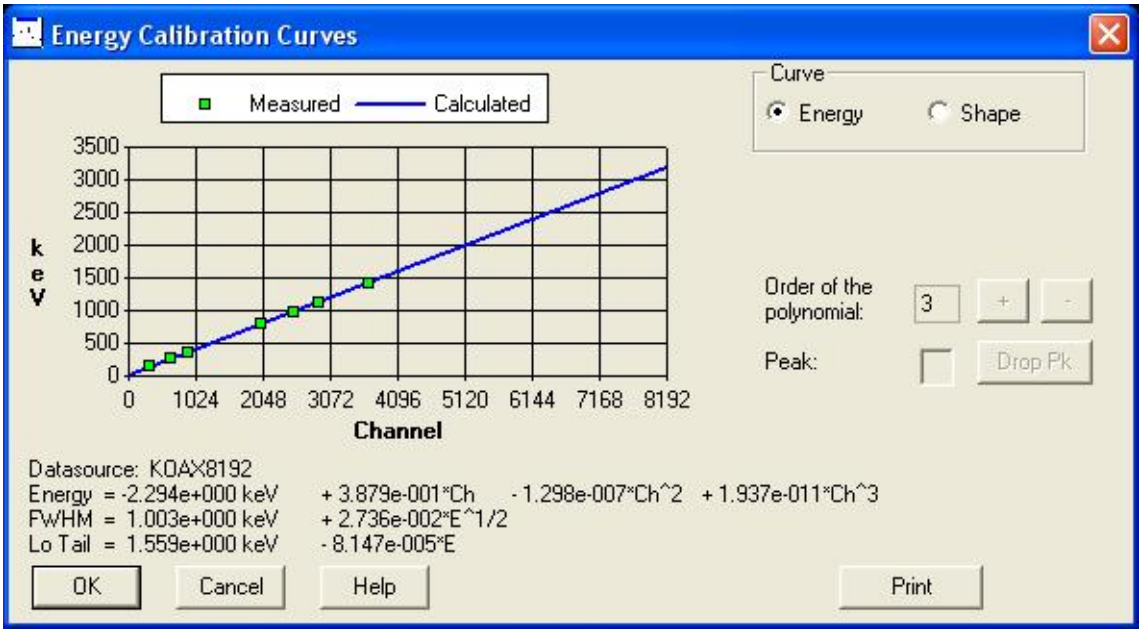

Figure 13.1.: Energy calibration curve of Seibersdorf detector

In order to figure out the influence of attenuating material between the calibration sources and the end cap peak-to-total calibration has been performed without any attenuating layers and with 1 cm high cylinders made from steel, aluminium and brass. Measurements were performed with the cylinder or point source positioned on axis and directly on as well 4.55 cm above the end cap.

Cylinder characterization

Steel cylinder

- Height: 1 cm
- Diameter: 4.1 cm

Aluminium cylinder

- Height: 1 cm
- Diameter: 4.0 cm

Brass cylinder

- Height: 1 cm
- Diameter: 4.0 cm

Figures 13.2, 13.3, 13.4 13.5 and 13.6 show the peak-to-total efficiency calibration curves of the Seibersdorf detector using the set of single-line emitters described above. The sources and attenuators were positioned on axis and directly on top of or 4.55 cm above the end cap respectively.

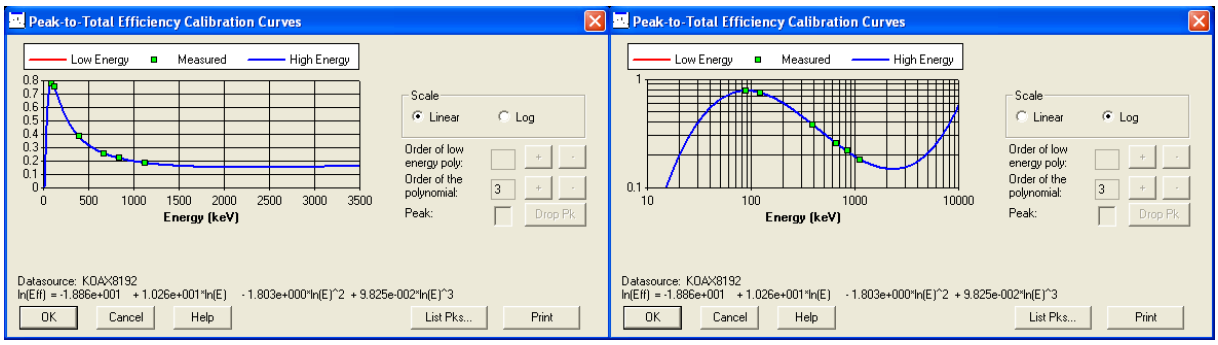

Figure 13.2.: Peak-to-total efficiency calibration curve of Seibersdorf detector using single-line emitters positioned on axis and directly on top of the end cap. No additional attenuating material was used. Left: linear calibration curve, right: log calibration curve

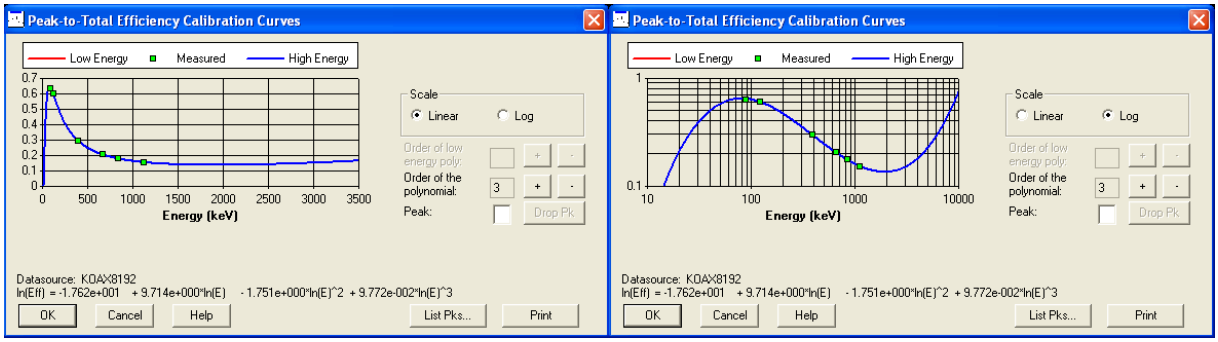

Figure 13.3.: Peak-to-total efficiency calibration curve of Seibersdorf detector using single-line emitters positioned on axis and directly on top of the end cap. Attenuator: Aluminium cylinder. Left: linear calibration curve, right: log calibration curve

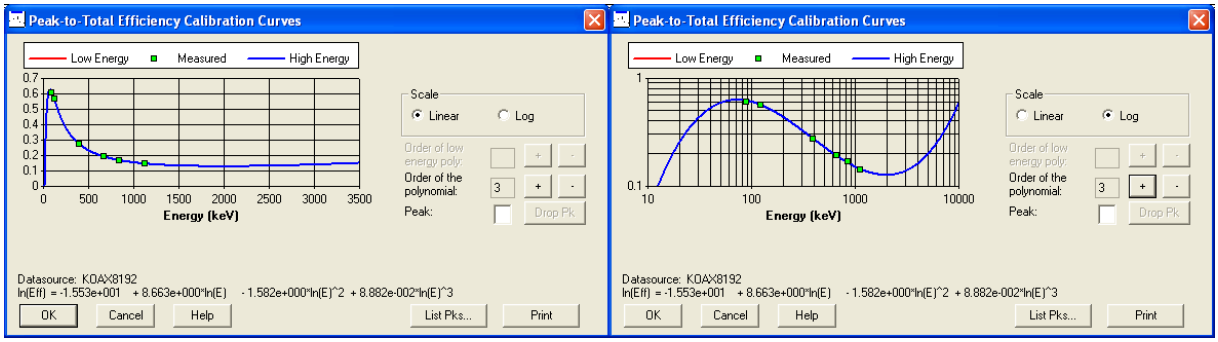

Figure 13.4.: Peak-to-total efficiency calibration curve of Seibersdorf detector using single-line emitters positioned on axis and 4.55 cm above the end cap. Attenuator: Aluminium cylinder. Left: linear calibration curve, right: log calibration curve

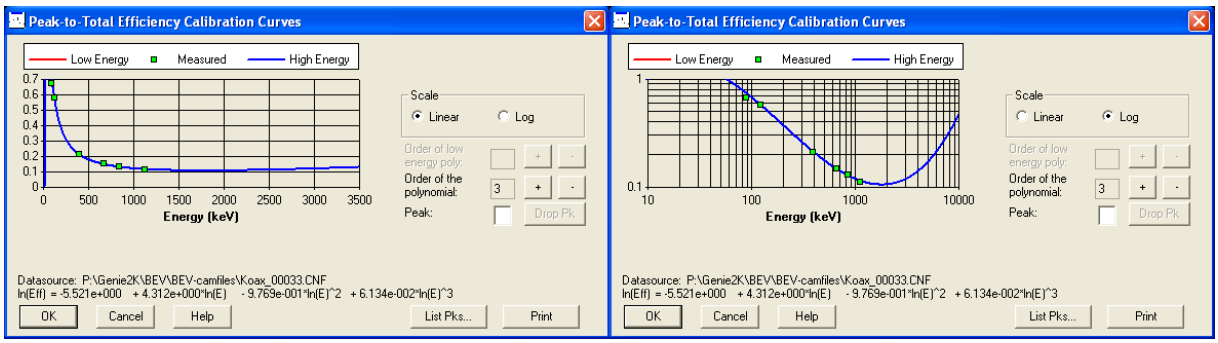

Figure 13.5.: Peak-to-total efficiency calibration curve of Seibersdorf detector using single-line emitters positioned on axis and directly on top of the end cap. Attenuator: Steel cylinder. Left: linear calibration curve, right: log calibration curve

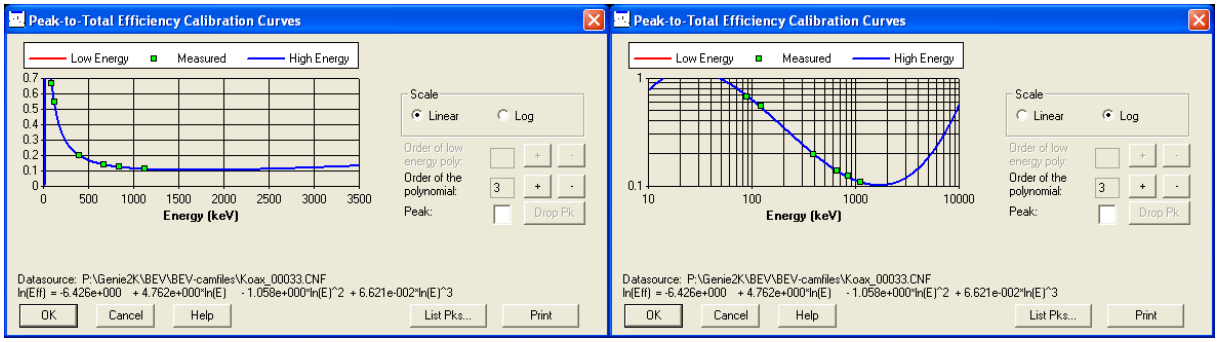

Figure 13.6.: Peak-to-total efficiency calibration curve of Seibersdorf detector using single-line emitters positioned on axis and 4.55 cm above the end cap. Attenuator: Steel cylinder. Left: linear calibration curve, right: log calibration curve

Comparison of the curves shows that the variation of attenuation material causes massive change in the peak-to-total efficiency calibration curve while the source positioning along the z-axis causes only minimal changes. This is expected as air is of very low density. Therefore, the amount of air between the sample and the detector impacts the resulting calibration curve only minimally compared to higher-density materials such as various metals.

The result of the measurement using the brass cylinder is not shown in here since no usable results could be obtained even after a long measuring time as brass, due to its high density of approximately 8.5 g/cm^3 is a highly effective attenuator.

14. Detector image calibration

The following tables show the calibration results of the detector image. As stated in the "materials & methods" section in the course of this work it became obvious that the physical dimensions of the detector provided by the manufacturer are inadequate for the purposes of Monte Carlo simulation. Table 14.1 and table 14.2 show the results of the Seibersdorf and Arsenal detectors obtained using manufacturer data only. The results of the Arsenal detector were obtained with the nearest possible position to the detector end cap. The results of the Seibersdorf detector were obtained with a sample-to-end cap distance of 4.55 cm. The errors are quoted at k=1. In both cases traceable point sources were used. The relatively high uncertainty values at the Seibersdorf detector can be explained by the low detection efficiency created by the used detector-sample geometry.

Since it was defined that only deviations in activity or peak efficiency of under 5 % are viewed as adequate it is obvious that the information provided by the manufacturer is not accurate enough.

Table 14.3 shows the results of simulations using the adapted detector properties of the Seibersdorf detector obtained by deploying the method described in the "materials & methods" section.

Parameters such as crystal diameter and length, distance of crystal to end cap, front and side dead layer thickness proved to have a significant impact on the simulation results whereas dimensions of the hole, hole dead layer thickness of the aluminium end cap, physical dimensions of the mounting had less impact on the simulation and where therefore kept at the nominal value or neglected completely.

As can be seen the results have improved drastically. Table 14.4 shows the adapted physical properties used in the simulation.

	A Arsenal detector (Bq)	ΔA/A Arsenal detector (%)	A source certificate (Bq)	ΔA/A source certificate (%)	difference (%) certificate vs. simulation
^{241}Am	1666.60	0.73	958.33	1.02	73.91
^{137}Cs	14004.14	0.42	16824.39	0.58	-16.76
^{60}Co	2150.53	0.86	1251.96	0.39	71.77

Table 14.1.: Results of simulation of Arsenal detector using physical dimensions provided by the manufacturer

	A Seibersdorf detector (Bq)	ΔA/A Seibersdorf detector (%)	A source certificate (Bq)	ΔA/A source certificate (%)	difference (%) certificate vs. simulation
^{241}Am	27523.23	2.57	42725.59	0.58	-35.58
^{137}Cs	12642.30	8.20	16699.71	0.58	-24.30
^{60}Co	54169.65	17.48	37224.85	0.23	45.52

Table 14.2.: Results of simulation of Seibersdorf detector using physical dimensions provided by the manufacturer

	A Seibersdorf detector (Bq)	ΔA/A Seibersdorf detector (%)	A source certificate (Bq)	ΔA/A source certificate (%)	difference (%) certificate vs. simulation
^{241}Am	42064.67	3.16	42721.98	0.58	-1.54
^{57}Co	100993.82	2.03	97081.17	0.57	4.03
^{109}Cd	263.03	7.86	272.87	0.85	-3.61
^{137}Cs	16292.31	3.67	16699.71	0.58	-2.44
^{60}Co	37162.19	4.85	37224.85	0.27	-0.17

Table 14.3.: Results of simulation of Seibersdorf detector using adapted physical dimensions

	Nominal value	Adapted value
Distance end cap to crystal	5.00 mm	9.40 mm
Crystal diameter	56.00 mm	55.84 mm
Crystal length	54.00 mm	52.92 mm
Dead layer front	1.00 mm	1.30 mm
Dead layer side	1.00 mm	1.60 mm
Hole diameter	10.50 mm	10.50 mm
Hole length	38.00 mm	36.92 mm
Dead layer hole	0.30 μm	0.00 μm

Table 14.4.: Physical dimensions of the Seibersdorf detector provided by the manufacturer vs. adapted

15. Results for MetroMETAL samples

Since the detector image was calibrated using only point sources the voluminous MetroMETAL sources were used to test the model and evaluate the use of the code for samples with non-negligible self absorption as found in real-life samples.

As stated in the summary report for Project IND04 MetroMETAL Ionising Radiation Metrology for the Metallurgical Industry the "development of reference standards for composite steel, cast steel, slag and fume dust containing a known activity of some radionuclides (^{60}Co, ^{137}Cs, ^{192}Ir, ^{226}Ra and ^{241}Am) considered as potential contaminants" that are "prepared in geometries/matrices that match the industrial environments for which they are designed" is a goal. [1] Prototypes of those standards were sent to the participating partners for evaluation. Part of the tasks was to simulate peak efficiency and compare it to the experimentally found values.

The results of the laboratory comparisons were submitted to Radiation Physics and Chemistry. The manuscript on fume dust can be found in the annex. [52]

The results show good agreement with the values of the intercomparison (see table 15.1). Comparison of peak efficiencies calculated by LabSOCS and PENELOPE (see table 15.2) also show good agreement except a larger discrepancy of about 6 % at the ^{226}Ra sample. This goes hand in hand with the fact that LabSOCS understated the a activity of ^{226}Ra in the sample by approximately 5 %. The reason for this could be a combination of insufficient data regarding the knowledge of the physical values of the source and limits to the input options of the geometry composer. Figure 15.1 shows the results of the participating laboratories.

	a simulation (Bq/g)	Δa/a simulation (%)	a intercomparison (Bq/g)	Δa/a intercomparison (%)	difference (%) intercomparison vs. simulation
VUHZ Nr. 002 (^{60}Co)	1.50	1.13	1.48	1.48	1.35
SK hFD ID03 (^{137}Cs)	9.59	4.84	9.58	1.46	0.10
^{226}Ra_HSlag13 (^{226}Ra)	9.91	5.83	9.72	0.90	1.29

Table 15.1.: Results of simulation of Seibersdorf detector using adapted physical dimensions

	ϵ PENELOPE 2011	$\Delta\epsilon/\epsilon$ PENELOPE 2011 (%)	ϵ LABSOCS	$\Delta\epsilon/\epsilon$ LABSOCS (%)	difference (%) LABSOCS vs. PENELOPE 2011
VUHZ Nr. 002 1173 keV (^{60}Co)	3.39E-3	5.42	3.39E-3	3.01	0.00
VUHZ Nr. 002 1332 keV (^{60}Co)	2.99E-3	5.77	3.11E-3	3.10	-3.86
SK hFD ID03 (^{137}Cs)	5.23E-3	4.36	5.12E-3	3.55	2.15
^{226}Ra_HSlag13 (^{226}Ra)	1.28E-2	0.00	1.21E-2	5.86	6.12

Table 15.2.: Results of simulation of Seibersdorf detector using adapted physical dimensions

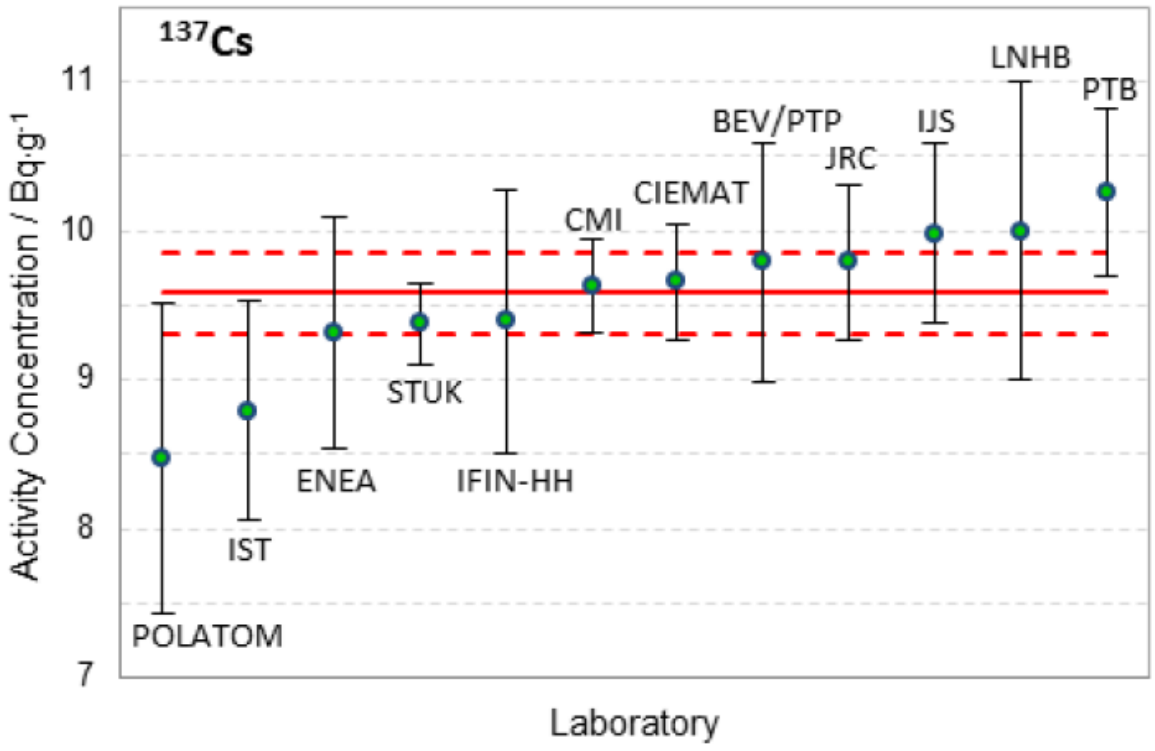

Figure 15.1.: Laboratory results for ^{137}Cs concentration in fume dust samples. BEV's results were obtained using LabSOCS only [52]

16. Results of Environmental samples

The Danube sediment samples were measured using the Seibersdorf detector and evaluated using LabSOCS.

Tables 16.1 - 16.5 show the results of the Danube power plant Wallsee-Mitterkirchen sediment samples for ^{40}K, ^{137}Cs, ^{228}Th, ^{226}Ra and ^{228}Ra. Due to the advanced age of the detector, limited measuring time and low γ-ray energy it was not possible to consistently analyse ^{210}Pb.

Tables Tables 16.6 - 16.10 show the results for the Danube power plant Ottensheim-Wilhering sediment samples.

Figures 16.1 - 16.10 show the development of the individual radionuclides over the course of the evaluation period.

In case of flooding more than one sample per month was taken. Some months there was no or not enough material to analyse due to environmental or maintenance processes.

The results show very high statistical uncertainties. The photo peaks barely rise above the Compton continuum. Some radionuclides, such as ^{210}Pb could not be identified in most of the samples. This is due to the fact that only poor shielding and little measuring time of approximately three days per sample was available at the Seibersdorf laboratory. Additionally, the relatively thick dead layer prevents the detection of low-energy photons. Still, the results are consistent with those of previous years, especially considering the assigned uncertainties.

The concentrations of ^{228}Ra and ^{22}Th mirror each other which is not surprising since ^{228}Th is a daughter of ^{228}Ra.

Sample acquisition date	Sample code	Nuclide	Activity (Bq/kg)	uncertainty (Bq/kg)
14.11.2013	B-010185	^{40}K	5.81E2	4.46E1
11.12.2013	B-010187	^{40}K	5.77E2	5.12E1
14.01.2014	B-010183	^{40}K	5.34E2	5.21E1
11.02.2014	B-010189	^{40}K	5.53E2	9.34E1
11.03.2014	B-010188	^{40}K	5.69E2	5.95E1
15.04.2014	B-010190	^{40}K	5.74E2	4.53E1
13.05.2014	B-010186	^{40}K	4.74E2	2.21E1
16.05.2014	B-010179	^{40}K	6.74E2	1.41E2
28.05.2014	B-010181	^{40}K	6.07E2	7.93E1
11.06.2014	B-010178	^{40}K	5.07E2	6.32E1
15.07.2014	B-010195	^{40}K	not enough material for evaluation available	
31.07.2014	B-010192	^{40}K	5.82E2	4.18E1
12.08.2014	B-010193	^{40}K	6.91E2	4.54E1
21.08.2014	B-010182	^{40}K	6.85E2	4.38E1

Table 16.1.: Results for ^{40}K of sediments taken in hydroelectric power plant Wallsee-Mitterkirchen in 2013/2014

Sample acquisition date	Sample code	Nuclide	Activity (Bq/kg)	uncertainty (Bq/kg)
14.11.2013	B-010185	^{137}Cs	4.11E1	3.26E0
11.12.2013	B-010187	^{137}Cs	3.96E1	4.23E0
14.01.2014	B-010183	^{137}Cs	4.02E1	2.41E0
11.02.2014	B-010189	^{137}Cs	4.26E1	2.37E0
11.03.2014	B-010188	^{137}Cs	3.54E1	1.68E0
15.04.2014	B-010190	^{137}Cs	3.31E1	1.36E0
13.05.2014	B-010186	^{137}Cs	3.54E1	1.80E0
16.05.2014	B-010179	^{137}Cs	3.23E1	3.05E0
28.05.2014	B-010181	^{137}Cs	3.11E1	7.56E0
11.06.2014	B-010178	^{137}Cs	3.36E1	1.87E0
15.07.2014	B-010195	^{137}Cs	not enough material for evaluation available	
31.07.2014	B-010192	^{137}Cs	3.03E1	2.92E0
12.08.2014	B-010193	^{137}Cs	2.49E1	1.26E0
21.08.2014	B-010182	^{137}Cs	1.7E1	9.13E-1

Table 16.2.: Results for ^{137}Cs of sediments taken in hydroelectric power plant Wallsee-Mitterkirchen

Sample acquisition date	Sample code	Nuclide	Activity (Bq/kg)	uncertainty (Bq/kg)
14.11.2013	B-010185	^{228}Th	4.36E1	4.29E0
11.12.2013	B-010187	^{228}Th	4.77E1	6.92E0
14.01.2014	B-010183	^{228}Th	6.60E1	1.04E1
11.02.2014	B-010189	^{228}Th	5.75E1	1.14E1
11.03.2014	B-010188	^{228}Th	4.87E1	7.94E0
15.04.2014	B-010190	^{228}Th	3.92E1	4.42E0
13.05.2014	B-010186	^{228}Th	4.86E1	6.85E0
16.05.2014	B-010179	^{228}Th	5.86E1	1.66E1
28.05.2014	B-010181	^{228}Th	5.08E1	3.25E0
11.06.2014	B-010178	^{228}Th	4.18E1	6.69E0
15.07.2014	B-010195	^{228}Th	not enough material for evaluation available	
31.07.2014	B-010192	^{228}Th	3.70E1	3.66E0
12.08.2014	B-010193	^{228}Th	5.68E1	6.30E0
21.08.2014	B-010182	^{228}Th	5.27E1	3.87E0

Table 16.3.: Results for ^{228}Th of sediments taken in hydroelectric power plant Wallsee-Mitterkirchen in 2013/2014

Sample acquisition date	Sample code	Nuclide	Activity (Bq/kg)	uncertainty (Bq/kg)
14.11.2013	B-010185	^{226}Ra	5.01E1	4.31E0
11.12.2013	B-010187	^{226}Ra	4.48E1	3.59E0
14.01.2014	B-010183	^{226}Ra	3.43E1	8.86E0
11.02.2014	B-010189	^{226}Ra	3.65E1	1.01E1
11.03.2014	B-010188	^{226}Ra	3.54E1	5.92E0
15.04.2014	B-010190	^{226}Ra	4.06E1	4.88E0
13.05.2014	B-010186	^{226}Ra	4.39E1	8.39E0
16.05.2014	B-010179	^{226}Ra	2.05E1	1.30E1
28.05.2014	B-010181	^{226}Ra	5.39E1	8.19E0
11.06.2014	B-010178	^{226}Ra	2.66E1	5.85E0
15.07.2014	B-010195	^{226}Ra	not enough material for evaluation available	
31.07.2014	B-010192	^{226}Ra	4.71E1	3.53E0
12.08.2014	B-010193	^{226}Ra	4.88E1	2.98E0
21.08.2014	B-010182	^{226}Ra	4.59E1	9.30E0

Table 16.4.: Results for ^{226}Ra of sediments taken in hydroelectric power plant Wallsee-Mitterkirchen in 2013/2014

Sample acquisition date	Sample code	Nuclide	Activity (Bq/kg)	uncertainty (Bq/kg)
14.11.2013	B-010185	^{228}Ra	3.68E1	4.34E0
11.12.2013	B-010187	^{228}Ra	4.22E1	5.28E0
14.01.2014	B-010183	^{228}Ra	5.87E1	7.87E0
11.02.2014	B-010189	^{228}Ra	5.63E1	1.90E1
11.03.2014	B-010188	^{228}Ra	5.37E1	5.35E0
15.04.2014	B-010190	^{228}Ra	3.56E1	3.33E0
13.05.2014	B-010186	^{228}Ra	5.21E1	4.83E0
16.05.2014	B-010179	^{228}Ra	3.93E1	1.16E1
28.05.2014	B-010181	^{228}Ra	5.27E1	1.48E1
11.06.2014	B-010178	^{228}Ra	3.55E1	6.75E0
15.07.2014	B-010195	^{228}Ra	not enough material for evaluation available	
31.07.2014	B-010192	^{228}Ra	4.014E1	2.72E0
12.08.2014	B-010193	^{228}Ra	4.61E1	5.12E0
21.08.2014	B-010182	^{228}Ra	5.12E1	4.04E0

Table 16.5.: Results for ^{228}Ra of sediments taken in hydroelectric power plant Wallsee-Mitterkirchen in 2013/2014

Sample acquisition date	Sample code	Nuclide	Activity (Bq/kg)	uncertainty (Bq/kg)
14.11.2013	B-01077	^{40}K	4.75E2	3.73E1
18.12.2013	B-01076	^{40}K	4.74E2	2.21E1
14.01.2014	-	^{40}K	no material to collect	
13.02.2014	-	^{40}K	no material to collect	
13.03.2014	-	^{40}K	no material to collect	
14.04.2014	-	^{40}K	no material to collect	
14.05.2014	B-010184	^{40}K	4.80E2	3.52E1
16.06.2014	B-010191	^{40}K	4.98E2	8.45E1
14.07.2014	B-010180	^{40}K	4.95E2	2.77E1
13.08.2014	B-010194	^{40}K	5.57E2	3.58E1

Table 16.6.: Results for ^{40}K of sediments taken in hydroelectric power plant Ottensheim-Wilhering in 2013/2014

Sample acquisition date	Sample code	Nuclide	Activity (Bq/kg)	uncertainty (Bq/kg)
14.11.2013	B-01077	^{137}Cs	8.60E0	6.74E-1
18.12.2013	B-01076	^{137}Cs	1.05E1	1.77E0
14.01.2014	-	^{137}Cs	no material to collect	
13.02.2014	-	^{137}Cs	no material to collect	
13.03.2014	-	^{137}Cs	no material to collect	
14.04.2014	-	^{137}Cs	no material to collect	
14.05.2014	B-010184	^{137}Cs	1.53E1	8.55E-1
16.06.2014	B-010191	^{137}Cs	1.21E1	4.34E0
14.07.2014	B-010180	^{137}Cs	1.15E1	7.58E-1
13.08.2014	B-010194	^{137}Cs	1.34E1	7.42E-1

Table 16.7.: Results for ^{137}Cs of sediments taken in hydroelectric power plant Ottenheim-Wilhering in 2013/2014

Sample acquisition date	Sample code	Nuclide	Activity (Bq/kg)	uncertainty (Bq/kg)
14.11.2013	B-01077	^{228}Th	4.66E1	3.77E0
18.12.2013	B-01076	^{228}Th	4.97E1	4.70E0
14.01.2014	-	^{228}Th	no material to collect	
13.02.2014	-	^{228}Th	no material to collect	
13.03.2014	-	^{228}Th	no material to collect	
14.04.2014	-	^{228}Th	no material to collect	
14.05.2014	B-010184	^{228}Th	4.09E1	3.69E0
16.06.2014	B-010191	^{228}Th	3.65E1	3.83E0
14.07.2014	B-010180	^{228}Th	5.04E1	5.29E0
13.08.2014	B-010194	^{228}Th	4.57E1	3.18E0

Table 16.8.: Results for ^{228}Th of sediments taken in hydroelectric power plant Ottensheim-Wilhering in 2013/2014

Sample acquisition date	Sample code	Nuclide	Activity (Bq/kg)	uncertainty (Bq/kg)
14.11.2013	B-01077	^{226}Ra	3.77E1	2.69E0
18.12.2013	B-01076	^{226}Ra	3.78E1	3.78E0
14.01.2014	-	^{226}Ra	no material to collect	
13.02.2014	-	^{226}Ra	no material to collect	
13.03.2014	-	^{226}Ra	no material to collect	
14.04.2014	-	^{226}Ra	no material to collect	
14.05.2014	B-010184	^{226}Ra	3.64E1	2.20E0
16.06.2014	B-010191	^{226}Ra	3.64E1	5.41E0
14.07.2014	B-010180	^{226}Ra	4.03E1	2.86E0
13.08.2014	B-010194	^{226}Ra	4.20E1	2.23E0

Table 16.9.: Results for ^{226}Ra of sediments taken in hydroelectric power plant Ottensheim-Wilhering in 2013/2014

Sample acquisition date	Sample code	Nuclide	Activity (Bq/kg)	uncertainty (Bq/kg)
14.11.2013	B-01077	^{228}Ra	3.76E1	3.17E0
18.12.2013	B-01076	^{228}Ra	4.09E1	2.63E0
14.01.2014	-	^{228}Ra	no material to collect	
13.02.2014	-	^{228}Ra	no material to collect	
13.03.2014	-	^{228}Ra	no material to collect	
14.04.2014	-	^{228}Ra	no material to collect	
14.05.2014	B-010184	^{228}Ra	4.18E1	2.83E0
16.06.2014	B-010191	^{228}Ra	5.12E1	8.49E0
14.07.2014	B-010180	^{228}Ra	4.66E1	4.98E0
13.08.2014	B-010194	^{228}Ra	3.63E1	2.92E0

Table 16.10.: Results for ^{228}Ra of sediments taken in hydroelectric power plant Ottensheim-Wilhering in 2013/2014

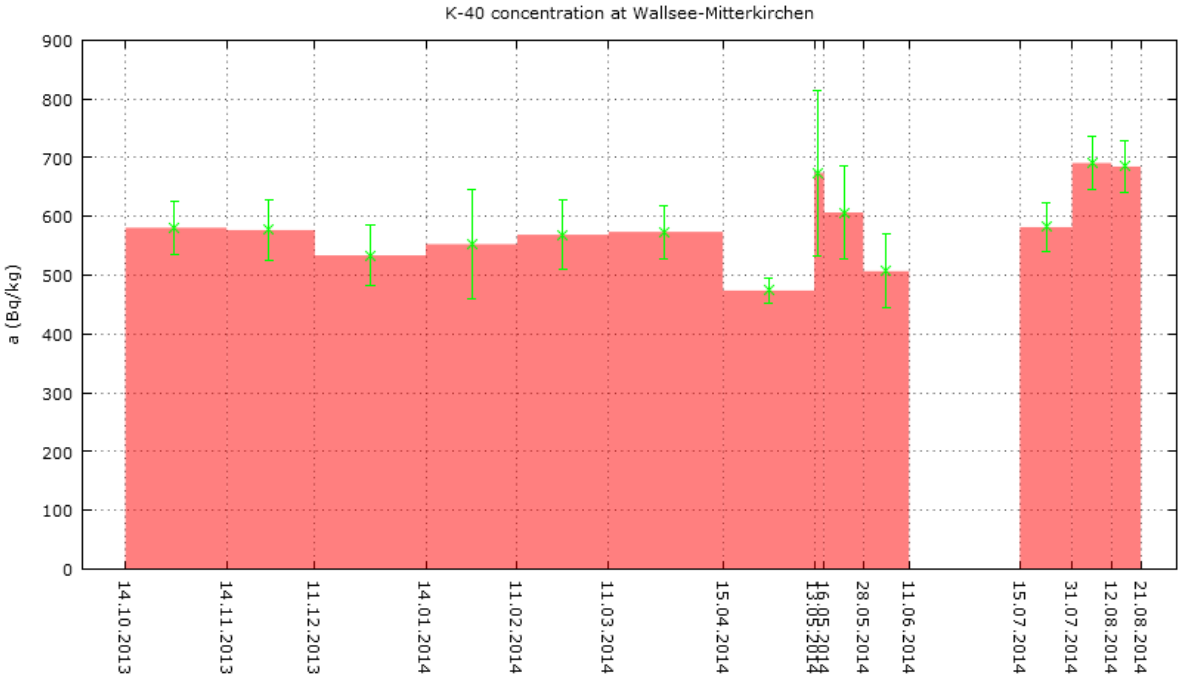

Figure 16.1.: Development of ^{40}K in Danube sediment samples taken at hydroelectric power plant Wallsee-Mitterkirchen in 2013/2014

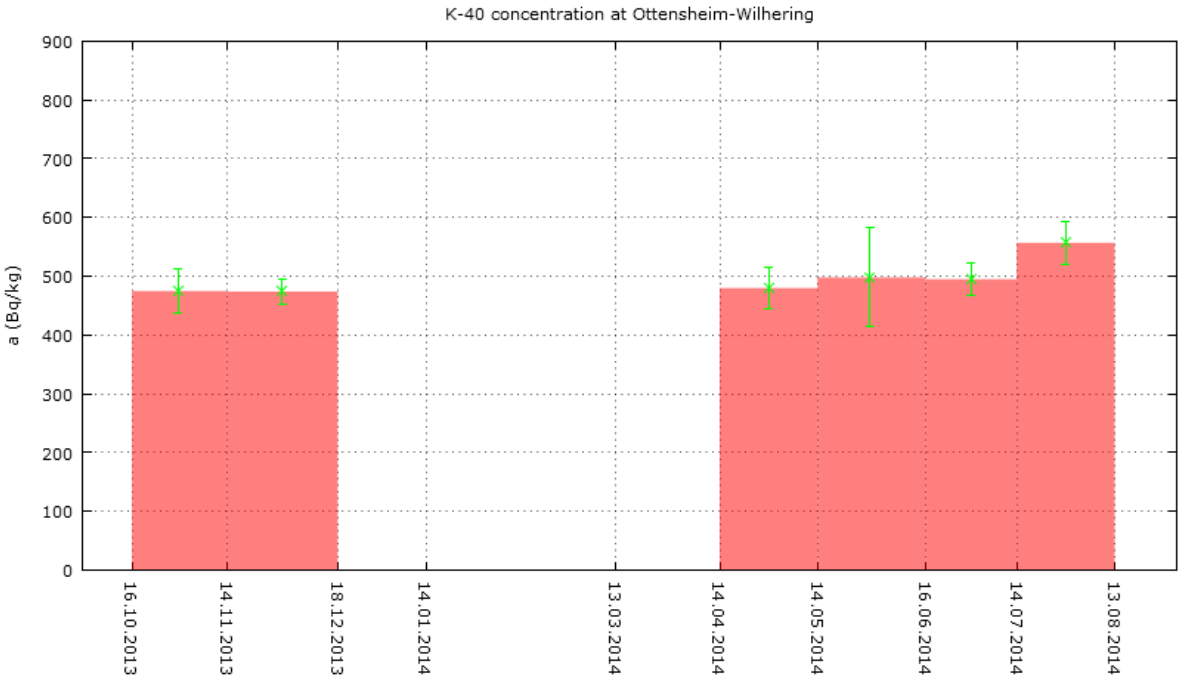

Figure 16.2.: Development of ^{40}K in Danube sediment samples taken at hydroelectric power plant Ottensheim-Wilhering in 2013/2014

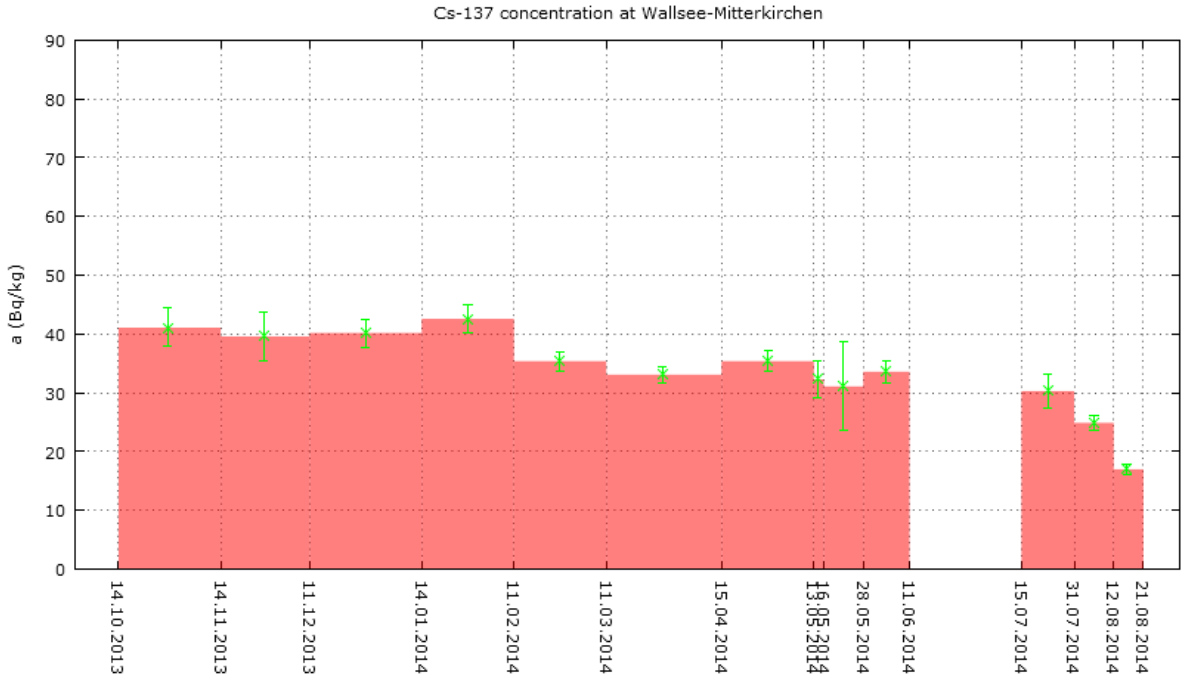

Figure 16.3.: Development of ^{137}Cs in Danube sediment samples taken at hydroelectric power plant Wallsee-Mitterkirchen in 2013/2014

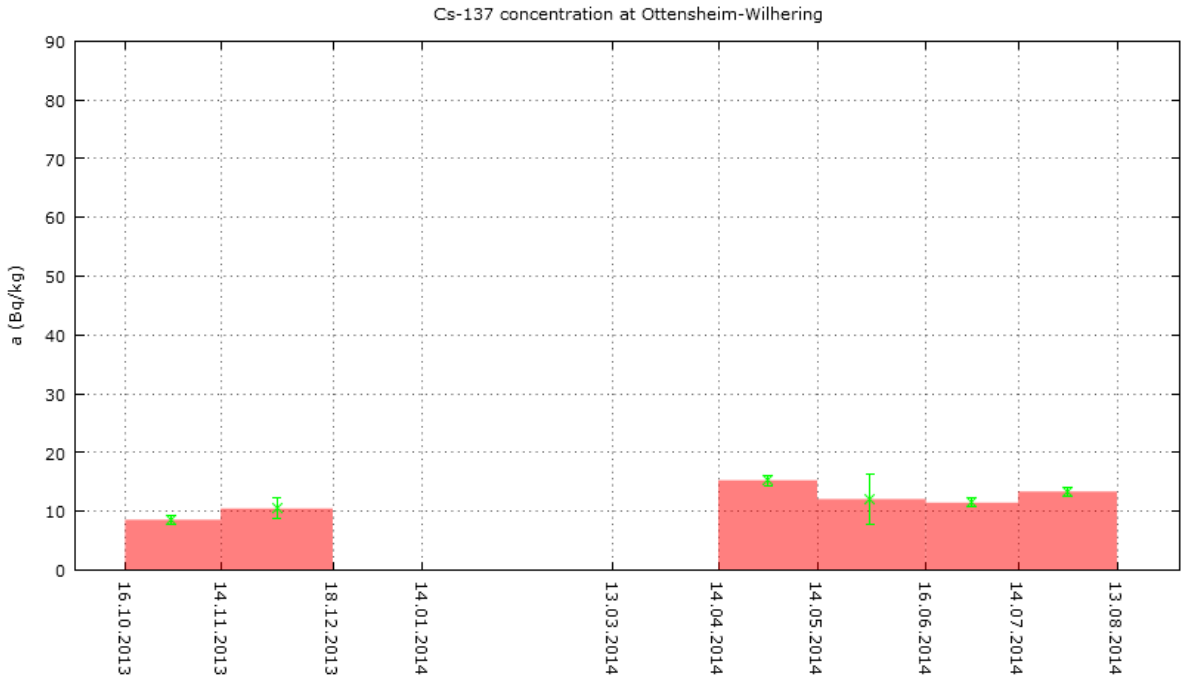

Figure 16.4.: Development of^{137}Cs in Danube sediment samples taken at hydroelectric power plant Ottensheim-Wilhering in 2013/2014

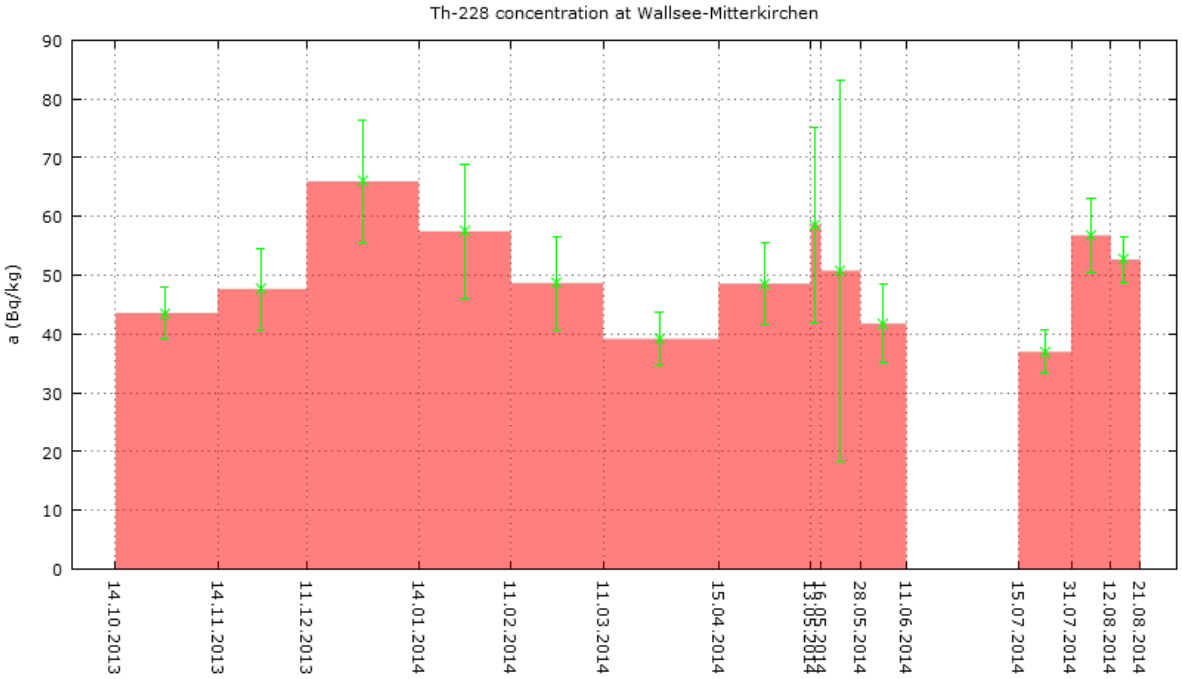

Figure 16.5.: Development of ^{228}Th in Danube sediment samples taken at hydroelectric power plant Wallsee-Mitterkirchen in 2013/2014

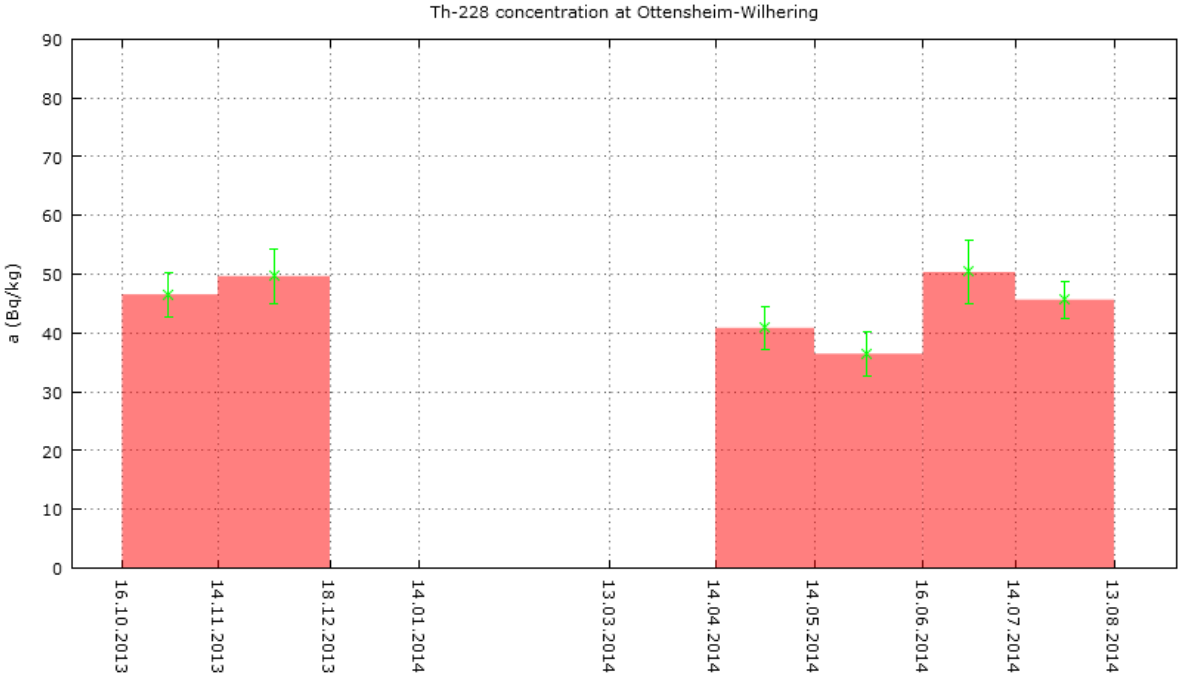

Figure 16.6.: Development of ^{228}Th in Danube sediment samples taken at hydroelectric power plant Ottensheim-Wilhering in 2013/2014

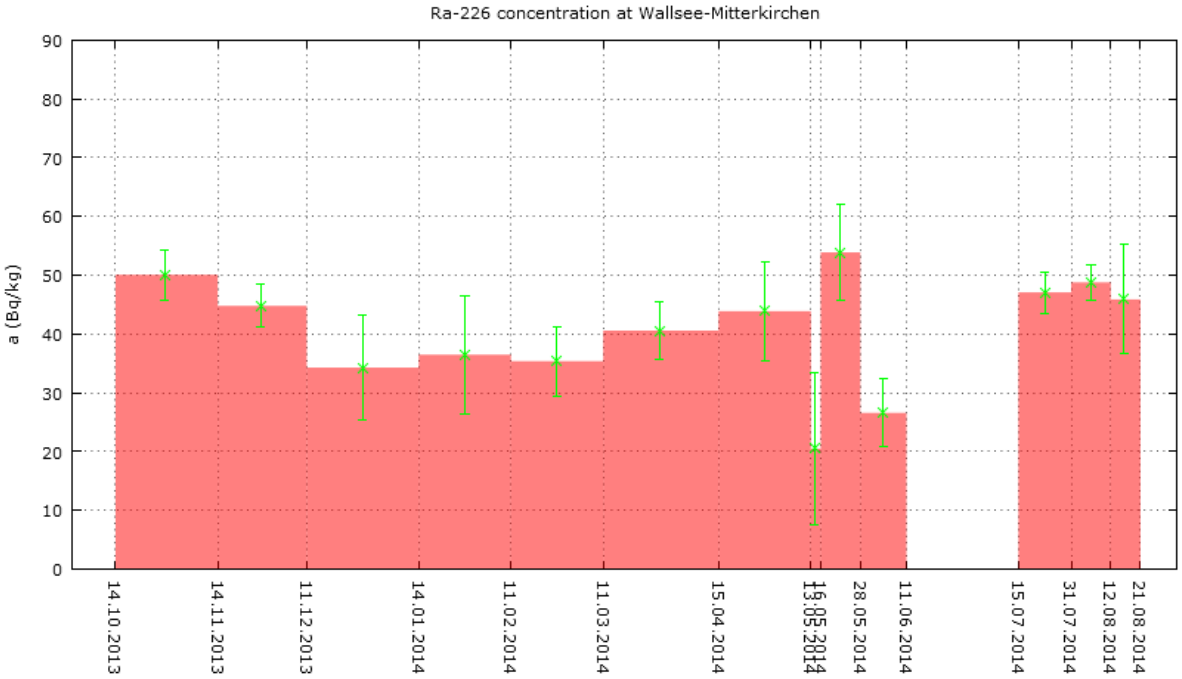

Figure 16.7.: Development of ^{226}Ra in Danube sediment samples taken at hydroelectric power plant Wallsee-Mitterkirchen in 2013/2014

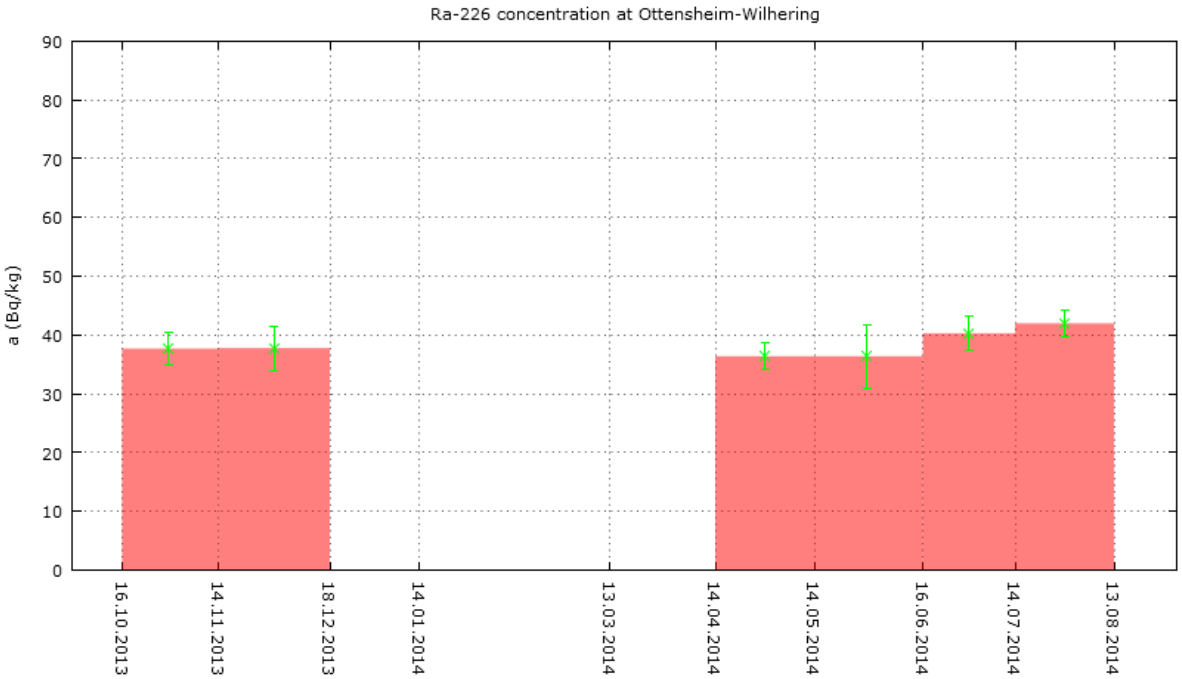

Figure 16.8.: Development of ^{226}Ra in Danube sediment samples taken at hydroelectric power plant Ottensheim-Wilhering in 2013/2014

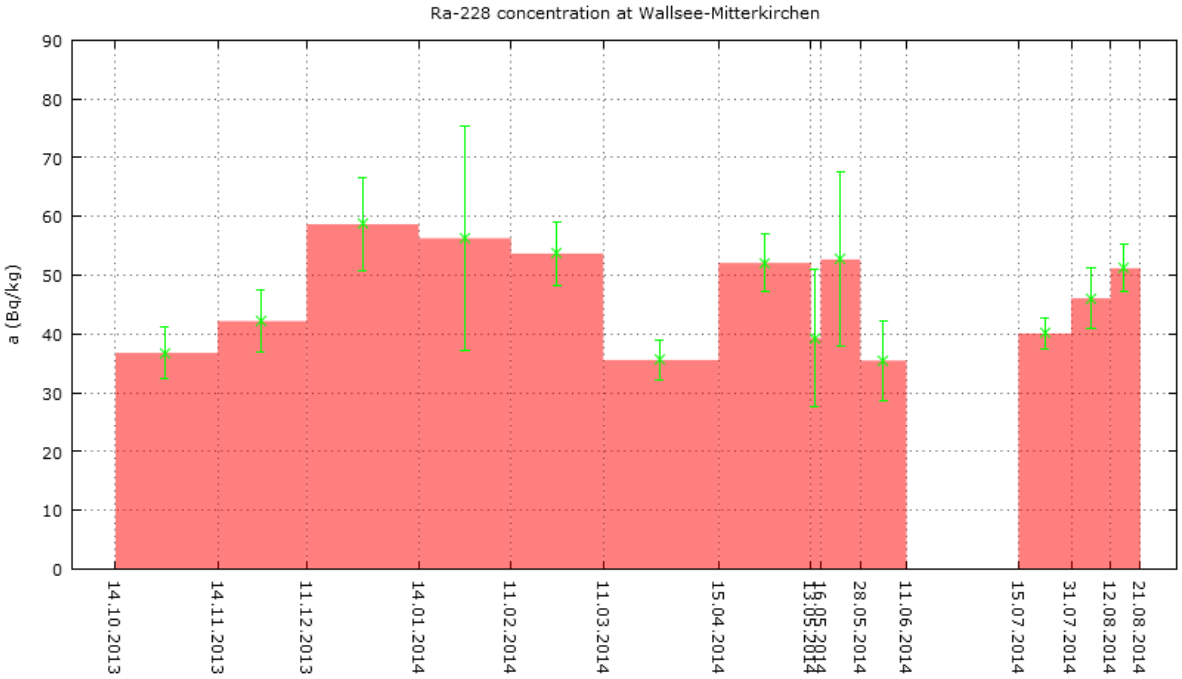

Figure 16.9.: Development of ^{228}Ra in Danube sediment samples taken at hydroelectric power plant Wallsee-Mitterkirchen in 2013/2014

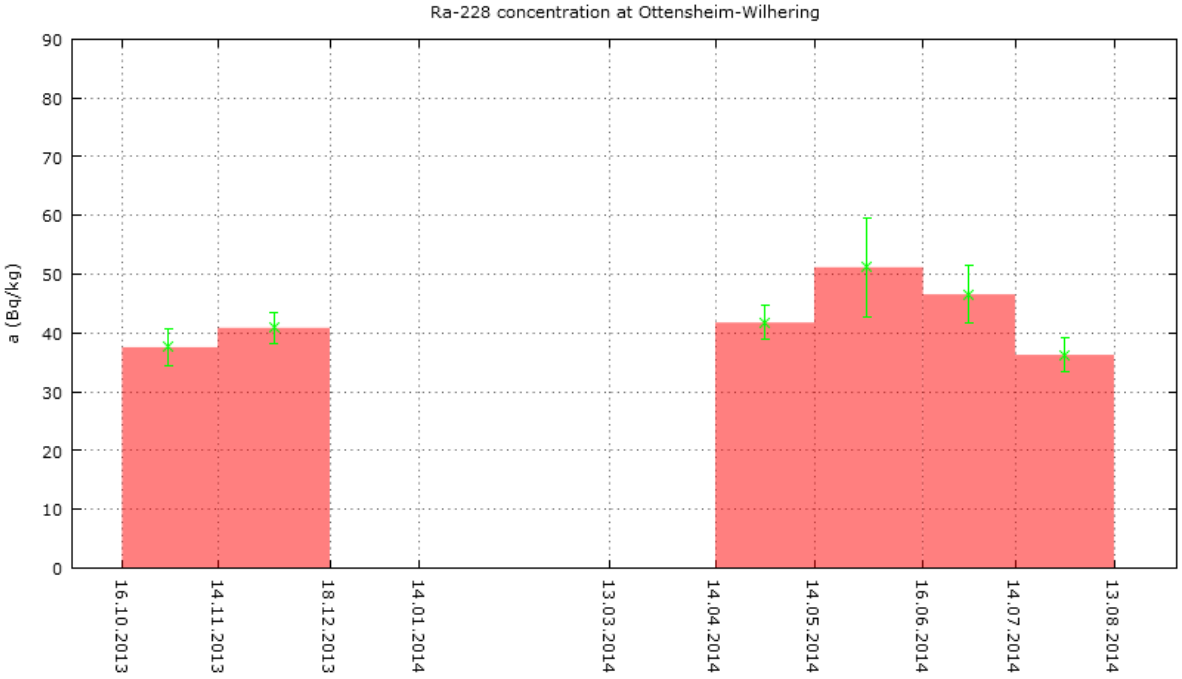

Figure 16.10.: Development of ^{228}Ra in Danube sediment samples taken at hydroelectric power plant Ottensheim-Wilhering in 2013/2014

17. Conclusions

In the course of this work a functioning and validated detector model has been created and tested by comparing simulated peak efficiencies and activities to the experimentally found values of the participating laboratories. The goal of reaching less than 5 % deviation from the experimentally found values could be reached.

Both detectors used in this diploma thesis are from different manufacturers. The big discrepancy of the simulation results of both detectors and the reference samples seems to suggest that generally the detector parameters provided by the manufacturer are less than adequate in order to perform Monte Carlo simulations of radiation transport.

In this work, some of the physical dimensions were kept at the nominal value and others were varied to obtain acceptable results, therefore, it is not possible to gauge if or which of the provided parameters are reliable. The user has to resort to different methods in order to get an acceptable result. One of the methods is described and applied in this work. It can be said with certainty, that the two main parameters influencing the simulation are dead layer thickness and source-to-end cap distance.

It is the opinion of the author that measuring the samples used to determine the dead layer at larger distances from the detector end cap (limited by the shielding) would enhance the applicability of the simulation to a more variable source positioning and improve the overall certainty of the model.

Since wiring and screws are used as little as possible and mostly on the back end of the detector where their impact is not as significant it is possible to neglect their influence on the simulation. That leaves only the dimension of the hole and the dead layers unknown, reducing the number of variables to be figured out significantly.

An important improvement to that procedure would be to obtain reliable data by conducting a radiography of the detector and calculation of the physical properties from the image. Using this method it is the belief of the author that the now obtained deviation of approximately 3 % could be reduced further.

Improved approaches have been shown by other authors but most procedures require a radiography and detailed measurements on every accessible part of the detector end cap

in order to figure out the behaviour of the dead layer. This approach is not feasible for small laboratories with limited resources and/or laboratories with immobile or heavily used detectors.

Comparison of the activity and efficiency values obtained using LabSOCS and PENELOPE 2011 are generally in good agreement. The use of LabSOCS is very convenient and user-friendly but limited in the accuracy with which composition data and sample geometry can be inserted while those parameters can be chosen freely in PENELOPE 2011.

The use of a properly calibrated detector is especially important when measuring low-activity environmental samples. In that respect sediment samples taken at two hydroelectric power plants located on the Danube river are evaluated. The ongoing measurement of environmental samples is necessary to establish a baseline for the amount of activity in nature. This is relevant for many purposes, such as radioecology, dose evaluation, the study of natural processes and the establishment of emergency procedures. For the measurement of environmental sources it is necessary to note the importance of reference standards and shielding. The density and matrix composition of the material is a very relevant factor in the evaluation of the spectra. Discrepancies in the source composition of reference standard and sample can lead to serious over- or underestimation of activity and. Furthermore, 10 cm of lead are insufficient to suppress the background as needed for environmental sources. Long measurement times of approximately three days still lead to high uncertainties.

The relatively high quoted uncertainties could be lowered significantly by a combination of longer measurement time, longer simulation time and better detector shielding.

18. Bibliography

[1] EURAMET. *Publishable JRP Summary Report for IND04 MetroMetal Ionising Radiation Metrology for the Metallurgical Industry.* https://www.euramet.org/fileadmin/docs/EMRP/JRP/JRP_Summaries_2010/IND04_Publishable_JRP_Summary.pdf, 2014. Access date: 05 December, 2014.

[2] W. Demtröder. *Experimentalphysik 4: Kern-, Teilchen- und Astrophysik, (2. überarbeitete Auflage).* Springer-Verlag, Berlin, Heidelberg, New York, 2005.

[3] H. Krieger. *Grundlagen der Strahlenphysik und des Strahlenschutzes (4. Auflage).* Springer Spektrum, Wiesbaden, 2012.

[4] INFORUM Verlags und Verwaltungsgesellschaft mbH. Informationskreis Kernenergie. *α-decay.* www.kernfragen.de/kernfragen/lexikon/a/alphazerfall.php, 2012. Access date: 28 August, 2014.

[5] INFORUM Verlags und Verwaltungsgesellschaft mbH. Informationskreis Kernenergie. *β^--decay.* www.kernfragen.de/kernfragen/lexikon/b/beta_minus_zerfall.php, 2012. Access date: 28 August, 2014.

[6] INFORUM Verlags und Verwaltungsgesellschaft mbH. Informationskreis Kernenergie. *Electron capture.* www.kernfragen.de/kernfragen/lexikon/e/elektroneneinfang.php, 2012. Access date: 28 August, 2014.

[7] INFORUM Verlags und Verwaltungsgesellschaft mbH. Informationskreis Kernenergie. *Electron capture.* www.kernfragen.de/kernfragen/lexikon/z/zustand_angeregter.php, 2012. Access date: 28 August, 2014.

[8] G. Pfennig et al. *Karlsruher Nuklidkarte.* Forschungszentrum Karlsruhe, Wiesbaden, 1998.

[9] J. Adams and P. Gasparini. *Gamma-ray spectrometry of rocks.* Elssevier Publishing Company, Amsterdam, 1970.

[10] W. Demtröder. *Experimentalphysik 3: Atome, Moleküle und Festkörper (3. Auflage).* Springer-Verlag, Berlin, Heidelberg, New York, 2005.

[11] K. Debertin and R. G. Helmer. *Gamma- and X-ray spectrometry with semiconductor detectors.* North Holland, Amsterdam, 1988.

[12] G. Knoll. *Radiation detection and measurement (second edition).* John Wiley & Sons, Inc., New York, Chichester, Brisbane, Toronto, Singapore, 1989.

[13] R. N. Cherry Jr. *Introduction.* www.ilo.org/oshenc/part-vi/radiation-ionizing/item/760-introduction, 2011. Access date: 2 September, 2014.

[14] F. J. Maringer. *Strahlenphysikalische und gesellschaftliche Aspekte des Strahlenschutzes*, 2011. Skriptum zur Vorlesung.

[15] H. Anderson. *Metropolis, Monte Carlo, and the MANIAC.* Los Alamos Science, 14 (1986).

[16] F. Salvat and J. Fernández-Varea. *Overview of physical interaction models for photon and electron transport used in Monte Carlo codes.* Metrologia, 46 (2009):112–138, 2009.

[17] F. Salvat and Fernández-Varea. *PENELOPE, a code system for Monte Carlo simulation of electron and photon transport.* Universitat de Barcelona, Barcelona, 2011.

[18] D. Kryeziu. *Enhancement of precision and accuracy by Monte-Carlo simulation of a well-type pressurized ionization chamber used in radionuclide metrology.* Atominstitut der Österreichischen Universitäten, Vienna, 2006.

[19] W. Feller. *An Introduction to Probability Theory and Its Applications, Volume 1 (Third Edition).* John Wiley & Sons Inc., New York, 1968.

[20] F. Adunka. *Messunsicherheiten - Theorie und Praxis, (2. Auflage).* Vulkan-Verlag, Essen, 2000.

[21] Joint Committee for Guides in Metrology. *International Vocabulary of Metrology - Basic and General Concepts and Associated Terms (third edition).* www.bipm.org/en/publications/guides/vim.html, 2012. Access date: 11 August, 2014.

[22] W. C. Röntgen. *Eine neue Art von Strahlen.* Stahel'sche K. Hof- und Universitätsbuch- und Kunsthandlung, Würzburg, 1895.

[23] Canberra Industries Inc. *Gamma and X-Ray Detection.* www.canberra.com/literature/fundamental-principles/pdf/Gamma-Xray-Detection.pdf, 2010. Access date: 6 August, 2014.

[24] K. Debertin and U. Schrötzig. *Bedeutung von Summationskorrektionen bei der Gammastrahlen-Spektrometrie mit Germaniumdetektoren.* Physikalisch-Technische Bundesanstalt, Braunschweig, 1990.

[25] Canberra Industries Inc. *Standard Electrode Coaxial Ge Detectors (SEGe).* www.canberra.com/products/detectors/pdf/SEGe-detectors-C40021.pdf, 2013. Access date: 6 August, 2014.

[26] R. G. Helmer et al. *The use of Monte Carlo calculations in the determination of a Ge detector efficiency curve.* Nuclear Instruments and Methods in Physics Research, A 511 (2003):360–381.

[27] T. Schröttner. *Implementierung von Summationskorrekturen für einen HPGe-Detektor mittels Monte-Carlo Simulation.* Technische Universität Graz, Graz, 2001.

[28] P. Jodlowski and S. J. Kalita. *Gamma-Ray Spectrometry Laboratory for high-precision measurements of radionuclide concentrations in environmental samples.* Nukleonika, 5(2), (2010):143–148.

[29] A. Arinc et al. *Decay Data Evaluation Project.* www.nucleide.org/DDEP.htm, 2014. Access date: 29 July, 2014.

[30] F. J. Schima and D. D. Hoppes. *The use of Monte Carlo calculations in the determination of a Ge detector efficiency curve.* International Journal of Applied Radiation & Isotopes, 34(1983):1109–1114.

[31] Canberra Industries Inc. *Detector repair sheet*, 2007.

[32] J. Ródenas et al. *Analysis of the influence of germanium dead layer on detector calibration simulation for environmental radioactive samples using Monte Carlo method.* Nuclear Instruments and Methods in Physics Research, A 496 (2003):390–399.

[33] A. Elanique et al. *Dead layer thickness characterization of an HPGe detector by measurements and Monte Carlo simulations.* Applied Radiation and Isotopes, 70 (2012):538–542.

[34] K. Seidl. *Private communication with Canberra Packard Central Europe GmbH employee on the subject of dead layer growth.* 26 March 2014.

[35] R. M. Keyser. *Resolution and sensitivity as a function of energy and incident geometry for germanium detectors.* Nuclear Instruments and Methods in Physics Research, B 213 (2004):236–240.

[36] M. Schläger. *Precise modelling of coaxial germanium detectors in preparation for a mathematical calibration.* Nuclear Instruments and Methods in Physics Research, A 580 (2007):137–140.

[37] H. Aiginger, F. J. Maringer et al. *A new laboratory for routine low-level measurements (BVFA ARSENAL, WIEN).* Nuclear Instruments and Methods in Physics Research, B17(1986):435–437.

[38] Baltic Scientific Industries. *Approval drawing Austria - Lead shield*, 2013.

[39] Canberra Industries Inc. *Genie^{TM}2000 Tutorials*, 2004.

[40] Canberra Industries Inc. *Genie^{TM}2000 Customization Tools Manual (v. 3.1).* Canberra Industries Inc., Meriden, 2006.

[41] Canberra Industries Inc. *Technical Advantages of ISOCS^{TM}/LabSOCS^{TM}.* www.canberra.com/literature/isocs/application_notes/ISOCS-LabSOCS-App-Note-C39530.pdf. Access date: 12 August, 2014.

[42] S. Hurtado et al. *GEANT4 code for simulation of a germanium gamma-ray detector and its application to efficiency calibration.* Nuclear Instruments and Methods in Physics Research, A 518 (2004):764–774.

[43] F. Padilla Cabal et al. *Monte Carlo based geometrical model for efficiency calculation of an n-type HPGe detector.* Applied Radiation and Isotopes, 68 (2010):2403–2408.

[44] J.C. Hardy et al. *Precise efficiency calibration of an HPGe detector: source measurements and Monte Calro calculations with sub-percent precision.* Applied Radiation and Isotopes, 56 (2002):65–69.

[45] Bureau International des Poids et Mesures. *Monographie BIPM-5 - "Table of Radionuclides".* www.bipm.org/fr/publications/monographie-ri-5.html, 2014. Access date: 29 July, 2014.

[46] J. Sŏlc. *Description of Monte Carlo simulations to be done in MetroMetal WP3 T3.1.3 and T3.2.3.* Private communication. January 2014.

[47] Google Inc. *Location of hydroelectric power plants.* http://www.google.at/mapmaker, 2014. Access date: 05 December, 2014.

[48] M. Kralik and K. Augustin-Gyurits. *Stauraumfeinsedimente als "Geochronometer" von Schad- oder Rohstoffen: Moderne Sedimentologie, Mineralogie, Geochemie und Verwertung der Donausedimente von Aschach (Oberösterreich).* Jubiläumsschrift 20 Jahre Geologische Zusammenarbeit Öesterreich - Ungarn, Teil 2:437–464.

[49] B. Downs. *RRUFF database of minerals.* www.rruff.info, 2014. Access date: 11 October, 2014.

[50] VERBUND AG. *Hydroelectric power plant Wallsee-Mitterkirchen.* http://www.verbund.com/pp/de/laufkraftwerk/wallsee-mitterkirchen, 2014. Access date: 05 December, 2014.

[51] VERBUND AG. *Hydroelectric power plant Ottensheim-Wilhering.* http://www.verbund.com/pp/de/laufkraftwerk/ottensheim-wilhering, 2014. Access date: 05 December, 2014.

[52] F. Tzika et al. *Interlaboratory comparison on ^{137}Cs activity concentration in fume dust.* Manuscript submitted to Radiation Physics and Chemistry.

Part IV.

Appendix

A. Manuscript: Interlaboratory comparison on ^{137}Cs activity concentration in fume dust

Interlaboratory comparison on ^{137}Cs activity concentration in fume dust

Faidra Tzika[1,*], Mikael Hult[1], Oleksiy Burda[2], Dirk Arnold[2], Goedele Sibbens[1], Belén Caro Marroyo[3], Maria Belén Gómez -Mancebo[3], Virginia Peyrés[3], Hannah Moser[4], Laurent Ferreux[5], Jaroslav Šolc[6], Pavel Dryák[6], Aldo Fazio[7], Aurelian Luca[8], Branko Vodenik[9], Mario Reis[10], Zbigniew Tyminski[11], Seppo Klemola[12]

[1] EC-JRC-IRMM-Institute for Reference Materials and Measurements, Retieseweg 111, 2440 Geel, Belgium;
[2] PTB-Physikalisch-Technische Bundesanstalt, Bundesallee 100, 38116 Braunschweig, Germany;
[3] CIEMAT, Metrología de Radiaciones Ionizantes & Unidad de Espectroscopía, Complutense 40, 28040 Madrid, Spain;
[4] BEV/PTP, Bundesamt für Eich- und Vermessungswesen, Arltgasse 35, A-1160 Wien, Austria;
[5] CEA-LIST, Centre de Saclay – LNHB, bât 602, 91191 Gif/Yvette Cedex, France;
[6] CMI, Czech Metrology Institute, Radiová 1a, CZ-102 00 Praha 10, Czech Republic;
[7] ENEA-INMRI, Via Anguillarese, 301 Santa Maria di Galeria, 00123 Roma, Italy;
[8] IFIN-HH, 30 Reactorului Street, 077125 Magurele, Ilfov, Romania;
[9] IJS, Institute Jožef Stefan, Jamova 39, 1000 Ljubljana, Slovenia;
[10] IST/CTN, Estrada Nacional 10 (km 139,7), 2695-066 Bobadela LRS - Portugal;
[11] NCBJ, Narodowe Centrum Badań Jądrowych, ul. Andrzeja Sołtana 7, 05-400 Ot`wock, Świerk, Poland;
[12] STUK, Radiation and Nuclear Safety Authority, P.O.Box 14, FIN-00881, Helsinki, Finland

Abstract-. A comparison was conducted, between 11 European National Metrology Institutes and EC-JRC, on measurement of ^{137}Cs activity concentration in fume dust. As comparison material an activity standard produced from real contaminated fume dust was used. The standard material consisted of 13 samples of compressed fume dust, each of 50 g mass and of well-defined cylindrical geometry (diameter 69.5 mm and height 18.7 mm). The material contained ^{137}Cs and ^{60}Co of reference activity concentrations of (9.72 ± 0.10) Bq/g and (0.450 ± 0.018) Bq/g, respectively, determined using the comparison results. The organisation and results of the intercomparison, as well as the process of obtaining reliable reference values are presented.

Key Words: metrology; ionising radiation measurements; interlaboratory comparisons; fume dust

* Corresponding author. Tel.: +32 (0) 14 571 288
E-mail address: faidra.tzika@ec.europa.eu (F. Tzika).

1. Introduction

More than one half of the yearly steel production in the European Union (EU) comes from recycling of metal scrap [1]. Radioactive 'orphan' sources may pass undetected through the radioactivity controls at the entrance of the metal works, and eventually be incorporated into the steel and/or its by-products. The dominating radionuclides occurring in melting incidents are ^{137}Cs and ^{60}Co [1]. They mainly originate from radioactive sources used in medical (e.g. from teletherapy units) and/or industrial applications and follow different routes in the steel production chain. The physical and chemical properties of ^{137}Cs favors its passing into the fumes and, after cooling, to the off-gas/fume dust of the melting process. The ^{60}Co is mostly trapped in the melt with a small fraction possible to be found in fume dust [2]. Together with slag, fume dust is one of the two main by-products of metal works. Samples of fume dust may be monitored for radioactivity using the same measurement system that is used for metal.

In 2011 the 'MetroMetal' (Ionising Radiation Metrology for the Metallurgical Industry) project, was launched in the framework of EMRP (European Metrology Research Programme) organized by Euramet and in which 13 European National Metrology Institutes (NMIs) participated. A main aim was to address the issue of reliable radioactivity monitoring in the steel industry. First, the current status of radioactivity monitoring in European Metal foundries was established concluding, among other facts, that there is a lack of traceable calibration standards for radioactivity measurement in cast steel, slag and fume dust matrices. The project responded to the identified needs by developing optimized radioactivity measurement systems and traceable calibration standards of these three matrices, which were also used to validate the proposed calibration methods of such systems [3]. In this context an interlaboratory comparison (ILC) was conducted for the determination of the ^{137}Cs activity concentration in the fume dust standard. This ILC was of particular importance, as it also tested the performance of the methods developed in the MetroMetal project for determining activity, which will be suggested as a standard for end-users. The methods are based on high resolution gamma-ray spectrometry using HPGe-detectors [4] and a well-defined geometry with pre-calculated correction factors for coincidence summing, geometry and sample composition. A key feature is calculation of detection efficiencies by Monte Carlo (MC) simulations using validated detector models [5]. The ILC participants employed in total 8 different MC codes and 2 numerical calculation approaches combined with experimental efficiencies for

determination of detection efficiency and various corrections (e.g. for coincidence summing).

The ILC further served as a means of characterization of the activity concentrations in the fume dust material. For this purpose, a second phase took place aiming to improve the analysis procedure, by correcting for deviations of the source shape from a perfect cylinder considered in MC simulations, and to extend the activity standardisation to include ^{60}Co.

2. Experimental

2.1. Organisation

The ILC was organized in two phases. Phase I included:

- Preparation of adequate number of samples and homogeneity testing (PTB) and composition analysis (JRC, CIEMAT).
- Distribution of samples, technical protocol and reporting template to participants.
- Measurements of samples at partners' laboratories and reporting results for ^{137}Cs activity concentrations to JRC.
- Final comparison and evaluation of ^{137}Cs results.

The ILC Phase II was agreed after the results of Phase I were disclosed and discussed among partners. The aim of Phase II was to improve the analytical procedure in order to reach a reliable reference value for the ^{137}Cs activity concentration in the fume dust standard and to extend the reporting to include ^{60}Co and establish a reference value for this additional radionuclide in the fume dust standard. The improved procedure in Phase II consisted on correcting the ^{137}Cs reported values for the slight curvature of container bottom.

Each of the 12 ILC-participants was provided one sample, and associated detailed information (sample mass, dimensions and elemental composition including container data). They were recommended to determine the ^{137}Cs activity concentration, for a reference date of 1 June 2013, by using gamma-ray spectrometry and without altering the provided sample geometry.

2.2. Samples

The raw fume dust material containing ^{137}Cs and ^{60}Co was provided by the Siempelkamp Nukleartechnik GmbH melting plant for radioactively contaminated residual substances in Krefeld, Germany [6].

The homogeneity testing and preparation of the intercomparison samples was realized at PTB. The total number of samples produced was 13. In order to achieve a fixed sample geometry, the fume dust of (50.20 ± 0.01) g was compressed to 54 % of its initial volume, using 3 inner plastic discs, in a hermetically closed polyethylene container (diameter 6.95 cm, height 1.87 cm, wall thickness 0.10 cm) (see Fig. 1). In such manner the reproducibility of the analysis, in terms of mathematical efficiency calibration, was estimated to be of better than 2 %.

For the elemental composition analysis (Table 1) of the fume dust, X-ray Fluorescence Analysis (XRF) was applied at CIEMAT using pellets of the same material prepared at JRC-IRMM (Fig. 2). The pressing of the pellet was applied at 250 kN using Fluxana Vaneox -25 t and 32 mm die and the mass was determined gravimetrically. The carbon content (Table 1) was obtained using Elemental Combustion Analysis (ECA).

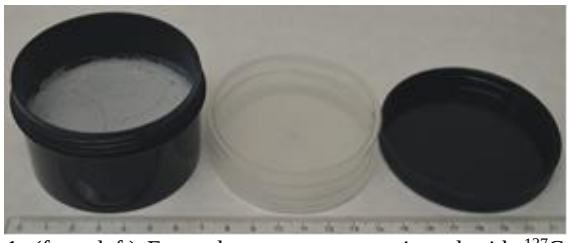

Fig. 1. (from left) Fume dust source contaminated with ^{137}Cs and ^{60}Co in the container, fixing inner discs and lid.

The homogeneity testing of the material was carried out using relative gamma-ray spectrometry measurements of all 13 samples performed under same measurement conditions and position on the PTB detector. The results of the count rates, normalized to sample mass, for the peaks of ^{137}Cs and ^{60}Co are shown in Fig. 3 in which homogeneity between samples is demonstrated with respect to the measurement uncertainties. The standard relative deviations of the results for ^{137}Cs and ^{60}Co, of 0.35 % and 3.74 %, respectively, were taken conservatively as homogeneity indicators. The higher inhomogeneity component of ^{60}Co as compared to the one of ^{137}Cs partially reflects the poorer counting statistics due to the lower activity concentration of this radionuclide.

Uncertainty due to material instability was disregarded based on the sample preparation procedure which did not allow changes with time or transport. The assumption was verified at JRC by repeating the measurement of one test sample after a period of 9 months which resulted in the same activity concentration for ^{137}Cs and ^{60}Co as the first analysis.

Table 1
Elemental composition of fume dust as determined by XRF and ECA performed on a fume dust pellet[1]

Element	Weight fraction, %	Element	Weight fraction, %
Zn	73(1)	Sb	0.05(3)
O[1]	23(1)	Al	0.050(6)
C	1.5(1)	Cd	0.027(4)
Fe	1.5(1)	Mn	0.024(5)
Pb	0.60(6)	Ca	0.013(1)
Br	0.33(4)	Ni	0.008(3)
Cl	0.20(2)	P	0.0043(4)
Si	0.083(6)		

[1] The oxygen content was calculated by difference

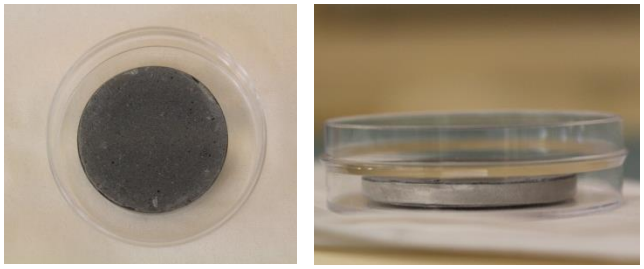

Fig. 2. Fume dust pellet (top and side views) of mass (6.6 ± 0.1) g in 32 mm × 7.9 mm Al cup, produced for XRF analysis.

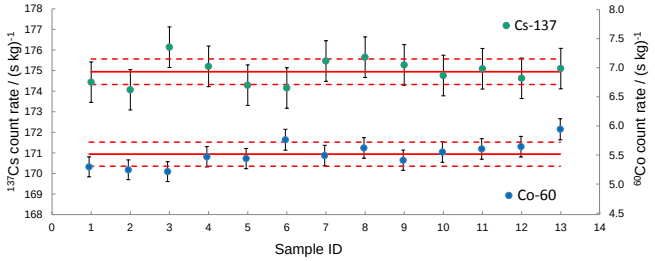

Fig. 3. Counts rate per unit mass for ^{137}Cs (662 keV) and ^{60}Co (1173 keV) peaks measured at the same position on PTB detector. The error bars correspond to counting statistical uncertainty and red lines to the mean ± 1 s.

2.3. *Analysis methods*

The participants analyzed the ILC samples applying the methods developed for end-users within the MetroMetal project [5]. More specifically, they used high resolution gamma-ray spectrometry and different calibration methods (experimental, mathematical and combined ones) to determine the activity concentration of ^{137}Cs. In total 8 different MC and 2 numerical codes were used to calculate the detection efficiencies and True Coincidence Summing (TCS) corrections, where applicable. Two partners applied absolute efficiency calibration using their validated MC detector models and the others applied efficiency corrections to the experimental efficiencies for standard sources (efficiency transfer approach). The distances from the detector end-cap to the bottom of the sample ranged from in-contact to 17 cm. The nuclear decay data was obtained from Monographie BIPM-5, which is identical to the DDEP (Decay Data Evaluation Project) data [7,8]. Participants reported their results of activity concentrations, A_{lab}, in Bq/g with the associated combined standard uncertainty, u_{lab}.

2.4. *Evaluation parameters*

The participants' results were evaluated against the ILC reference values, A_{ref}, for each nuclide. A_{ref} represented the ILC consensus value derived as the power moderated mean (pmm) [9] of all reported activity concentrations, A_{lab}, for each nuclide. The standard uncertainty of A_{ref} for each nuclide, u_{ref}, combined the uncertainty components from characterisation, u_{pmm}, and homogeneity, u_{hom}, as following:

$$u_{ref} = \sqrt{u_{pmm}^2 + u_{hom}^2} \quad . \qquad (1)$$

Performance statistics were calculated including relative deviations from the reference values, D_{rel}:

$$D_{rel} = \frac{A_{lab} - A_{ref}}{A_{ref}} 100 \qquad (2)$$

and E_n numbers [10]:

$$E_n = \frac{A_{lab} - A_{ref}}{U(d_i)} \overset{k=2}{=} \frac{\zeta}{2} \qquad (3)$$

where $U(d_i) = k\, u(d_i)$ is the expanded uncertainty of the difference $d_i = A_{lab} - A_{ref}$ and ζ the zeta-score for the lab i for coverage factor k = 2. Since A_{lab} and A_{ref} are correlated $u(d_i)$ is calculated using the following equation [9,11]:

$$u^2(d_i) = (1 - 2w_i)u_i^2 + u_{ref}^2 \qquad (4)$$

where w_i are the normalized weights used in the calculation of the pmm and u_{pmm} [9]. The E_n values $|E_n| \leq 1$, $|E_n| > 1$, and $|E_n| > 1.5$, were interpreted as showing compatibility, significant difference from A_{ref}, or need for investigation (action signal), respectively, at 95 % confidence level.

3. Results and discussion

All 12 participants reported results for activity concentrations of ^{137}Cs (Phase I) and ^{60}Co (Phase II).

The reported results for ^{137}Cs of Phase I, are shown in Fig.4. They were obtained considering cylindrical source shape in a container of flat bottom. Exceptions were PTB and POLATOM (NCBJ) who took into consideration the slight curvature of the container bottom, by using a calibration standard in identical container as the ILC sample. After the disclosure of the results it was agreed for POLATOM to apply a correction of +3.2 %, to compensate for the difference in density between their standard (0.65 g·cm^{-3}) and the ILC sample (0.707 g·cm^{-3}), which was not included initially. From the 12 reported results for ^{137}Cs, 9 deviated by <5 % from the reference value, 2 in the range between 5 % and 10 % and 1 by >10 %. The latter deviation (POLATOM) was associated with the instability of the one of two detectors used in the measurements at the specific laboratory.

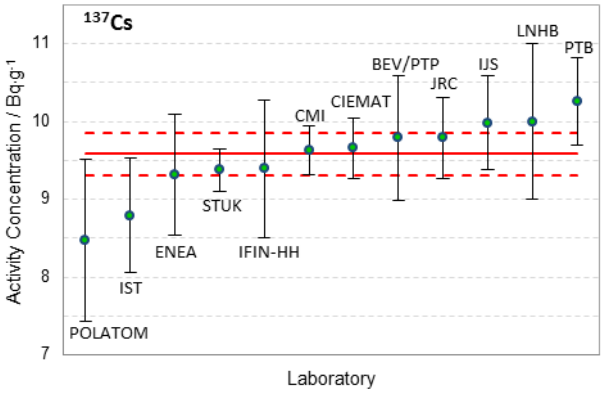

Fig. 4. Laboratory results (Phase I) for ^{137}Cs activity concentration in fume dust (ref. date 1 June 2013). Error bars represent U_{lab}, calculated from the reported combined standard uncertainties, for k = 2 and red lines the $A_{ref} \pm U_{ref}$ (k = 2).

The results of ^{60}Co activity concentrations (see Fig. 5) were analyzed and reported during the Phase II of the ILC. The participants applied the improved analytical method by accounting for the container curvature which in turn biases the geometry of the source. Of the 12 ^{60}Co reported results, 9 deviated by <5 % from the reference value, 2 in the range between 5 % and 10 % and 1 by >10 %. The latter corresponds to the sample (number 13) showing the higher deviation, of 8 %, from the mean during the homogeneity measurements (Fig. 3). A comparison between the two plots a) the reported ^{60}Co values *vs* sample number (not shown here) and b) homogeneity plot (Fig. 3), revealed a similar pattern. Plotting the independent participant values as a function of homogeneity measurements indicates possible linear correlation for ^{60}Co. The apparent inhomogeneity of

^{60}Co was accounted for in the uncertainty of its reference value (Eq. 1). During conducting the same test for ^{137}Cs, no correlation was observed.

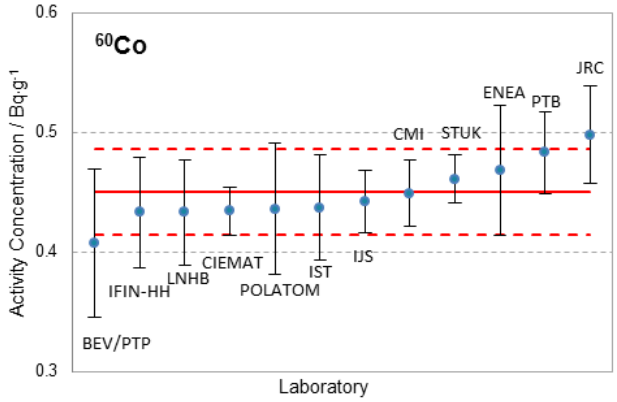

Fig. 5. Laboratory results (Phase II) for ^{60}Co activity concentration in Siempelkamp Fume Dust (ref. date 1 June 2013). Error bars and red lines as in Fig.4.

The improved analytical procedure (taking into account the curved container bottom) of ILC Phase II resulted in an effect on the calculated detection efficiencies for ^{137}Cs which ranged between 0 % and 7 % depending on the detector type and measurement distance used by each participant. In Table 2 the evaluation parameters and the reduced observed χ-values of the ILC are summarized for both phases of the ILC and ^{137}Cs and ^{60}Co nuclides. No 'action signal' was recorded with respect to E_n statistics, which indicates the validity of uncertainty estimations by the participants. The values of the evaluation parameters shown in Table 2 are improved for ^{137}Cs Phase II as compared to the ones of Phase I, reflecting the optimisation of efficiency calculations with respect to container/source shape definition. E_n compatibility of 100 % is observed for the case of ^{60}Co.

The results of Phase II, were used to derive the reference activity concentrations in the fume dust standard of (9.72 ± 0.10) Bq/g and (0.450 ± 0.018) Bq/g, respectively, for the reference date of 1 June 2013. It is noted that the value for ^{60}Co is not altered if the reported results are corrected for inhomogeneity (case ^{60}Co-IIb in Table 2) although the spread of the results is improved in this case.

Table 2
Summary of ILC evaluation parameters

Nuclide-Phase[1]	A_{ref} Bq g^{-1}	χ	No of labs with				
			$\lvert D_{rel}\rvert$			$\lvert E_n\rvert$	
			≤5%	>5% & ≤10%	>10 %	≤1	>1& ≤1.5
^{137}Cs-I	9.58(14)	1.40	9	2	1	9	3
^{137}Cs-II	9.72(10)	1.04	10	1	1	11	1
^{60}Co-II	0.450(18)	1.26	9	2	1	12	-
^{60}Co-IIb[2]	0.450(18)	0.82	11	-	1	11	1

[1] ^{137}Cs results reported in ILC Phase I and II and ^{60}Co only in Phase II.
[2] ^{60}Co results of Phase II after applying corrections for inhomogeneity.

4. Conclusion

This ILC was part of the MetroMetal research project. It did not aim at testing the proficiency of the participants, but at assisting the development of a reference procedure and a standard for radioactivity monitoring in metal foundries. The ILC results demonstrated the validity of the proposed methods for the measurement of ^{137}Cs and ^{60}Co in fume dust. The validated MC detector models proved to be an important tool assisting the improvement of the analysis. The ILC results were further used to determine the reference activity concentrations in the material.

The availability of tested methods and of the new fume dust activity standard will contribute in ensuring reliable measurements of radioactivity in the EU metal industry. The study can be further projected to production of a certified reference material (CRM) of fume dust with ^{137}Cs and ^{60}Co. Following this exercise it is now possible to better design a larger scale undertaking for production of such a material.

Acknowledgements

This work was supported by the EMRP joint research project 'Ionising radiation metrology for the metallurgical industry' (MetroMetal) which has received funding from the European Union on the basis of Decision No 912/2009/EC. The EMRP is jointly funded by the EMRP participating countries within EURAMET and the European Union. The authors are grateful to all contributors to this work at the partners' laboratories and in particular to André Moens for preparing the fume dust pellets and also to Eduardo García-Toraño, Uwe Wätjen, Stefaan Pommé, Timos Atzitzoglou, Franz-Josef Maringer, Maria Sahagia, Pierluigi Carconi and Andrea Petrucci for the valuable discussions.

References

1. IAEA SSS, SSG-17, Control of Orphan Sources and Other Radioactive Material in the Metal Recycling and Production Industries, Vienna, 2012.
2. UNECE, Report on the Improvement of the Management of Radiation Protection Aspects in the Recycling of Metal Scrap, Geneva, 2002.
3. E. García-Toraño, Ionising Radiation Metrology for the Metallurgical Industry, Int. J. Metrol. & Qual. Eng. (accepted).
4. E. García-Toraño et. al., A Novel Radionuclide Specific Detector System for the Measurement of Radioactivity at Steelworks, 8th International Conference on Isotopes, Hyatt Regency Chicago, 24-29, August, 2014.
5. J. Šolc et. al., Characterization of a Radionuclide Specific Laboratory Detection System for the Metallurgical Industry, Rad. Phys. Chem. (to be submitted)
6. http://www.siempelkamp.com/index.php?id=2003&L=0
7. http://www.bipm.org/en/publications/monographie-ri-5.html
8. http://www.nucleide.org/DDEP_WG/DDEPdata.htm
9. S. Pommé, Determination of a Reference Value, Associated Standard Uncertainty and Degrees of Equivalence, EUR JRC25355 EN, doi: 10.2787/61338, 2012.
10. ISO 13528:2005, Statistical Methods for Use in Proficiency Testing by Interlaboratory Comparisons, Geneva, Switzerland.
11. G. Ratel, Evaluation of the uncertainty of the degree of equivalence. Metrologia 42 (2005) 140-144.

B. Seibersdorf Detector (BEV)

DETECTOR SPECIFICATIONS AND PERFORMANCE DATA

Specifications

Model GC3020-7935-7 Serial Number b 94028

The purchase specifications and therefore the warranted performance of this detector are as follows :

Nominal volume ____ cc Relative efficiency 30 %

Resolution 2.0 keV (FWHM) at 1.33 MeV

____ keV (FWTM) at 1.33 MeV

1.2 keV (FWHM) at 122 keV

____ keV (FWTM) at

Peak/Compton 54 :1 Cryostat well diameter ____ mm Well depth ____ mm

Cryostat description or Drawing Number if special Multi Attitude Cryostat, type 7935-7

Physical Characteristics

Geometry Coaxial one open end, closed end facing window

Diameter 56.5 mm Active volume ____ cc

Length 55 mm Well depth ____ mm

Distance from window 5 mm Well diameter ____ mm

Electrical Characteristics

Depletion voltage (+)2500 Vdc

Recommended bias voltage Vdc (+)3500 Vdc

Leakage current at recommended bias .01 nA

Preamplifier test point voltage at recommended voltage -.8 Vdc

Capacitance at recommended bias ___/ pF

Resolution and Efficiency

With amp time constant of 4 µs

Isotope	^{57}Co	^{60}Co			
Energy (KeV)	122	1332			
FWHM (keV)	.931	1.78			
FWTM (keV)		3.35			
Peak/Compton		60.8:1			
Rel. Efficiency		30.2%			

Tests are performed following IEEE standard test ANSI/IEEE std325-1986

Tested by : Date : February 14 1995

Approved by : Date : February 14 1995

Docum : GDAME001	*Date : 29/10/93*
Issue : Spec. Sheet GC	*Name : PVE*
Revue : A	*Page : 1/1*
Basis : 0.M001PVE.08	*Appr :*

CSNV Repair nr :	*GHR3169*
Date of arrival :	*11/3/02*
Subs repair nr :	*AT-4/440/21*
Customer order nr :	

CANBERRA

DETECTOR SERVICE REPORT

Customer identification

Subsidiary : **CPCE**
Customer name :
Contacted person :
Address :

Detector elements

Detector Model :	**GC3020-7935SL-7**	s/n	**b 94028**
Preamp model :	**2001CSL**	s/n	
Dewar :		s/n	
Collar :			
Cables :			
HV shut-off	**yes**		
Manuals			
Carry handle	**yes**		
Other			

Visual Inspection

Endcap	☐	broken	☐	bent	☐	dented	☐ **OK**
Cryostat	☐	broken	☐	bent	☐	dented	☐ **OK**
Dewar	☐	broken	☐	bent	☐	dented	☐
Preamp	☐	broken	☐	bent	☐	dented	☐ **OK**

Tests before cool down

Test point ☒YES ☐ NO

Defective cooled fet assembly ☐ YES ☒ NO

Defective :☐Field Effect Transistor ☐Feedback Resistor ☐Feedback capacitor ☐Protection diode ☐Test Capacitor ☐No contact

Defective preamp ☐ YES ☒NO

Defective : ☐HV network ☐Electronics

Detector tests (cooled down)

☐ Resolution conform to specs : ☐ YES ☐ No . keV

☒ Vacuum ~~or insulation problem~~ +/-OK
☐ HV leakage to the ground
☐ Internal ☐ External
☐ Detector leakage current
☒ OK
☐ Increased
☐ Breakdown at
☐Microphonics : ☐ YES ☐ NO

☐ Damaged components of preamp
☐ Defective components of preamp
☐ Peak shift
☐ Pole zero
☐ Drain current
☐ Oscillations
☐ Neutron damage
☐

Replaced parts

☐ Feedthroughs ☐Preamplifier ☐ Dewar ☐Crystal ☐ Endcap ☐ Collar ☐ Cryostat ☒ internal hardware + electronics

Comments : Crystal has been reprocessed completely (grinded, new style diffusion, new implantation and etch). It has been remounted in completely new upgraded holder construction with new electronics. Vacuum has been reconditioned and checked after a cycle. Detector has been 4 times tested and cycled and has had a long term stability test and ISOCS calibration measurements before shipment.

SERVICE MANAGER : P. VERMEULEN
Date : May 6, 2002
Signature :

CANBERRA

DETECTOR SPECIFICATION AND PERFORMANCE DATA AFTER REPAIR

Specifications

Detector Model GC3020 **Serial number** b 94028
Cryostat Model 7935SL-7
Preamplifier Model 2001CSL

Cryostat description or Drawing Number if special Multi Attitude cryostat, type 7935SL-7

Physical Characteristics

Geometry Coaxial one open end, closed end facing window

Diameter	56	mm	Active volume	_____	cc
Length	54	mm	Crystal well depth	_____	mm
Distance from window (outside)	5	mm	Crystal well diameter	_____	mm

Electrical Characteristics

Depletion voltage (+)2500 Vdc
Recommended bias voltage Vdc (+)3500 Vdc
Leakage current at recommended bias 0.01 nA
Preamplifier test point voltage at recommended voltage -0.8 Vdc

Resolution and Efficiency after repair

With amp time constant of 4 µs

Isotope	^{57}Co	^{60}Co			
Energy (keV)	122	1332			
FWHM (keV)	.843	1.77			
FWTM (keV)		3.33			
Peak/Compton		58.0:1			
Rel. Efficiency		26.8%			

- Test are performed following IEEE standard test ANSI/IEEE std325-1996
- Standard Canberra electronics used - See Germanium detector manual Section 7

Tested by : Date : May 6, 2002

Approved by : Date : May 6, 2002

CANBERRA Semiconductor is an ISO 9000 certified company

Table 1: Comparison of measured activity to true activity using MCNP efficiency for initial data set acquired in April 2002. The top table is for 0 degree source position and the bottom table is for 90 degree source position.

Source located at 0 degree		Measured Efficiency		MCNP Efficiency		Ratio of MCNP eff. over Measured eff.	
Nuclide	E (keV)	Efficiency	1 sd %	Efficiency	1 sd %	MCNP/Meas	1 σ error
AM-241	59.54	6.57E-04	3.61%	6.32E-04	0.74%	0.961	0.035
Eu-152	121.78	1.24E-03	3.31%	1.24E-03	0.53%	0.999	0.034
	244.6	9.33E-04	3.39%	9.38E-04	0.61%	1.006	0.035
	344.27	7.09E-04	3.33%	6.93E-04	0.71%	0.978	0.033
	778.89	3.55E-04	3.41%	3.50E-04	0.99%	0.987	0.035
	1112.02	2.72E-04	3.44%	2.66E-04	1.14%	0.977	0.035
	1407.95	2.26E-04	3.41%	2.23E-04	1.24%	0.985	0.036
				Weighted Average		0.981	0.014

Source located at 90 degrees		Measured Efficiency		MCNP Efficiency		Ratio of MCNP eff. over Measured eff.	
Nuclide	E (keV)	Efficiency	1 sd %	Efficiency	1 sd %	MCNP/Meas	1 σ error
AM-241	59.54	3.09E-04	3.69%	3.00E-04	1.45%	0.971	0.038
EU-152	121.78	1.22E-03	3.99%	1.26E-03	0.68%	1.029	0.042
	244.6	1.01E-03	4.01%	1.03E-03	0.76%	1.026	0.042
	344.27	7.57E-04	3.99%	7.75E-04	0.87%	1.024	0.042
	778.89	3.86E-04	4.01%	3.86E-04	1.25%	1.000	0.042
	1112.02	2.96E-04	4.02%	2.84E-04	1.45%	0.961	0.041
	1407.95	2.42E-04	4.01%	2.46E-04	1.56%	1.014	0.044
				Weighted Average		0.998	0.017

Table 2: Comparison of measured activity to true activity using MCNP efficiency for data acquired in February 2003. The top table is for 0 degree source position and the bottom table is for 90 degree source position.

Source located at 0 degree		Measured Efficiency		MCNP Efficiency		Ratio of MCNP eff. over Measured eff.	
Nuclide	E (keV)	Efficiency	1 sd %	Efficiency	1 sd %	Ratio	1 σ error
AM-241	59.54	6.83E-04	3.62%	6.32E-04	0.74%	0.925	0.034
Eu-152	121.78	1.23E-03	3.33%	1.24E-03	0.53%	1.007	0.034
	244.6	9.19E-04	3.43%	9.38E-04	0.61%	1.021	0.036
	344.27	7.01E-04	3.34%	6.93E-04	0.71%	0.989	0.034
	778.89	3.45E-04	3.48%	3.50E-04	0.99%	1.015	0.037
	1112.02	2.75E-04	3.51%	2.66E-04	1.14%	0.967	0.036
	1407.95	2.19E-04	3.42%	2.23E-04	1.24%	1.017	0.037
				Weighted Average		0.985	0.014

Source located at 90 degrees		Measured Efficiency		MCNP Efficiency		Ratio of MCNP eff. over Measured eff.	
Nuclide	E (keV)	Efficiency	1 sd %	Efficiency	1 sd %	Ratio	1 σ error
AM-241	59.54	3.13E-04	3.56%	3.00E-04	1.45%	0.958	0.037
EU-152	121.78	1.21E-03	3.44%	1.26E-03	0.68%	1.040	0.036
	244.6	9.59E-04	3.48%	1.03E-03	0.76%	1.077	0.038
	344.27	7.49E-04	3.44%	7.75E-04	0.87%	1.034	0.037
	778.89	3.81E-04	3.49%	3.86E-04	1.25%	1.013	0.038
	1112.02	2.90E-04	3.50%	2.84E-04	1.45%	0.980	0.037
	1407.95	2.39E-04	3.47%	2.46E-04	1.56%	1.028	0.039
				Weighted Average		1.009	0.015

CSNV Repair nr :	*GHR4169*
Date of arrival :	*20/11/06*
Subs repair nr :	*SVA26325*
Customer order nr :	

Isocs: ☒YES / ☐NO
Quote: ☐YES / ☐NO

CANBERRA

DETECTOR SERVICE REPORT

Customer identification

Subsidiary : **CPCE A**
Customer name :
Contacted person :
Address :

Detector elements

Detector Model :	**GC3020**	s/n	**b 94028**
Cryostat Model :	**7935SL-7**		
Preamp model :	**2001CSL**	s/n	
Dewar :		s/n	
Collar :			
Cables :			
HV shut-off	**yes**		
Manuals			
Carry handle	**yes**		
Muffler			
Other			

Visual Inspection

Endcap	☐	broken	☐	bent	☐	dented	☐ **OK**
Cryostat	☐	broken	☐	bent	☐	dented	☐ **OK**
Dewar	☐	broken	☐	bent	☐	dented	☐
Preamp	☐	broken	☐	bent	☐	dented	☐ **OK**

Tests before cool down

Test point ☒YES ☐NO

Defective cooled fet assembly ☐YES ☒NO

Defective :☐Field Effect Transistor ☐Feedback Resistor ☐Feedback capacitor ☐Protection diode ☐Test Capacitor ☐No contact

Defective preamp ☐YES ☒NO

Defective : ☐HV network ☐Electronics

Detector tests (cooled down)

☐ Resolution conform to specs : ☐ YES ☐ No . keV

☒ Vacuum OK
☐ Vacuum problem
☐ HV leakage to the ground
  ☐ Internal ☐ External
☐ Detector leakage current
  ☐ OK
  ☒ Increased
  ☐ Breakdown at
☐ Microphonics : ☐ YES ☐ NO

☐ Damaged components of preamp
☐ Defective components of preamp
☐ Peak shift
☐ Pole zero
☐ Drain current
☐ Oscillations
☐ Neutron damage
☐

Replaced parts

☐ Feedthroughs ☐Preamplifier ☐ Dewar ☐Crystal ☐ Endcap ☐ Collar ☐ Cryostat ☐

Comments : Incoming test showed us an increased crystal leakage current. Crystal has been re-implanted, re-etched and remounted. Vacuum has been reconditioned and checked after a cycle. Detector has been 4 times tested and cycled and has had 1 long term stability test. Also ISOCS cal val measurements have been performed before shipment.

SERVICE MANAGER : P. VERMEULEN
Date : February 16, 2007
Signature :

C. Reference sources and sample information

Physikalisch-Technische Bundesanstalt

G13-ST
(1351)

Radioaktives Standardpräparat

Radionuklid:	Americium-241
Halbwertszeit:	432,0 Jahre
Präparat Nr.:	155-86
Typ:	punktförmig
Abdeckfolie:	Polyäthylen, beidseitig 22 mg cm^{-2}
Aktivität:	44,7 kBq
Relative Unsicherheit: (Vertrauensniveau 99 %)	1,5 %
Bezugszeit:	1.1.1986

Dichtheitsprüfung

ausgeführt am:	5.12.86
Prüfverfahren:	Wischtest
Ergebnis:	Aktivität kleiner als 4 Bq

Braunschweig, 09.12.86

Im Auftrag

(Dipl.-Phys. K.F. Walz)

Physikalisch-Technische Bundesanstalt

G14-ST

(14 St)

Radioaktives Standardpräparat

Radionuklid:	Caesium-137
Halbwertszeit:	30,0 Jahre
Präparat Nr.:	252-83
Typ:	punktförmig
Abdeckfolie:	Polyäthylen, beidseitig 22 mg cm^{-2}
Aktivität:	32,0 kBq
Relative Unsicherheit: (Vertrauensniveau 99 %)	1,5 %
Bezugszeit:	1.1.1986

Dichtheitsprüfung

ausgeführt am:	5.12.86
Prüfverfahren:	Wischtest
Ergebnis:	Aktivität kleiner als 4 Bq

Braunschweig, 09.12.86

Im Auftrag

(Dipl.-Phys. K.F. Walz)

PKSI - 4

ORSZÁGOS MÉRÉSÜGYI HIVATAL
NATIONAL OFFICE OF MEASURES
BUDAPEST XII., NÉMETVÖLGYI ÚT 37-39.
1535 Budapest, Pf.: 919. HUNGARY
Telephone:(36-1) 156-7722
Telefax:(36-1) 212-0147

Our ref.: 1956/96
Your ref.: 1082/96
Purchaser: BEV
Number of bill of delivery: 508 059

Budapest, 11 April 1996

CERTIFICATE

SOLID RADIOACTIVE REFERENCE SOURCE

No.: 96 - 025

Expiration date	:	1 May 1998
Code	:	Am - OMH - 1 - SP
Symbol	:	OMH; Am-241; 96 - 025
Radionuclide	:	americium - 241
Activity	:	398.5 kBq ± 1.0 % *
Measuring method	:	4 π α - gamma coincidence counting
Reference date	:	1 May 1996
Half - life	:	(1.5785 ± 0.0024) x 10^5 d **

* The expanded uncertainty of radioactive concentration (%)
is the combined standard uncertainty multiplied by the coverage factor k=3
(See Guidelines for the Expression of the Uncertainty of Measurement
in Calibration, WECC Doc. 19 - 1990.)

** IAEA-TECDOC-619; VIENNA, 1991

ORSZÁGOS MÉRÉSÜGYI HIVATAL

Source holder

- **material** : polystyrene
- **thickness** : 0,5 mm
- **diameter** : 35 mm

Sample encapsulated in : aluminium ring

Radionuclidic impurities : At the reference date , activities other than that of the principal nuclide and its daughter nuclide(s), were estimated to be (in percentage of the principal activity):

no gamma - emitting impurities were detected

The detection limits over 100 - 2500 keV energy range varied between 0,0001-0,0005 %.

ORSZÁGOS MÉRÉSÜGYI HIVATAL Sugárfizikai- és Kémiai Mérések Főosztály

/Jenő Vágvölgyi /
Head, Section of
Radioactivity

PKS7-4

ORSZÁGOS MÉRÉSÜGYI HIVATAL
NATIONAL OFFICE OF MEASURES
BUDAPEST XII., NÉMETVÖLGYI ÚT 37-39.
1535 Budapest, Pf.: 919. HUNGARY
Telephone:(36-1) 156-7722
Telefax:(36-1) 212-0147

Our ref.: 1956/96
Your ref.: 1082/96
Purchaser: BEV
Number of bill of delivery: 508 059

Budapest, 11 April 1996

CERTIFICATE

SOLID RADIOACTIVE REFERENCE SOURCE

No.: 96 - 019

Expiration date	:	1 May 1998
Code	:	Co - OMH - 4 - SP
Symbol	:	OMH; Co-60; 96 - 019
Radionuclide	:	cobalt - 60
Activity	:	390.0 kBq ± 0.7 % *
Measuring method	:	4 π beta - gamma coincidence counting
Reference date	:	1 May 1996
Half - life	:	(1925.5 ± 0.5) d **

* The expanded uncertainty of radioactive concentration (%)
is the combined standard uncertainty multiplied by the coverage factor k=3
(See Guidelines for the Expression of the Uncertainty of Measurement
in Calibration, WECC Doc. 19 - 1990.)

** IAEA-TECDOC-619; VIENNA, 1991

ORSZÁGOS MÉRÉSÜGYI HIVATAL

Source holder

- **material** : polystyrene
- **thickness** : 0,5 mm
- **diameter** : 35 mm

Sample encapsulated in : aluminium ring

Radionuclidic impurities : At the reference date , activities other than that of the principal nuclide and its daughter nuclide(s), were estimated to be (in percentage of the principal activity):

Cs-137: (0.07 ± 0.01) % ; $T_{1/2} = 1.102 \times 10^4$ d

The detection limits over 100 - 2500 keV energy range varied between 0,002-0,04 % .

ORSZÁGOS MÉRÉSÜGYI HIVATAL Sugárfizikai- és Kémiai Mérések Főosztálya

/Jenő Vágvölgyi / h.
Head, Section of
Radioactivity

Physikalisch-Technische Bundesanstalt

Braunschweig und Berlin

Kalibrierschein

Calibration certificate

Gegenstand: *Object:*	Aktivitätsnormal *Activity standard*
Hersteller: *Manufacturer:*	Physikalisch-Technische Bundesanstalt Fachbereich 6.1
Typ: *Type:*	Punktförmiges Präparat *Point source*
Kenn-Nummer: *Serial number:*	2005-1073
Auftraggeber: *Applicant:*	Bundesamt für Eich- und Vermessungswesen Arltgasse 35 A-1160 Wien Austria
Anzahl der Seiten: *Number of pages:*	4
Geschäftszeichen: *Reference number:*	PTB-6.11-234/13.2005
Kalibrierzeichen: *Calibration mark:*	PTB-6.11-2005-1073
Datum der Kalibrierung: *Date of calibration:*	02.08.2005

Im Auftrag
By order

Dr. K. Kossert

Braunschweig, 02.08.2005

Siegel
Seal

Bearbeiter:
Examiner:

M. Ehlers

Physikalisch-Technische Bundesanstalt

Gegenstand: *Object*	Aktivitätsnormal *Activity standard*
Typ: *Type*	Punktförmiges Präparat *Point source*
Kenn-Nummer: *Serial number*	2005-1073
Radionuklid: *Radionuclide*	Cadmium-109 *Cadmium-109*
Abdeckfolie: *Backing*	Polyester, beidseitig (2,20 ± 0,07) mg·cm^{-2} *Polyester, (2,20 ± 0,07) mg·cm^{-2} each*
Kalibrierverfahren: *Method of calibration*	Das Präparat wurde durch Aufbringen einer radioaktiven Lösung auf die Präparatunterlage mit Hilfe einer Pipette hergestellt. Die spezifische Aktivität der verwendeten Lösung wurde durch Messung der Photonenstrahlung mit einer 4π-Ionisationskammer bestimmt. Die 4π-Ionisationskammer ist eine Sekundärnormal-Messeinrichtung, kalibriert mit Aktivitätsnormalen der PTB. Die Aktivität des Präparates ergibt sich aus der spezifischen Aktivität und der Masse der aufgebrachten Lösung, die durch Wägung der Pipette vor und nach dem Aufbringen ermittelt wurde. *The source was prepared by dispensing a radioactive solution to the source carrier by means of a pipette. The specific activity (activity divided by mass of solution) of the used solution was determined by measuring the photon radiation with a 4π-ionization chamber. The 4π-ionization chamber is a secondary-standard measuring system calibrated by activity standards from primary standardization of the PTB. The activity of the source follows from the specific activity and the mass of the dispensed solution, which was determined by weighing the pipette prior to and after dispensation of the solution.*
Aktivität: *Activity*	A = (46,9 ± 0,8) kBq
Bezugszeitpunkt: *Reference date*	1. Januar 2005, 00:00 Uhr MEZ *00:00 CET on 1 January 2005*

PHYSIKALISCH-TECHNISCHE BUNDESANSTALT 18

Messunsicherheit:
Uncertainty of measurement

Angegeben ist die erweiterte Messunsicherheit, die sich aus der Standardmessunsicherheit durch Multiplikation mit dem Erweiterungsfaktor $k = 2$ ergibt. Sie wurde gemäß dem *"Guide to the Expression of Uncertainty in Measurement"* (ISO, 1995) ermittelt. Der Wert der Messgröße liegt im Regelfall mit einer Wahrscheinlichkeit von annähernd 95 % im zugeordneten Werteintervall.

The uncertainty stated is the expanded uncertainty obtained by multiplying the standard uncertainty by the coverage factor k = 2. It has been determined in accordance with the "Guide to the Expression of Uncertainty in Measurement" (ISO, 1995). Normally, the value of the measurand lies within the assigned range of values with a coverage probability of approximately 95%.

ISO-Klassifikation:
ISO classification

ISO/C 11111 gemäß DIN 25426-1 und ISO 2919.
ISO/C 11111 in compliance with DIN 25426-1 and ISO 2919.

Dichtheitsprüfung
Leakage test

ausgeführt am:
Date of test

2. August 2005
2 August 2005

Prüfverfahren:
Method of test

Wischprüfung gemäß DIN 25426-3.
Wipe test in compliance with DIN 25426-3.

Ergebnis:
Result of test

Die Aktivität der Wischprobe war zum Zeitpunkt der Probenahme kleiner als 30 Bq.

Die Umhüllung des Präparates ist dicht und kontaminationsfrei.

The activity of the wipe sample was less than 30 Bq at the time of sampling.

The cover of the source is leakproof and free of radioactive contamination.

Die Physikalisch-Technische Bundesanstalt (PTB) in Braunschweig und Berlin ist das natur- und ingenieurwissenschaftliche Staatsinstitut und die technische Oberbehörde der Bundesrepublik Deutschland für das Messwesen und Teile der Sicherheitstechnik. Die PTB gehört zum Dienstbereich des Bundesministeriums für Wirtschaft. Sie erfüllt die Anforderungen an Kalibrier- und Prüflaboratorien auf der Grundlage der Normen der Reihe DIN EN ISO/IEC 17025.

Zentrale Aufgabe der PTB ist es, die gesetzlichen Einheiten in Übereinstimmung mit dem Internationalen Einheitensystem (SI) darzustellen, zu bewahren und - insbesondere im Rahmen des gesetzlichen und industriellen Messwesens - weiterzugeben. Die PTB steht damit an oberster Stelle der metrologischen Hierarchie in Deutschland. Kalibrierscheine der PTB dokumentieren die Rückführung des Kalibriergegenstandes auf nationale Normale.

Zur Sicherstellung der weltweiten Einheitlichkeit der Maße arbeitet die PTB mit anderen nationalen metrologischen Instituten auf regionaler europäischer Ebene in EUROMET und auf internationaler Ebene im Rahmen der Meterkonvention zusammen. Das Ziel wird durch einen intensiven Austausch von Forschungsergebnissen und durch umfangreiche internationale Vergleichsmessungen erreicht.

The Physikalisch-Technische Bundesanstalt *(PTB) in Braunschweig and Berlin is the national institute for science and technology and the highest technical authority of the Federal Republic of Germany for the field of metrology and certain sectors of safety engineering. The PTB comes under the auspices of the Federal Ministry of Economics. It meets the requirements for calibration and testing laboratories as defined in the EN ISO/IEC 17025.*

It is the fundamental task of the PTB to realize and maintain the legal units in compliance with the International System of Units (SI) and to disseminate them, above all within the framework of legal and industrial metrology. The PTB thus is on top of the metrological hierarchy in Germany. Calibration certificates issued by it document that the object calibrated is traceable to national standards.

To ensure worldwide coherence of measures, the PTB cooperates with other national metrology institutes within EUROMET on the regional European level and on the international level within the framework of the Metre Convention. The aim is achieved by an intensive exchange of results of research work carried out and by comprehensive international comparison measurements.

Physikalisch-Technische Bundesanstalt

Braunschweig und Berlin

Empfohlene Radionukliddaten

Stand: 01.08.1999

Radionuklid: Cd-109

Halbwertszeit: $T_{½}$ = 462,1(14) Tage

Photonen-Energien *E* und –Emissionswahrscheinlichkeiten *p* pro Zerfall:

Strahlungs-typ	*E* in keV	*p*	Kommentar
Ag-L	3,1	0,1034(26)	
Ag-K_{α_2}	21,99	0,2899(25)	
Ag-K_{α_1}	22,16	0,547(4)	
Ag-K_{β_1}	24,9	0,1514(18)	
Ag-K_{β_2}	25,5	0,0263(10)	
γ	88,03	0,03626(20)	

Messunsicherheiten:
Die Ziffern in Klammern hinter dem Zahlenwert einer Messgröße geben die Messunsicherheit in der(n) letzten Stelle(n) des Zahlenwertes an. Die Messunsicherheiten entsprechen der einfachen Standardabweichung.

Literatur:
Schötzig, U. und Schrader, H.:
Halbwertszeiten und Photonen-Emissionswahrscheinlichkeiten von häufig verwendeten Radionukliden; PTB-Bericht PTB-Ra-16/5, Braunschweig 1998, ISBN 3-89701-279-0

Physikalisch-Technische Bundesanstalt

Braunschweig und Berlin

AKTIVITÄTSNORMAL
PUNKTFÖRMIGES PRÄPARAT MIT NIEDERENERGETISCHER PHOTONENSTRAHLUNG

Beschreibung, Hinweise

Das vorliegende Aktivitätsnormal, ein punktförmiges Präparat mit niederenergetischer Photonenstrahlung, ist in erster Linie für die Kalibrierung von Messanordnungen mit Halbleiterdetektoren bis herab zu etwa 5 keV vorgesehen.

Beim Aufbau des Präparats wurde auf möglichst geringe Absorption und Streuung der Strahlung geachtet. Die radioaktive Substanz liegt in Form einer sehr dünnen Schicht vor, die sich auf einer Kreisfläche von weniger als 5 mm Durchmesser in der Mitte zwischen zwei runden Polyester-Folien von je (2,20 ± 0,07) $mg \cdot cm^{-2}$ flächenbezogener Masse befindet. Durch Erhitzen unter Druck wurden die beiden Folien auf ihrer gesamten Fläche dicht miteinander verschweißt.

Da bei dem vorgesehenen Verwendungszweck die mechanische Beanspruchung gering ist, kann das Präparat als umschlossener radioaktiver Stoff im Sinne der Strahlenschutzverordnung angesehen werden. Es ist jedoch darauf zu achten, dass das Präparat nicht starken Lösungsmitteln oder Temperaturen oberhalb von 100 °C ausgesetzt wird. Vor der Auslieferung werden die Präparate durch Wischtest auf Dichtheit und Kontaminationsfreiheit geprüft; eine Freigabe erfolgt nur dann, wenn die Aktivität der Wischprobe 20 Bq nicht übersteigt.

Die im Kalibrierschein angegebene Aktivität A wurde entweder aus der Masse und der spezifischen Aktivität der aufgetropften radioaktiven Lösung oder aus dem Vergleich mit einem gleichartigen Aktivitätsnormal mittels einer geeigneten Sekundärmesseinrichtung bestimmt.

Aus der Aktivität läßt sich die Emissionsrate B für Photonen, d. h. die auf ein Zeitintervall bezogene Anzahl der in dem Zeitintervall **erzeugten** Photonen, gemäß $B = p \cdot A$ bestimmen; dabei ist p die Photonen-Emissionswahrscheinlichkeit.

Ein Teil der emittierten niederenergetischen Photonen wird beim Durchgang durch die radioaktive Substanz und die Präparatfolien absorbiert oder gestreut. Absorption und Streuung sind umso größer, je kleiner die Energie ist. Der Photonenfluß Φ, d. h. die auf ein Zeitintervall bezogene Anzahl der in diesem Zeitintervall aus dem Präparat **austretenden** Photonen, ist somit kleiner als die Emissionsrate und außerdem abhängig von der Durchstrahlungsrichtung. In der Richtung senkrecht zur Präparatunterlage ist der Einfluß der radioaktiven Substanz und der Präparatfolien am geringsten und abschätzbar.

Tabelle: Korrektionsfaktoren K_F für Strahlabschwächung in der Folie.

Radio-nuklid	Strahlungs-typ	Energie in keV	K_F
Cr-51	V-K_α	4,95	1,065
	V-K_β	5,43	1,049
Mn-54	Cr-K_α	5,41	1,050
	Cr-K_β	5,95	1,037
Fe-55	Mn-K_α	5,89	1,038
	Mn-K_β	6,49	1,028
Co-57	Fe-K_α	6,40	1,030
	Fe-K_β	7,06	1,022
Zn-65	Cu-K_α	8,04	1,015
	Cu-K_β	8,91	1,011
Sr-85	Rb-K_α	13,37	1,003
	Rb-K_β	15,0	1,003
Nb-93m	Nb-K_α	16,58	1,002
	Nb-K_β	18,7	<1,002
		17,0	<1,002
		24,0	<1,001

Die Korrektionsfaktoren für die Schwächung in der radioaktiven Substanz lassen sich nur schwer abschätzen. Aufgrund von Vergleichen zwischen Präparaten der beschriebenen Art und Präparaten ohne Schwächung [2] kann angenommen werden, dass bei den angewandten Herstellungsverfahren K_S für die Röntgenstrahlung zwischen 1,005 und 1,02 liegt. Da K_S bei dem vorliegenden Präparat nicht bestimmbar ist, wird $d\Phi/d\Omega$ nicht nach Gleichung (1) berechnet, sondern an einem mit Präparaten ohne Schwächung kalibrierten Halbleiterspektrometer der PTB bestimmt und ebenfalls im Kalibrierschein aufgeführt.

Im beiliegenden Datenblatt sind für die in der Messpraxis relevanten Photonen des betreffenden Nuklids die Emissionswahrscheinlichkeiten zusammengestellt. Sie wurden entweder in der PTB gemessen, aus publizierten Daten evaluiert oder den neuesten Datenwerken entnommen [3].

Achtung

Die Haltbarkeit dieses Präparates ist begrenzt. Erfahrungsgemäß sind besonders Am-241-Präparate (Alpha-Strahler) mit Aktivitäten über 50 kBq betroffen. Nach etwa einem halben Jahr wird die Folie im Bereich der radioaktiven Substanz brüchig, dieser Teil kann bei unsachgemäßer Handhabung sogar herausfallen. Die Unversehrtheit des Präparates sollte daher stets, vor allem während des Gebrauchs, durch Sichtprüfung überwacht werden.

Physikalisch-Technische Bundesanstalt

Braunschweig und Berlin

Kalibrierschein

Calibration Certificate

Gegenstand: *Object:*	Aktivitätsnormal *Activity standard*
Hersteller: *Manufacturer:*	Physikalisch-Technische Bundesanstalt Fachbereich 6.1
Typ: *Type:*	Punktförmiges Präparat *Point source*
Kenn-Nummer: *Serial number:*	2001-1686
Auftraggeber: *Applicant:*	Bundesamt für Eich- und Vermessungswesen - BEV Faradaygasse 3 A-1030 Wien Austria
Anzahl der Seiten: *Number of pages:*	5
Geschäftszeichen: *Reference number:*	PTB-6.11-245/30.2008
Kalibrierzeichen: *Calibration mark:*	PTB-6.11-2001-1686
Datum der Kalibrierung: *Date of calibration:*	18.02.2008

Im Auftrag
By order

Dr. K. Kossert

Braunschweig, 18.02.2008

Siegel
Seal

Bearbeiter:
Examiner:

M. Ehlers

Physikalisch-Technische Bundesanstalt

Gegenstand: *Object*	Aktivitätsnormal *Activity standard*
Typ: *Type*	Punktförmiges Präparat *Point source*
Kenn-Nummer: *Serial number*	2001-1686
Radionuklid: *Radionuclide*	Europium-152 *Europium-152*
Abdeckfolie: *Backing*	Polyethylen, beidseitig (21,3 ± 1,8) mg·cm^{-2} *Polyethylene, (21,3 ± 1,8) mg·cm^{-2} each*
Kalibrierverfahren: *Method of calibration*	Das Präparat wurde durch Aufbringen einer radioaktiven Lösung auf die Präparatunterlage mit Hilfe einer Pipette hergestellt. Die spezifische Aktivität der verwendeten Lösung wurde durch Messung der Photonenstrahlung mit einer 4π-Ionisationskammer bestimmt. Die 4π-Ionisationskammer ist eine Sekundärnormal-Messeinrichtung, kalibriert mit Aktivitätsnormalen der PTB. Die Aktivität des Präparates ergibt sich aus der spezifischen Aktivität und der Masse der aufgebrachten Lösung, die durch Wägung der Pipette vor und nach dem Aufbringen ermittelt wurde. *The source was prepared by dispensing a radioactive solution to the source carrier by means of a pipette. The specific activity (activity divided by mass of solution) of the used solution was determined by measuring the photon radiation with a 4π-ionization chamber. The 4π-ionization chamber is a secondary-standard measuring system calibrated by activity standards from primary standardization of the PTB. The activity of the source follows from the specific activity and the mass of the dispensed solution, which was determined by weighing the pipette prior to and after dispensation of the solution.*
Aktivität: *Activity*	A = (17,41 ± 0,25) kBq
Bezugszeitpunkt: *Reference date*	1. März 2008, 00:00 Uhr MEZ *00:00 CET on 1 March 2008*

PHYSIKALISCH-TECHNISCHE BUNDESANSTALT 18

Radioaktive Verunreinigungen:
Radioactive impurities

Die zur Herstellung des Präparats benutzte Lösung wurde mit einem kalibrierten Halbleiterspektrometer auf gammastrahlende radioaktive Verunreinigungen geprüft. Dabei wurde Eu-154 mit folgendem Aktivitätsanteil nachgewiesen:

$A(\text{Eu-154})/A(\text{Eu-152}) = (2{,}8 \pm 0{,}4)\cdot 10^{-3}$

am Bezugszeitpunkt.

Die oben angegebene Aktivität bezieht sich allein auf Eu-152.

The solution used for the preparation of the source was checked for gamma-emitting radioactive impurities using a calibrated semiconductor spectrometer. The following activity portion of Eu-154 was detected:

$A(\text{Eu-154})/A(\text{Eu-152}) = (2{,}8 \pm 0{,}4)\cdot 10^{-3}$

at the reference date.

The above stated activity refers to Eu-152 only.

Messunsicherheit:
Uncertainty of measurement

Angegeben ist die erweiterte Messunsicherheit, die sich aus der Standardmessunsicherheit durch Multiplikation mit dem Erweiterungsfaktor $k = 2$ ergibt. Sie wurde gemäß dem *"Guide to the Expression of Uncertainty in Measurement"* (ISO, 1995) ermittelt. Der Wert der Messgröße liegt im Regelfall mit einer Wahrscheinlichkeit von annähernd 95 % im zugeordneten Werteintervall.

The uncertainty stated is the expanded uncertainty obtained by multiplying the standard uncertainty by the coverage factor k = 2. It has been determined in accordance with the "Guide to the Expression of Uncertainty in Measurement" (ISO, 1995). Normally, the value of the measurand lies within the assigned range of values with a coverage probability of approximately 95%.

ISO-Klassifikation:
ISO classification

ISO/C 11111 gemäß DIN 25426-1 und ISO 2919.
ISO/C 11111 in compliance with DIN 25426-1 and ISO 2919.

PHYSIKALISCH-TECHNISCHE BUNDESANSTALT 18

Physikalisch-Technische Bundesanstalt

Dichtheitsprüfung
Leakage test

ausgeführt am: *Date of test*	18. Februar 2008 *18 February 2008*
Prüfverfahren: *Method of test*	Wischprüfung gemäß DIN 25426-3. *Wipe test in compliance with DIN 25426-3.*
Ergebnis: *Result of test*	Die Aktivität der Wischprobe war zum Zeitpunkt der Probenahme kleiner als 4 Bq. *The activity of the wipe sample was less than 4 Bq at the time of sampling.* Die Umhüllung des Präparates ist dicht und kontaminationsfrei. *The cover of the source is leakproof and free of radioactive contamination.*

PHYSIKALISCH-TECHNISCHE BUNDESANSTALT 18

Die Physikalisch-Technische Bundesanstalt (PTB) in Braunschweig und Berlin ist das nationale Metrologieinstitut und die technische Oberbehörde der Bundesrepublik Deutschland für das Messwesen und Teile der Sicherheitstechnik. Die PTB gehört zum Dienstbereich des Bundesministeriums für Wirtschaft und Technologie. Sie erfüllt die Anforderungen an Kalibrier- und Prüflaboratorien auf der Grundlage der DIN EN ISO/IEC 17025.

Zentrale Aufgabe der PTB ist es, die gesetzlichen Einheiten in Übereinstimmung mit dem Internationalen Einheitensystem (SI) darzustellen, zu bewahren und – insbesondere im Rahmen des gesetzlichen und industriellen Messwesens – weiterzugeben. Die PTB steht damit an oberster Stelle der metrologischen Hierarchie in Deutschland. Kalibrierscheine der PTB dokumentieren die Rückführung des Kalibriergegenstandes auf nationale Normale.

Zur Sicherstellung der weltweiten Einheitlichkeit der Maße arbeitet die PTB mit anderen nationalen metrologischen Instituten auf regionaler europäischer Ebene in EUROMET und auf internationaler Ebene im Rahmen der Meterkonvention zusammen. Das Ziel wird durch einen intensiven Austausch von Forschungsergebnissen und durch umfangreiche internationale Vergleichsmessungen erreicht.

The Physikalisch-Technische Bundesanstalt *(PTB) in Braunschweig and Berlin is the National Metrology Institute and the highest technical authority of the Federal Republic of Germany for the field of metrology and certain sectors of safety engineering. The PTB comes under the auspices of the Federal Ministry of Economics and Technology. It meets the requirements for calibration and testing laboratories as defined in the EN ISO/IEC 17025.*

It is fundamental task of the PTB to realize and maintain the legal units in compliance with the International System of Units (SI) and to disseminate them, above all within the framework of legal and industrial metrology. The PTB thus is on top of the metrological hierarchy in Germany. Calibration certificates issued by it document that the object calibrated is traceable to national standards.

To ensure worldwide coherence of measures, the PTB cooperates with other national metrology institutes within EUROMET on the regional European level and on the international level within the framework of the Metre Convention. The aim is achieved by an intensive exchange of results of research work carried out and by comprehensive international comparison measurements.

Physikalisch-Technische Bundesanstalt

Braunschweig und Berlin

Empfohlene Radionukliddaten

Stand: 01.08.1999

Radionuklid: Eu-152

Halbwertszeit: $T_{½}$ = 4943(5) Tage [13,534 (14) Jahre]

Photonen-Energien *E* und –Emissionswahrscheinlichkeiten *p* pro Zerfall:

Strahlungs-typ	*E* in keV	*p*	Kommentar
Sm-L	6,0	0,127(7)	
Gd-L	6,5	0,00163(8)	
Sm-K_{α_2}	39,52	0,211(7)	
Sm-K_{α_1}	40,12	0,380(11)	
Gd-K_{α_2}	42,31	0,00233(11)	
Gd-K_{α_1}	43,00	0,00415(19)	
Sm-K_{β_1}	45,4	0,119(4)	
Sm-K_{β_2}	46,6	0,0296(8)	
Gd-K_{β_1}	48,7	0,00141(15)	
Gd-K_{β_2}	50,0	0,000355(4)	
γ	121,78	0,2858(9)	
γ	244,70	0,07580(30)	
γ	295,94	0,00447(6)	
γ	329,43	0,00128(8)	
γ	344,28	0,265(6)	
γ	367,79	0,00861(11)	
γ	411,12	0,02234(25)	
γ	443,96	0,03148(20)	Doppellinie
γ	488,68	0,00419(4)	
γ	503,47	0,00149(9)	
γ±	511,00	0,00030(9)	Vernichtungsstrahlung
γ	563,99	0,00489(7)	
γ	566,44	0,0013(4)	
γ	586,26	0,00459(8)	
γ	656,49	0,0014(5)	
γ	674,67	0,00189(5)	Doppellinie
γ	678,0	0,0198(7)	

Physikalisch-Technische Bundesanstalt

Braunschweig und Berlin

AKTIVITÄTSNORMAL
PUNKTFÖRMIGES PRÄPARAT MIT PHOTONENSTRAHLUNG

Beschreibung, Hinweise

Das vorliegende Aktivitätsnormal, ein punktförmiges Präparat mit Photonenstrahlung, ist in erster Linie für die Kalibrierung von Messanordnungen mit Halbleiterdetektoren vorgesehen. Beim Aufbau des Präparates wurde auf möglichst geringe Absorption und Streuung der Strahlung geachtet. Die radioaktive Substanz liegt in Form einer sehr dünnen Schicht vor, die sich auf einer Kreisfläche von weniger als 5 mm Durchmesser in der Mitte zwischen zwei runden Polyethylen-Folien von je $(21{,}3 \pm 1{,}8)$ mg·cm^{-2} flächenbezogener Masse befindet. Durch Erhitzen unter Druck werden die beiden Folien auf ihrer gesamten Fläche dicht miteinander verschweißt. Zur leichteren Handhabung ist die Präparatfolie in einem Aluminium-Ring von 30 mm Durchmesser gefasst, aus dem sie bei Bedarf durch Abheben des Sprengrings entnommen werden kann.

Da bei dem vorgesehenen Verwendungszweck die mechanische Beanspruchung gering ist, kann das Präparat als umschlossener radioaktiver Stoff im Sinne der Strahlenschutzverordnung angesehen werden. Es ist jedoch darauf zu achten, dass das Präparat nicht starken Lösungsmitteln oder Temperaturen oberhalb von 100 °C ausgesetzt wird. Vor ihrer Auslieferung werden die Präparate durch Wischtest auf Dichtheit und Kontaminationsfreiheit geprüft; eine Freigabe erfolgt nur dann, wenn die Aktivität der Wischprobe 20 Bq nicht übersteigt. Bei ^{60}Co-, ^{134}Cs-, ^{137}Cs-, ^{152}Eu- und ^{241}Am-Präparaten mit Aktivitäten $A > 200$ kBq kann die Polyethylenfolie nach einigen Jahren infolge von Strahlenschäden brüchig werden. Es wird deshalb empfohlen, diese Präparate nach längerer Lagerung vor der Entnahme aus dem Lager einer Sichtprüfung und vor der Wiederverwendung einer Dichtheitsprüfung zu unterziehen.

Auf dem Kalibrierschein wird die Aktivität A des Präparats für ein Referenzdatum angegeben. Die für den Gebrauch des Präparats wesentlichen Zerfallsdaten (Halbwertszeit $T_{1/2}$ und Photonen-Emissionswahrscheinlichkeiten p) sind auf dem beigefügten Datenblatt zusammengestellt. Sie wurden entweder in der PTB gemessen oder den neuesten Datenwerken entnommen [1]. Die häufig interessierende Emissionsrate B für Photonen einer bestimmten Energie, d. h. die auf ein Zeitintervall bezogene Anzahl der in dem Zeitintervall erzeugten Photonen, ergibt sich gemäß $B = p \cdot A$. Die so errechneten Emissionsraten berücksichtigen nicht die Strahlenabschwächung in der Polyethylen-Folie, die allerdings in den meisten Fällen zu vernachlässigen ist. Der Korrektionsfaktor K_F für senkrecht zur Präparatfläche austretende Strahlung kann aus der Abbildung entnommen werden.

SPECTECH **SPECTRUM TECHNIQUES**

106 Union Valley Road
Oak Ridge, TN 37830 USA
Tel. 865-482-9937
Fax. 865-483-0473
E-mail: sales@spectrumtechniques.com
Web site: www.spectrumtechniques.com

SOURCE DATA SHEET

PART NUMBER: S-PTC SOURCE SET

Purchase Order Number: 14/068/12-AT

Nuclide	Activity(+/- 20%)	Reference Date	Serial Number
Cd-109	1.0 uCi (37 kBq)	30614	1
462.6 days			
Co-57	1.0 uCi (37 kBq)	30614	2
271.8 days			
Cs-137	0.25 uCi (9.25 kBq)	30614	3
30.1 yrs			
Mn-54	1.0 uCi (37 kBq)	30614	4
312.3 days			
Sn-113	1.0 uCi (37 kBq)	30614	5
115.09 days			
Zn-65	1.0 uCi (37 kBq)	30614	6
244.3 days			

PKTST 19
PKTST 20
PKTST 21
PKTST 22
PKTST 23
PKTST 24

The source is of sealed construction and wipe tested for surface contamination and leakage.
This is to certify that the enclosed Check Sources were manufactured by Spectrum Techniques.
Sources are manufactured in Oak Ridge, Anderson County, Tennessee, USA.

Certified by: *Larry Webb* **Date:** 6-Mar-14

Physikalisch-Technische Bundesanstalt

Braunschweig und Berlin

Kalibrierschein

Calibration Certificate

Gegenstand: *Object:*	Aktivitätsnormal *Activity standard*
Hersteller: *Manufacturer:*	Physikalisch-Technische Bundesanstalt Fachbereich 6.1
Typ: *Type:*	Punktförmiges Präparat *Point source*
Kenn-Nummer: *Serial No.:*	2014-1348
Auftraggeber: *Applicant:*	Bundesamt für Eich- und Vermessungswesen (BEV) 2444 Seibersdorf Austria
Anzahl der Seiten: *Number of pages:*	4
Geschäftszeichen: *Reference No.:*	PTB-6.11-273/15.2014
Kalibrierzeichen: *Calibration mark:*	PTB-6.11-2014-1348
Datum der Kalibrierung: *Date of calibration:*	23.07.2014

Im Auftrag
On behalf of PTB

Dr. K. Kossert

Braunschweig, 23.07.2014

Siegel
Seal

PHYSIKALISCH-TECHNISCHE BUNDESANSTALT 18

Im Auftrag
On behalf of PTB

M. Ehlers

Gegenstand: *Object*	Aktivitätsnormal *Activity standard*
Typ: *Type*	Punktförmiges Präparat *Point source*
Kenn-Nummer: *Serial number*	2014-1348
Radionuklid: *Radionuclide*	Cobalt-57 *Cobalt-57*
Abdeckfolie: *Backing*	Polyester, beidseitig (2,20 ± 0,07) mg·cm^{-2} *Polyester, (2.20 ± 0.07) mg·cm^{-2} on both sides*
Kalibrierverfahren: *Method of calibration*	Das Präparat wurde durch Aufbringen einer radioaktiven Lösung auf die Präparatunterlage mit Hilfe einer Pipette hergestellt. Die spezifische Aktivität der verwendeten Lösung wurde durch Messung der Photonenstrahlung mit einer 4π-Ionisationskammer bestimmt. Die 4π-Ionisationskammer ist eine Sekundärnormal-Messeinrichtung, kalibriert mit Aktivitätsnormalen der PTB. Die Aktivität des Präparates ergibt sich aus der spezifischen Aktivität und der Masse der aufgebrachten Lösung, die durch Wägung der Pipette vor und nach dem Aufbringen ermittelt wurde. *The source was prepared by dispensing a radioactive solution to the source backing by means of a pipette. The specific activity (activity divided by mass of solution) of the used solution was determined by measuring the photon radiation with a 4π ionization chamber. The 4π ionization chamber is a secondary-standard measuring system calibrated by means of activity standards of PTB. The activity of the source follows from the specific activity and the mass of the dispensed solution, which was determined by weighing the pipette prior to and after dispensing the solution.*
Aktivität: *Activity*	A = (104,8 ± 1,1) kBq
Bezugszeitpunkt: *Reference date*	1. Juli 2014, 00:00 Uhr MEZ *00:00 CET on 1 July 2014*

PHYSIKALISCH-TECHNISCHE BUNDESANSTALT 18

Messunsicherheit:
Uncertainty of measurement

Angegeben ist die erweiterte Messunsicherheit, die sich aus der Standardmessunsicherheit durch Multiplikation mit dem Erweiterungsfaktor $k = 2$ ergibt. Sie wurde gemäß dem „Guide to the Expression of Uncertainty in Measurement (GUM)" ermittelt. Der Wert der Messgröße liegt dann im Regelfall mit einer Wahrscheinlichkeit von annähernd 95 % im zugeordneten Überdeckungsintervall.

The uncertainty stated is the expanded measurement uncertainty obtained by multiplying the standard measurement uncertainty by the coverage factor k = 2. It has been determined in accordance with the "Guide to the Expression of Uncertainty in Measurement (GUM)". The value of the measurand then normally lies, with a probability of approximately 95 %, within the attributed coverage interval.

ISO-Klassifikation:
ISO classification

ISO/12/C11111 gemäß DIN 25426-1 und ISO 2919.
ISO/12/C11111 in compliance with DIN 25426-1 and ISO 2919.

Dichtheitsprüfung
Leakage test

ausgeführt am:
Date of test

22. Juli 2014
22 July 2014

Prüfverfahren:
Method of test

Wischprüfung gemäß DIN 25426-3.
Wipe test in compliance with DIN 25426-3.

Ergebnis:
Result of test

Die Aktivität der Wischprobe war zum Zeitpunkt der Probenahme kleiner als 4 Bq.

The activity of the wipe sample was less than 4 Bq at the time of sampling.

Die Umhüllung des Präparates ist dicht und kontaminationsfrei.

The cover of the source is leakproof and free of radioactive contamination.

PHYSIKALISCH-TECHNISCHE BUNDESANSTALT 18

Die Physikalisch-Technische Bundesanstalt (PTB) in Braunschweig und Berlin ist das nationale Metrologieinstitut und die technische Oberbehörde der Bundesrepublik Deutschland für das Messwesen. Die PTB gehört zum Geschäftsbereich des Bundesministeriums für Wirtschaft und Energie. Sie erfüllt die Anforderungen an Kalibrier- und Prüflaboratorien auf der Grundlage der DIN EN ISO/IEC 17025.

Zentrale Aufgabe der PTB ist es, die gesetzlichen Einheiten in Übereinstimmung mit dem Internationalen Einheitensystem (SI) darzustellen, zu bewahren und weiterzugeben. Die PTB steht damit an oberster Stelle der metrologischen Hierarchie in Deutschland. Die Kalibrierscheine der PTB dokumentieren eine auf nationale Normale rückgeführte Kalibrierung.

Dieser Ergebnisbericht ist in Übereinstimmung mit den Kalibrier- und Messmöglichkeiten (CMCs), wie sie im Anhang C des gegenseitigen Abkommens (MRA) des Internationalen Komitees für Maße und Gewichte enthalten sind. Im Rahmen des MRA wird die Gültigkeit der Ergebnisberichte von allen teilnehmenden Instituten für die im Anhang C spezifizierten Messgrößen, Messbereiche und Messunsicherheiten gegenseitig anerkannt (nähere Informationen unter http://www.bipm.org).

CIPM MRA

The Physikalisch-Technische Bundesanstalt *(PTB) in Braunschweig and Berlin is the National Metrology Institute and the supreme technical authority of the Federal Republic of Germany for metrology. The PTB comes under the auspices of the Federal Ministry of Economics and Energy. It meets the requirements for calibration and testing laboratories as defined in DIN EN ISO/IEC 17025.*

The central task of PTB is to realize, to maintain and to disseminate the legal units in compliance with the International System of Units (SI). PTB thus is at the top of the metrological hierarchy in Germany. The calibration certificates issued by PTB document a calibration traceable to national measurement standards.

This certificate is consistent with the Calibration and Measurement Capabilities (CMCs) that are included in Appendix C of the Mutual Recognition Arrangement (MRA) drawn up by the International Committee for Weights and Measures (CIPM). Under the MRA, all participating institutes recognize the validity of each other's calibration and measurement certificates for the quantities, ranges and measurement uncertainties specified in Appendix C (for details, see http://www.bipm.org).

Physikalisch-Technische Bundesanstalt

Braunschweig und Berlin

Empfohlene Radionukliddaten

Stand: 01.01.2005

Radionuklid: Co-57

Halbwertszeit: $T_{½}$ = 271,83(8) Tage

Photonen-Energien *E* und –Emissionswahrscheinlichkeiten *p*:

Strahlungs-typ	*E* in keV	*p*	Kommentar
Fe-L	0,71	0,0127(21)	
Fe-K_α	6,40	0,510(7)	
Fe-K_β	7,06	0,069(1)	
γ	14,41	0,0916(15)	
γ	122,06	0,8560(17)	
γ	136,47	0,1068(8)	
γ	230,40	0,0000040(12)	
γ	339,69	0,000037(11)	
γ	352,33	0,000030(9)	
γ	366,80	0,000012(4)	
γ	570,09	0,00016(5)	
γ	692,41	0,00149(10)	
γ	706,54	0,000050(15)	

Messunsicherheiten:
Die Ziffern in Klammern hinter dem Zahlenwert einer Messgröße geben die Messunsicherheit in der(n) letzten Stelle(n) des Zahlenwertes an. Die Messunsicherheiten entsprechen der einfachen Standardabweichung.

Literatur:
Schötzig, U. und Schrader, H.:
Halbwertszeiten und Photonen-Emissionswahrscheinlichkeiten von häufig verwendeten Radionukliden, 5. erweiterte und korrigierte Auflage; PTB-Bericht PTB-Ra-16/5, Braunschweig, Mai 2000, ISBN 3-89701-279-0

Physikalisch-Technische Bundesanstalt

Braunschweig und Berlin

AKTIVITÄTSNORMAL
PUNKTFÖRMIGES PRÄPARAT MIT NIEDERENERGETISCHER PHOTONENSTRAHLUNG

Beschreibung, Hinweise

Das vorliegende Aktivitätsnormal, ein punktförmiges Präparat mit niederenergetischer Photonenstrahlung, ist in erster Linie für die Kalibrierung von Messanordnungen mit Halbleiterdetektoren bis herab zu etwa 5 keV vorgesehen.

Beim Aufbau des Präparats wurde auf möglichst geringe Absorption und Streuung der Strahlung geachtet. Die radioaktive Substanz liegt in Form einer sehr dünnen Schicht vor, die sich auf einer Kreisfläche von weniger als 5 mm Durchmesser in der Mitte zwischen zwei runden Polyester-Folien von je (2,20 ± 0,07) $mg \cdot cm^{-2}$ flächenbezogener Masse befindet. Durch Erhitzen unter Druck wurden die beiden Folien auf ihrer gesamten Fläche dicht miteinander verschweißt.

Da bei dem vorgesehenen Verwendungszweck die mechanische Beanspruchung gering ist, kann das Präparat als umschlossener radioaktiver Stoff im Sinne der Strahlenschutzverordnung angesehen werden. Es ist jedoch darauf zu achten, dass das Präparat nicht starken Lösungsmitteln oder Temperaturen oberhalb von 100 °C ausgesetzt wird. Vor der Auslieferung werden die Präparate durch Wischtest auf Dichtheit und Kontaminationsfreiheit geprüft; eine Freigabe erfolgt nur dann, wenn die Aktivität der Wischprobe 20 Bq nicht übersteigt.

Die im Kalibrierschein angegebene Aktivität A wurde entweder aus der Masse und der spezifischen Aktivität der aufgetropften radioaktiven Lösung oder aus dem Vergleich mit einem gleichartigen Aktivitätsnormal mittels einer geeigneten Sekundärmesseinrichtung bestimmt.

Aus der Aktivität lässt sich die Emissionsrate B für Photonen, d. h. die auf ein Zeitintervall bezogene Anzahl der in dem Zeitintervall **erzeugten** Photonen, gemäß $B = p \cdot A$ bestimmen; dabei ist p die Photonen-Emissionswahrscheinlichkeit.

Ein Teil der emittierten niederenergetischen Photonen wird beim Durchgang durch die radioaktive Substanz und die Präparatfolien absorbiert oder gestreut. Absorption und Streuung sind umso größer, je kleiner die Energie ist. Der Photonenfluss Φ, d. h. die auf ein Zeitintervall bezogene Anzahl der in diesem Zeitintervall aus dem Präparat **austretenden** Photonen, ist somit kleiner als die Emissionsrate und außerdem abhängig von der Durchstrahlungsrichtung. In der Richtung senkrecht zur Präparatunterlage ist der Einfluss der radioaktiven Substanz und der Präparatfolien am geringsten und abschätzbar.

Tabelle: Korrektionsfaktoren K_F für Strahlabschwächung in der Folie.

Radio-nuklid	Strahlungs-typ	Energie in keV	K_F
Cr-51	V-K_α	4,95	1,065
	V-K_β	5,43	1,049
Mn-54	Cr-K_α	5,41	1,050
	Cr-K_β	5,95	1,037
Fe-55	Mn-K_α	5,89	1,038
	Mn-K_β	6,49	1,028
Co-57	Fe-K_α	6,40	1,030
	Fe-K_β	7,06	1,022
Zn-65	Cu-K_α	8,04	1,015
	Cu-K_β	8,91	1,011
Sr-85	Rb-K_α	13,37	1,003
	Rb-K_β	15,0	1,003
Nb-93m	Nb-K_α	16,58	1,002
	Nb-K_β	18,7	<1,002
		17,0	<1,002
		24,0	<1,001

Die Korrektionsfaktoren für die Schwächung in der radioaktiven Substanz lassen sich nur schwer abschätzen. Aufgrund von Vergleichen zwischen Präparaten der beschriebenen Art und Präparaten ohne Schwächung [2] kann angenommen werden, dass bei den angewandten Herstellungsverfahren je nach Radionuklid K_S für die Röntgenstrahlung zwischen 1,00 und 1,02 liegt.

Im beiliegenden Datenblatt sind für die in der Messpraxis relevanten Photonen des betreffenden Nuklids die Emissionswahrscheinlichkeiten zusammengestellt. Sie wurden entweder in der PTB gemessen, aus publizierten Daten evaluiert oder den neuesten Datenwerken entnommen [3].

Wichtiger Hinweis

Die Haltbarkeit dieses Präparates ist begrenzt. Erfahrungsgemäß sind besonders Am-241-Präparate (Alpha-Strahler) mit Aktivitäten über 50 kBq betroffen. Nach etwa einem halben Jahr wird die Folie im Bereich der radioaktiven Substanz brüchig, dieser Teil kann bei unsachgemäßer Handhabung sogar herausfallen. Die Unversehrtheit des Präparates sollte daher stets, vor allem während des Gebrauchs, durch Sichtprüfung überwacht werden.

MCNP (v5) calculations to estimate the effect of steel composition on the FEP efficiency

Detector: Ge5
Sample: Siempelkamp cast steel disk (r=1.74 cm h=0.98 cm ρ=7.55 g/cm^3)
Position: Sample on Ge5 end cup

Calculations were performed by changing the steel composition of the disk and keeping the density constant. The simulated compositions are given bellow.
The three last rows of the table correspond to IJS reported composition (normalised) with additional carbon content (of 4, 8 and 16 %).

	elemental weight fraction %																
steel composition	Fe	Cr	Mn	Mo	Ni	C	Si	S	P	**Cu**	**Al**	**Co**	Zn	Nb	Pb	Sn	V
Fe	100																
IJS	99.30	0.28	0.37	0.014													
S275	97.61		1.6			0.25	0.5	0.05	0.04								
S355	97.63		1.6			0.2	0.55	0.025	0.025								
high Cr steel	70.00	20			10												
IJS+C4%	95.33	0.269	0.355	0.01344		4											
IJS+C8%	91.36	0.258	0.340	0.01288		8											
IJS+C16%	83.41	0.235	0.311	0.01176		16											
VUHZ	98.623	0.2	0.3	0.03	0.16	0.16	0.21	0.049	0.018	0.2	0.04	0.01					
CIEMAT - Full	95.747	0.19	0.349	0.0213	0.107	3.1	0.339	0.058	0.0165	0.107	0.011	0.012	0.0378	0.0019	0.0048	0.00562	0.0039

Results 1.17 MeV			
composition	**FEP eff/ per gamma**	**relErr FEP eff**	**Err eff / per gamma**
Fe	0.027824	0.0019	0.00005
IJS	0.027827	0.0019	0.00005
S275	0.027825	0.0019	0.00005
S355	0.027826	0.0019	0.00005
High Cr steel	0.027819	0.0019	0.00005
IJS+C4%	0.027807	0.0019	0.00005
IJS+C8%	0.027785	0.0059	0.00016
IJS+C16%	0.027754	0.0059	0.00016
VUHZ-S355	0.027829	0.0059	0.000164
CIEMAT-full	0.027811	0.0019	0.00005

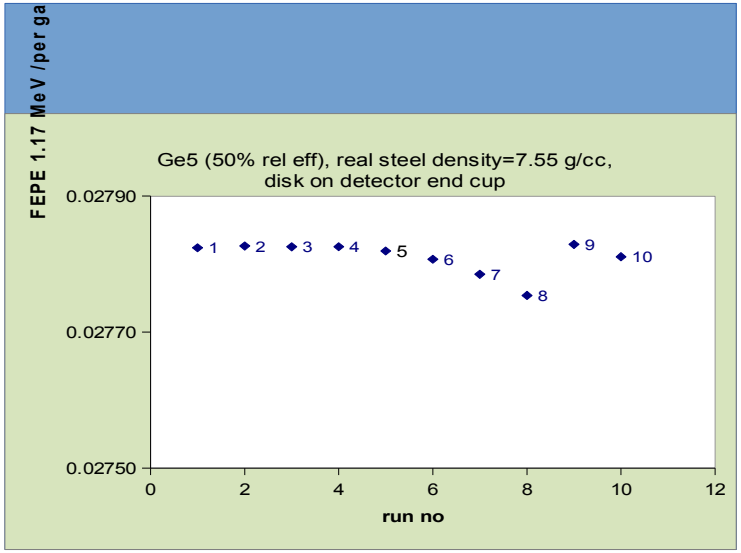

D. Geometry view of detector images

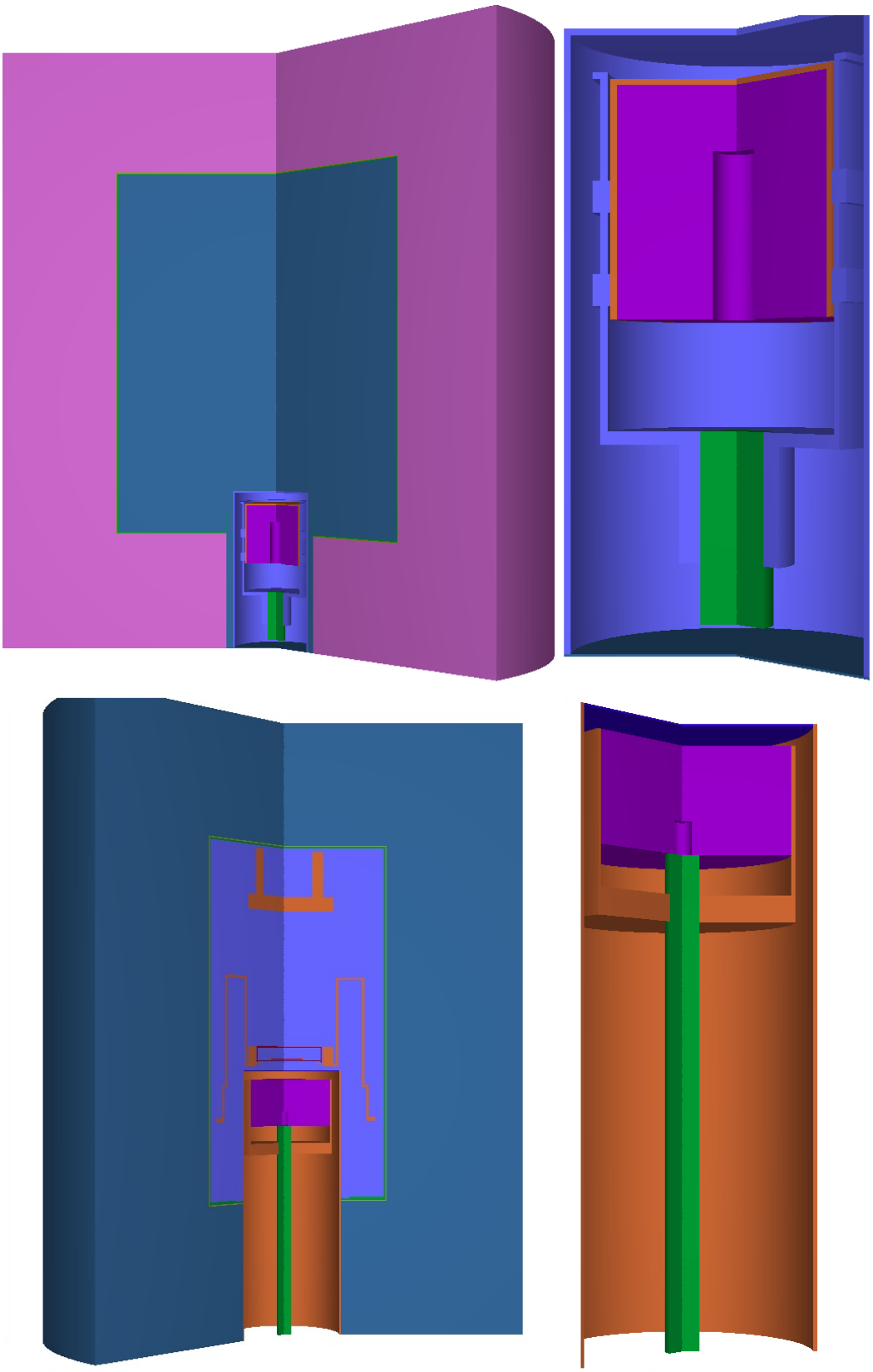

Figure D.1.: 3d detector overview, above: Seibersdorf detector, below: Arsenal detector

D.1. Arsenal detector

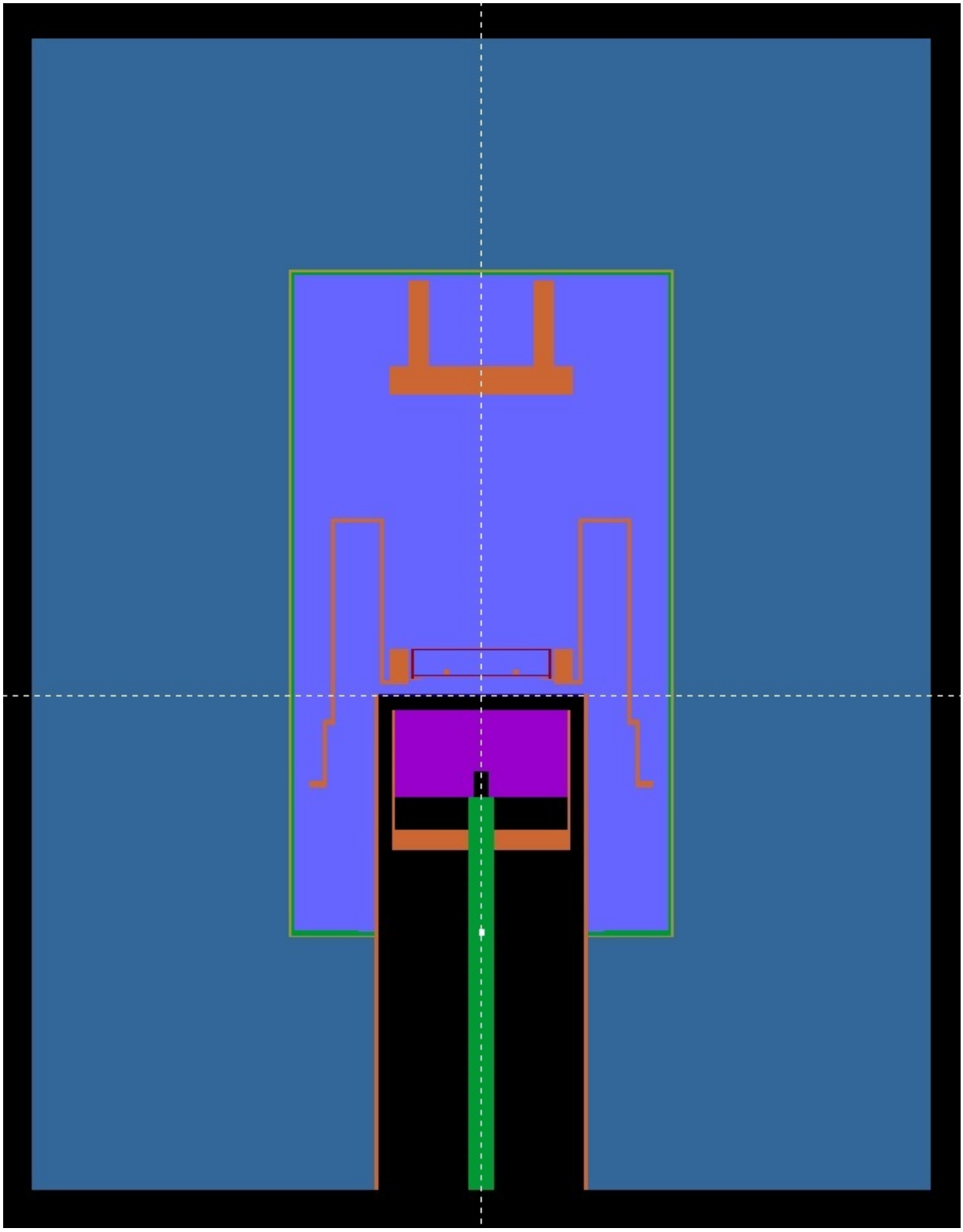

Figure D.2.: Arsenal detector 2d

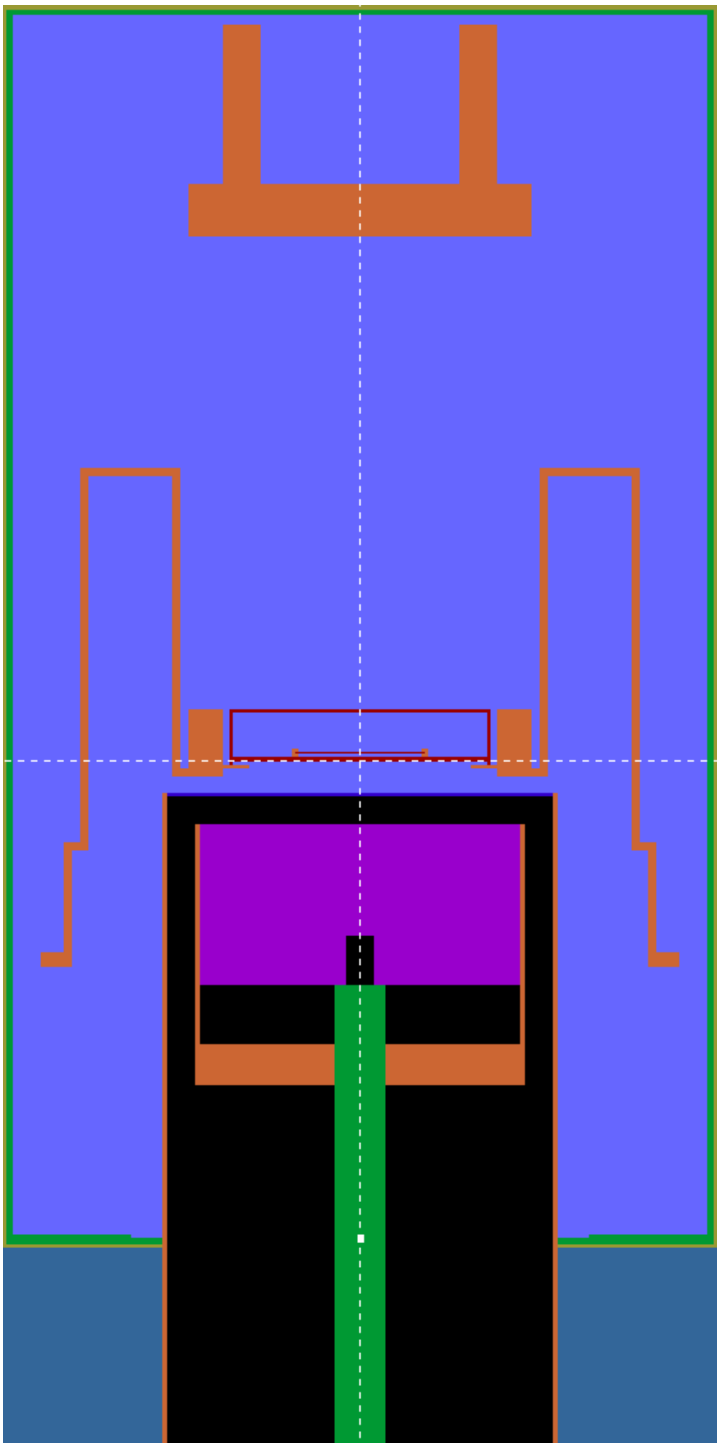

Figure D.3.: Close-up Arsenal detector 2d

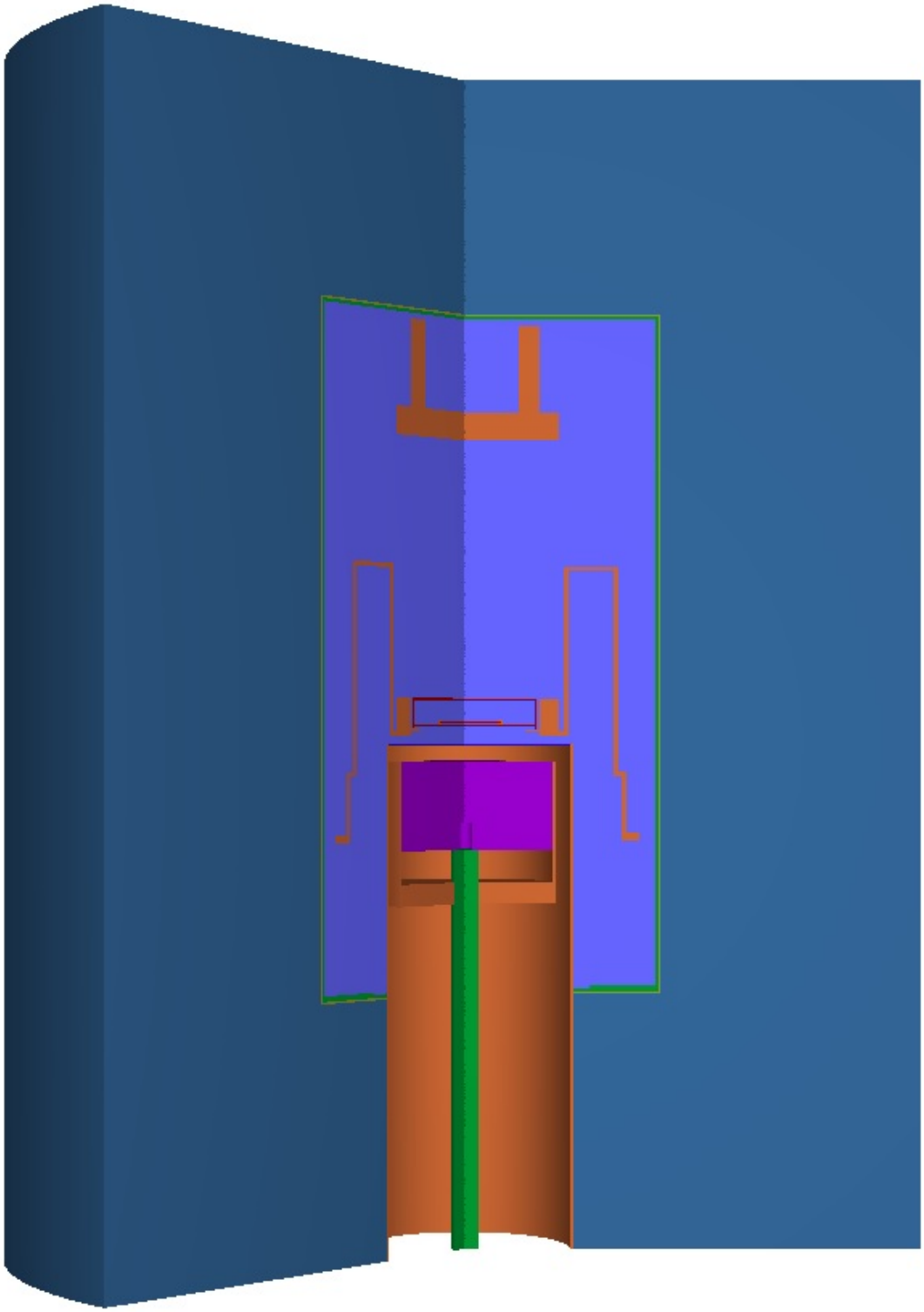

Figure D.4.: Arsenal detector 3d

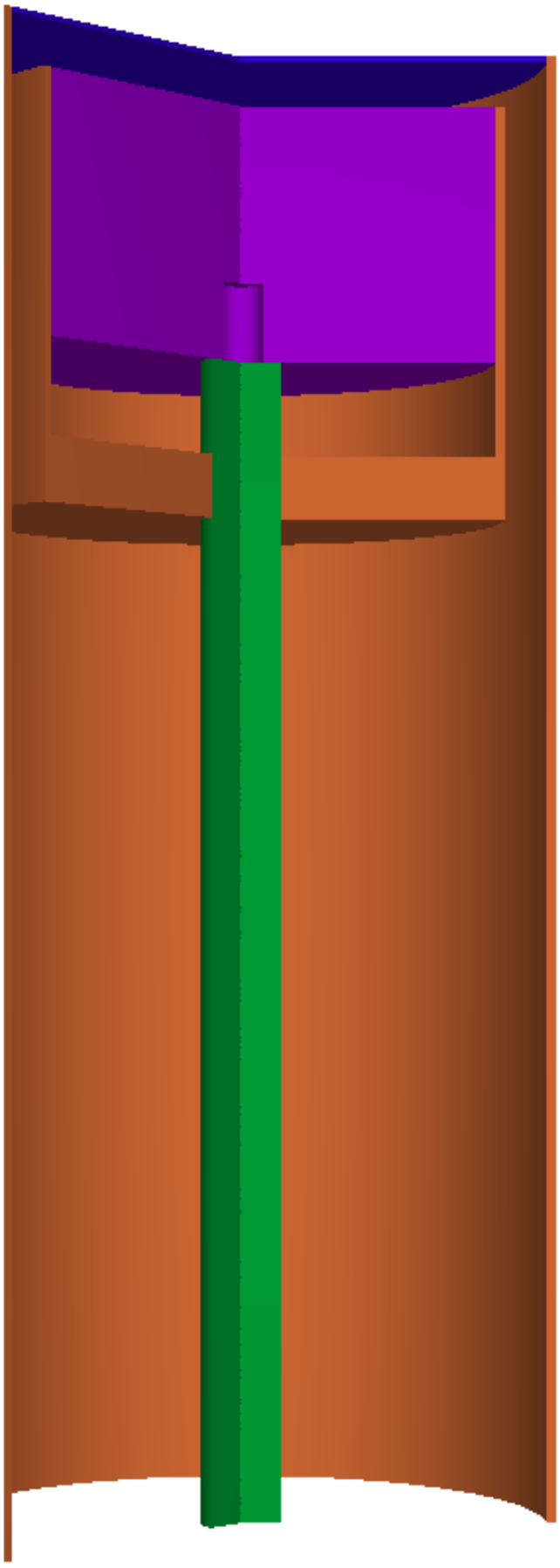

Figure D.5.: Close-up Arsenal detector 3d

D.2. Seibersdorf detector

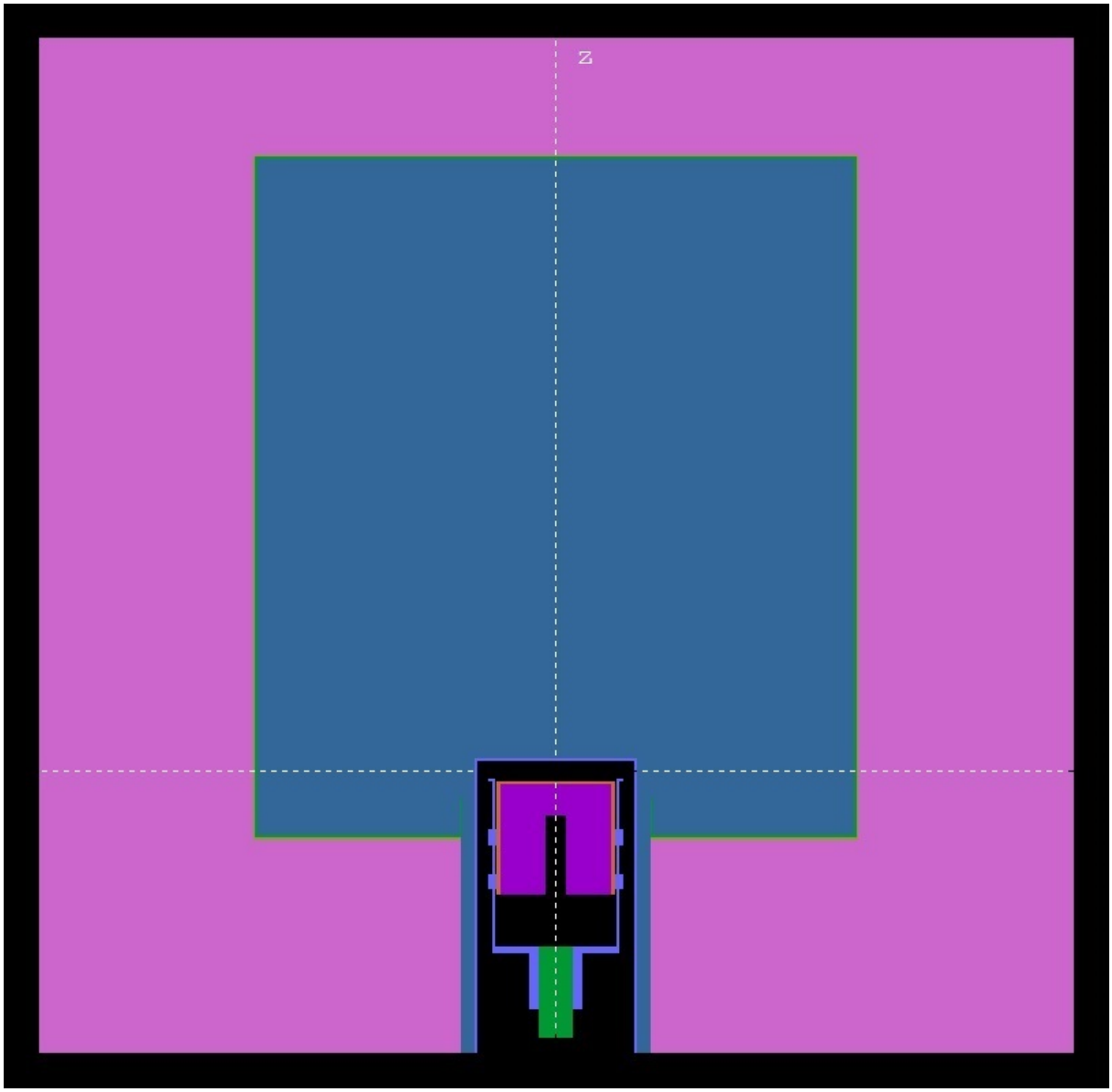

Figure D.6.: Seibersdorf detector 2d

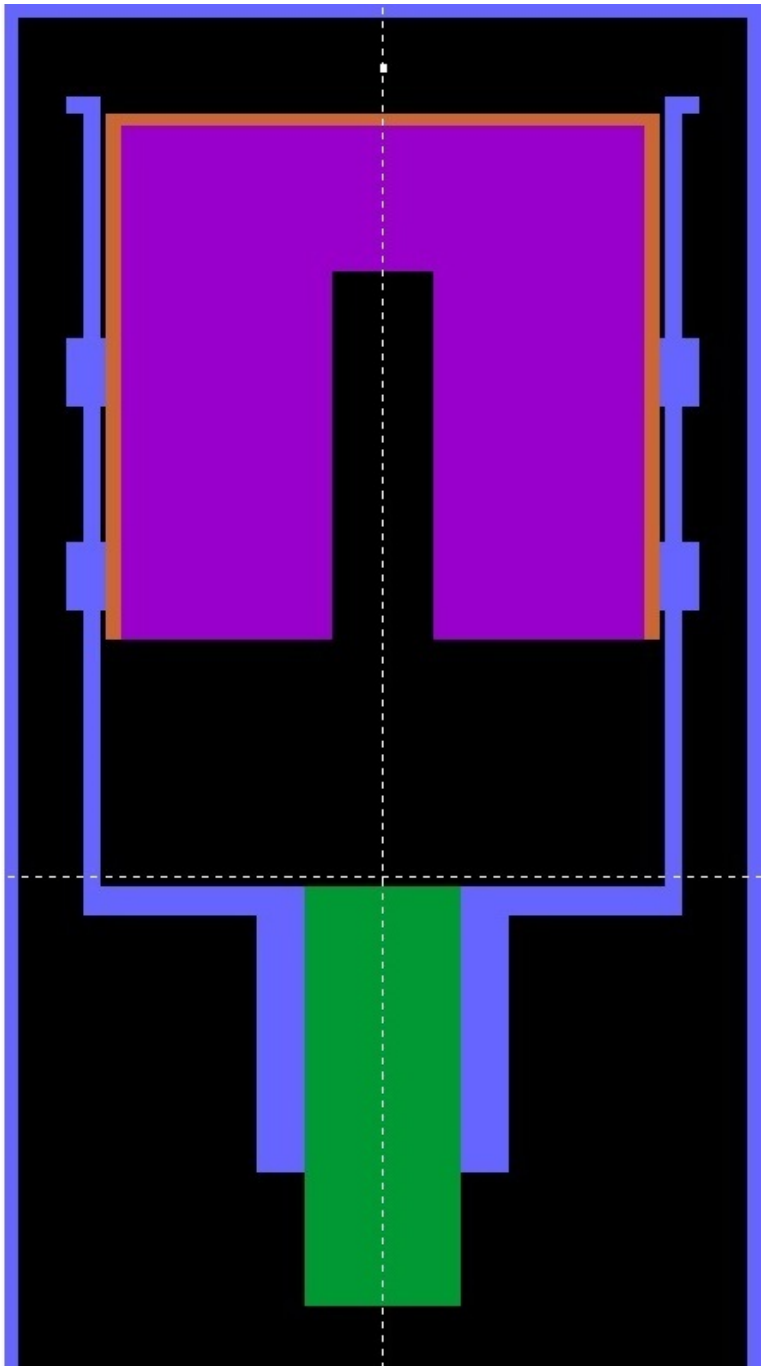

Figure D.7.: Close-up Seibersdorf detector 2d

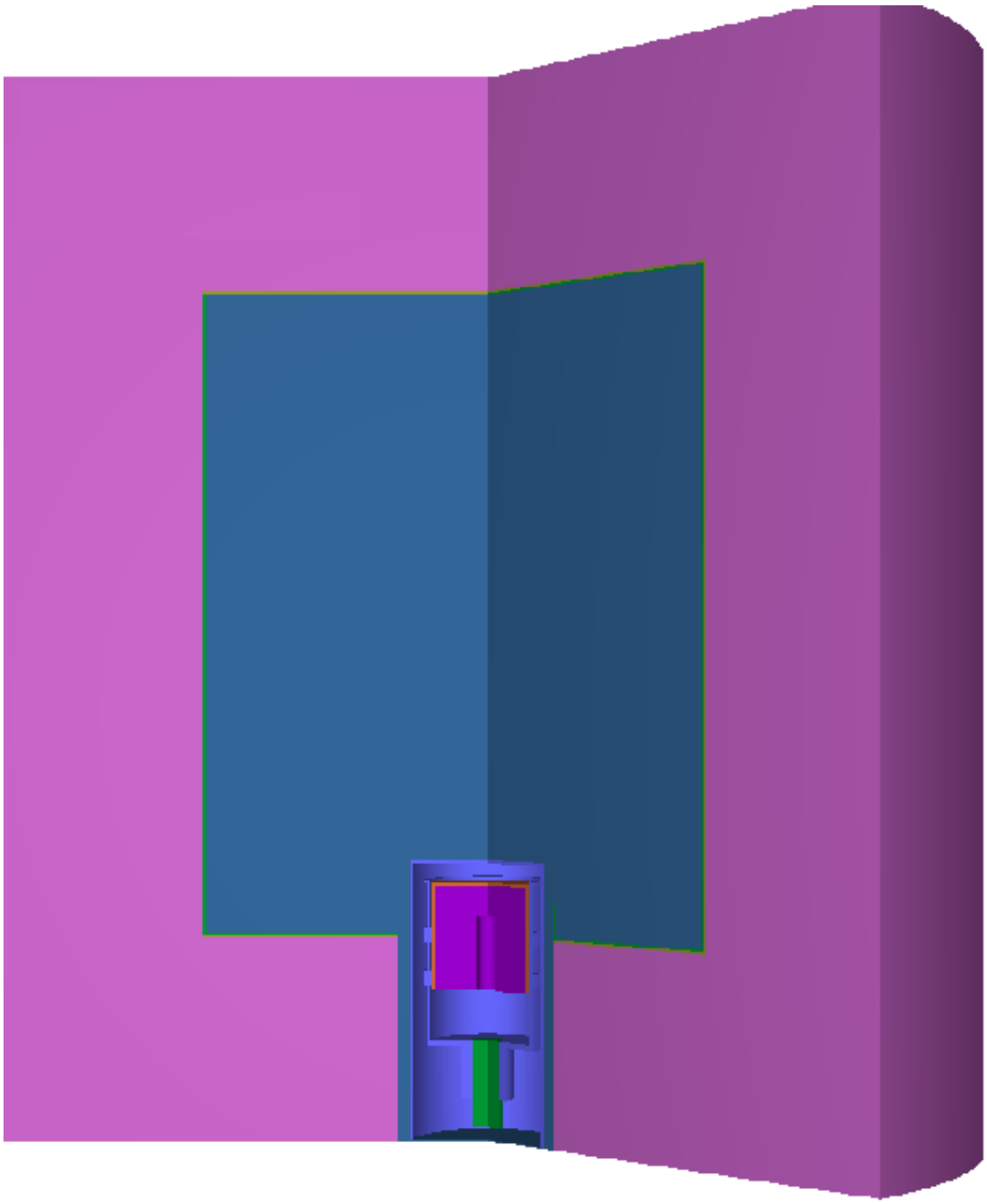

Figure D.8.: Seibersdorf detector 3d

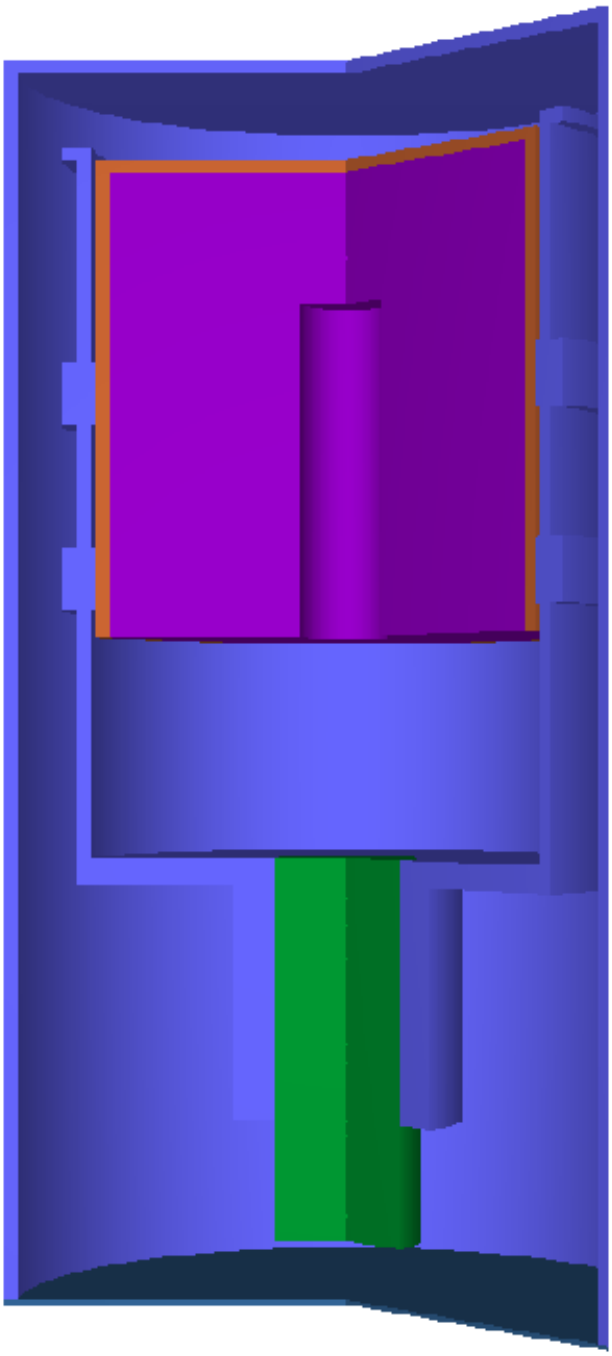

Figure D.9.: Close-up Seibersdorf detector 3d

E. PENELOPE 2011 sample in-files

```
TITLE  MetroMETAL fume dust sample, Cs-137 PQ, Seibersdorf
.
>>>>>>>> Source definition.
SKPAR  2                          [Primary particles: 1=electron, 2=photon, 3=positron]
SPECTR 6.6166e5  8.499e-1                      [E bin: lower-end and total probability]
SPECTR 6.6166e5 -1.0e0                         [E bin: lower-end and total probability]
SPOSIT 0 0 6.336
SBOX   6.95 6.95 1.872
SBODY  19
SCONE  0 0 180
.
>>>>>>>> Material data and simulation parameters.
MFNAME Ge.mat                                          [Material file, up to 20 chars]
MSIMPA 6.6E3 6.6E2  6.6E3 0.1 0.1 6.6E3  6.6E2                  [M,EABS,C1,C2,WCC,WCR]
MFNAME GeINAC.mat                                      [Material file, up to 20 chars]
MSIMPA 6.6E3 6.6E2  6.6E3 0.1 0.1 6.6E3  6.6E2                  [M,EABS,C1,C2,WCC,WCR]
MFNAME POLYSTYRENE.mat                                 [Material file, up to 20 chars]
MSIMPA 6.6E3 6.6E2  6.6E3 0.1 0.1 6.6E3  6.6E2                  [M,EABS,C1,C2,WCC,WCR]
MFNAME Cu.mat                                          [Material file, up to 20 chars]
MSIMPA 6.6E3 6.6E2  6.6E3 0.1 0.1 6.6E3  6.6E2                  [M,EABS,C1,C2,WCC,WCR]
MFNAME Be.mat                                          [Material file, up to 20 chars]
MSIMPA 6.6E3 6.6E2  6.6E3 0.1 0.1 6.6E3  6.6E2                  [M,EABS,C1,C2,WCC,WCR]
MFNAME Al.mat                                          [Material file, up to 20 chars]
MSIMPA 6.6E3 6.6E2  6.6E3 0.1 0.1 6.6E3  6.6E2                  [M,EABS,C1,C2,WCC,WCR]
MFNAME Cd.mat                                          [Material file, up to 20 chars]
MSIMPA 6.6E3 6.6E2  6.6E3 0.1 0.1 6.6E3  6.6E2                  [M,EABS,C1,C2,WCC,WCR]
MFNAME Air.mat                                         [Material file, up to 20 chars]
MSIMPA 6.6E3 6.6E2  6.6E3 0.1 0.1 6.6E3  6.6E2                  [M,EABS,C1,C2,WCC,WCR]
MFNAME Pb.mat                                          [Material file, up to 20 chars]
MSIMPA 6.6E3 6.6E2  6.6E3 0.1 0.1 6.6E3  6.6E2                  [M,EABS,C1,C2,WCC,WCR]
MFNAME fumedust.mat                                    [Material file, up to 20 chars]
MSIMPA 6.6E3 6.6E2  6.6E3 0.1 0.1 6.6E3  6.6E2                  [M,EABS,C1,C2,WCC,WCR]
.
>>>>>>>> Geometry definition file.
GEOMFN PQneu100.geo                                    [Geometry file, up to 20 chars]
.
>>>>>>>> Energy deposition detectors (up to 25).
ENDETC 0 6.6166e5 440                            [Energy window and number of bins]
EDSPC  spc-enddet-001.dat
EDBODY 2                                      [Active body; one line for each body]
EDBODY 3
.
>>>>>>>> Job properties
RESUME dump0.dmp                               [Resume from this dump file, 20 chars]
DUMPTO dump0.dmp                                 [Generate this dump file, 20 chars]
DUMPP  60                                                    [Dumping period, in sec]
.
NSIMSH 1.0e9                        [Desired number of simulated showers, max=2*31-1]
.
END                                                 [Ends the reading of input data]
```

```
TITLE  MetroMETAL slag sample, 226Ra HSlag13, 186 keV, Seibersdorf
.
>>>>>>>> Source definition.
SKPAR  2                          [Primary particles: 1=electron, 2=photon, 3=positron]
SPECTR 1.86211e5  1                             [E bin: lower-end and total probability]
SPECTR 1.86211e5 -1.0e0                         [E bin: lower-end and total probability]
SPOSIT 0 0 6.3185
SBOX   7.2 7.2 1.805
SBODY  19
SCONE  0 0 180
.
>>>>>>>> Material data and simulation parameters.
MFNAME Ge.mat                                          [Material file, up to 20 chars]
MSIMPA 1.9E3 1.9E2  1.9E3 0.1 0.1 1.9E3  1.9E2        [M,EABS,C1,C2,WCC,WCR]
MFNAME GeINAC.mat                                      [Material file, up to 20 chars]
MSIMPA 1.9E3 1.9E2  1.9E3 0.1 0.1 1.9E3  1.9E2                 [M,EABS,C1,C2,WCC,WCR]
MFNAME POLYSTYRENE.mat                                 [Material file, up to 20 chars]
MSIMPA 1.9E3 1.9E2  1.9E3 0.1 0.1 1.9E3  1.9E2                 [M,EABS,C1,C2,WCC,WCR]
MFNAME Cu.mat                                          [Material file, up to 20 chars]
MSIMPA 1.9E3 1.9E2  1.9E3 0.1 0.1 1.9E3  1.9E2                 [M,EABS,C1,C2,WCC,WCR]
MFNAME Be.mat                                          [Material file, up to 20 chars]
MSIMPA 1.9E3 1.9E2  1.9E3 0.1 0.1 1.9E3  1.9E2                 [M,EABS,C1,C2,WCC,WCR]
MFNAME Al.mat                                          [Material file, up to 20 chars]
MSIMPA 1.9E3 1.9E2  1.9E3 0.1 0.1 1.9E3  1.9E2                 [M,EABS,C1,C2,WCC,WCR]
MFNAME Cd.mat                                          [Material file, up to 20 chars]
MSIMPA 1.9E3 1.9E2  1.9E3 0.1 0.1 1.9E3  1.9E2                 [M,EABS,C1,C2,WCC,WCR]
MFNAME Air.mat                                         [Material file, up to 20 chars]
MSIMPA 1.9E3 1.9E2  1.9E3 0.1 0.1 1.9E3  1.9E2                 [M,EABS,C1,C2,WCC,WCR]
MFNAME Pb.mat                                          [Material file, up to 20 chars]
MSIMPA 1.9E3 1.9E2  1.9E3 0.1 0.1 1.9E3  1.9E2                 [M,EABS,C1,C2,WCC,WCR]
MFNAME slag.mat                                        [Material file, up to 20 chars]
MSIMPA 1.9E3 1.9E2  1.9E3 0.1 0.1 1.9E3  1.9E2                 [M,EABS,C1,C2,WCC,WCR]
.
>>>>>>>> Geometry definition file.
GEOMFN PQneu100.geo                                    [Geometry file, up to 20 chars]
.
>>>>>>>> Energy deposition detectors (up to 25).
ENDETC 0 1.86211e5 124                          [Energy window and number of bins]
EDSPC  spc-enddet-001.dat
EDBODY 2                                     [Active body; one line for each body]
EDBODY 3
.
>>>>>>>> Job properties
RESUME dump0.dmp                            [Resume from this dump file, 20 chars]
DUMPTO dump0.dmp                               [Generate this dump file, 20 chars]
DUMPP  60                                                  [Dumping period, in sec]
.
NSIMSH 1.0e9                                  [Desired number of simulated showers]
.
END                                                [Ends the reading of input data]
```

```
TITLE  MetroMETAL steel disk sample, Co-60, 1173 keV, Seibersdorf
.
>>>>>>>> Source definition.
SKPAR  2                          [Primary particles: 1=electron, 2=photon, 3=positron]
SPECTR 1.1732e6  1                              [E bin: lower-end and total probability]
SPECTR 1.1732e6 -1.0e0                          [E bin: lower-end and total probability]
SPOSIT 0 0 5.7015
SBOX   3.506 3.506 1.003
SBODY  19
SCONE  0 0 180
.
>>>>>>>> Material data and simulation parameters.
MFNAME Ge.mat                                          [Material file, up to 20 chars]
MSIMPA 1.2E4 1.2E3  1.2E4 0.1 0.1 1.2E4  1.2E3                  [M,EABS,C1,C2,WCC,WCR]
MFNAME GeINAC.mat                                      [Material file, up to 20 chars]
MSIMPA 1.2E4 1.2E3  1.2E4 0.1 0.1 1.2E4  1.2E3                  [M,EABS,C1,C2,WCC,WCR]
MFNAME POLYSTYRENE.mat                                 [Material file, up to 20 chars]
MSIMPA 1.2E4 1.2E3  1.2E4 0.1 0.1 1.2E4  1.2E3                  [M,EABS,C1,C2,WCC,WCR]
MFNAME Cu.mat                                          [Material file, up to 20 chars]
MSIMPA 1.2E4 1.2E3  1.2E4 0.1 0.1 1.2E4  1.2E3                  [M,EABS,C1,C2,WCC,WCR]
MFNAME Be.mat                                          [Material file, up to 20 chars]
MSIMPA 1.2E4 1.2E3  1.2E4 0.1 0.1 1.2E4  1.2E3                  [M,EABS,C1,C2,WCC,WCR]
MFNAME Al.mat                                          [Material file, up to 20 chars]
MSIMPA 1.2E4 1.2E3  1.2E4 0.1 0.1 1.2E4  1.2E3                  [M,EABS,C1,C2,WCC,WCR]
MFNAME Cd.mat                                          [Material file, up to 20 chars]
MSIMPA 1.2E4 1.2E3  1.2E4 0.1 0.1 1.2E4  1.2E3                  [M,EABS,C1,C2,WCC,WCR]
MFNAME Air.mat                                         [Material file, up to 20 chars]
MSIMPA 1.2E4 1.2E3  1.2E4 0.1 0.1 1.2E4  1.2E3                  [M,EABS,C1,C2,WCC,WCR]
MFNAME Pb.mat                                          [Material file, up to 20 chars]
MSIMPA 1.2E4 1.2E3  1.2E4 0.1 0.1 1.2E4  1.2E3                  [M,EABS,C1,C2,WCC,WCR]
MFNAME VUHZ.mat                                        [Material file, up to 20 chars]
MSIMPA 1.2E4 1.2E3  1.2E4 0.1 0.1 1.2E4  1.2E3                  [M,EABS,C1,C2,WCC,WCR]
.
>>>>>>>> Geometry definition file.
GEOMFN PQneu100.geo                                    [Geometry file, up to 20 chars]
.
>>>>>>>> Energy deposition detectors (up to 25).
ENDETC 0 1.1732e6 782                            [Energy window and number of bins]
EDSPC  spc-enddet-001.dat
EDBODY 2                                      [Active body; one line for each body]
EDBODY 3
.
>>>>>>>> Job properties
RESUME dump0.dmp                               [Resume from this dump file, 20 chars]
DUMPTO dump0.dmp                                  [Generate this dump file, 20 chars]
DUMPP  60                                                    [Dumping period, in sec]
.
NSIMSH 1.0e9                        [Desired number of simulated showers, max=2*31-1]
.
END                                                 [Ends the reading of input data]
```

```
TITLE  MetroMETAL steel disk sample, Co-60, 1332 keV, Seibersdorf
.
>>>>>>>> Source definition.
SKPAR  2                          [Primary particles: 1=electron, 2=photon, 3=positron]
SPECTR 1.3325e6  1                              [E bin: lower-end and total probability]
SPECTR 1.3325e6 -1.0e0                          [E bin: lower-end and total probability]
SPOSIT 0 0 5.7015
SBOX   3.506 3.506 1.003
SBODY  19
SCONE  0 0 180
.
>>>>>>>> Material data and simulation parameters.
MFNAME Ge.mat                                          [Material file, up to 20 chars]
MSIMPA 1.3E4 1.3E3  1.3E4 0.1 0.1 1.3E4  1.3E3                  [M,EABS,C1,C2,WCC,WCR]
MFNAME GeINAC.mat                                      [Material file, up to 20 chars]
MSIMPA 1.3E4 1.3E3  1.3E4 0.1 0.1 1.3E4  1.3E3                  [M,EABS,C1,C2,WCC,WCR]
MFNAME POLYSTYRENE.mat                                 [Material file, up to 20 chars]
MSIMPA 1.3E4 1.3E3  1.3E4 0.1 0.1 1.3E4  1.3E3                  [M,EABS,C1,C2,WCC,WCR]
MFNAME Cu.mat                                          [Material file, up to 20 chars]
MSIMPA 1.3E4 1.3E3  1.3E4 0.1 0.1 1.3E4  1.3E3                  [M,EABS,C1,C2,WCC,WCR]
MFNAME Be.mat                                          [Material file, up to 20 chars]
MSIMPA 1.3E4 1.3E3  1.3E4 0.1 0.1 1.3E4  1.3E3                  [M,EABS,C1,C2,WCC,WCR]
MFNAME Al.mat                                          [Material file, up to 20 chars]
MSIMPA 1.3E4 1.3E3  1.3E4 0.1 0.1 1.3E4  1.3E3                  [M,EABS,C1,C2,WCC,WCR]
MFNAME Cd.mat                                          [Material file, up to 20 chars]
MSIMPA 1.3E4 1.3E3  1.3E4 0.1 0.1 1.3E4  1.3E3                  [M,EABS,C1,C2,WCC,WCR]
MFNAME Air.mat                                         [Material file, up to 20 chars]
MSIMPA 1.3E4 1.3E3  1.3E4 0.1 0.1 1.3E4  1.3E3                  [M,EABS,C1,C2,WCC,WCR]
MFNAME Pb.mat                                          [Material file, up to 20 chars]
MSIMPA 1.3E4 1.3E3  1.3E4 0.1 0.1 1.3E4  1.3E3                  [M,EABS,C1,C2,WCC,WCR]
MFNAME VUHZ.mat                                        [Material file, up to 20 chars]
MSIMPA 1.3E4 1.3E3  1.3E4 0.1 0.1 1.3E4  1.3E3                  [M,EABS,C1,C2,WCC,WCR]
.
>>>>>>>> Geometry definition file.
GEOMFN PQneu100.geo                                    [Geometry file, up to 20 chars]
.
>>>>>>>> Energy deposition detectors (up to 25).
ENDETC 0 1.3325e6 888                            [Energy window and number of bins]
EDSPC  spc-enddet-001.dat
EDBODY 2                                    [Active body; one line for each body]
EDBODY 3
.
>>>>>>>> Job properties
RESUME dump1.dmp                           [Resume from this dump file, 20 chars]
DUMPTO dump0.dmp                              [Generate this dump file, 20 chars]
DUMPP  60                                                  [Dumping period, in sec]
.
NSIMSH 1.0e9                       [Desired number of simulated showers, max=2*31-1]
.
END                                                 [Ends the reading of input data]
```

F. Geometry composer files

Geometry Composer Report

Date: Wednesday, December 10, 2014
Description: Stahlzylinder_VUHZ
Comment: Stahlzylinder_VUHZ
File Name: C:\GENIE2K\isocs\data\GEOMETRY\Laboratory\CYLINDER_DISK_AND_POINT\getestet\Stahlzylinder\PTB\vuhz.geo
Software: LabSOCS
Template: CYLINDER_DISK_AND_POINT, Version: cylinder
Detector: B94028
Environment: Temperature= 22 C, Pressure= 760 mmHg, Rel.Humidity= 30%
Integration: Convergence= 1.00%, MDRPN= 2^(4) CRPN= 2^(44)

#	Geometry Compon.	Dimensions (cm): d1	d2	d3	d4	d5	d6	Material	D(g/cm3)	R.Conc.
1	Side Walls		3.51					none		
2	Bottom Wall							none		
3	Sample	1.00						csteel	7.74	
4	Absorber1	4.35						dryair	0.00	
5	Absorber2	0.20						plexigls	1.18	
6	Source-Detector	4.55								

List of energies for efficiency curve generation:

100.0 150.0 200.0 300.0 500.0 700.0 1000.0 1400.0 2000.0

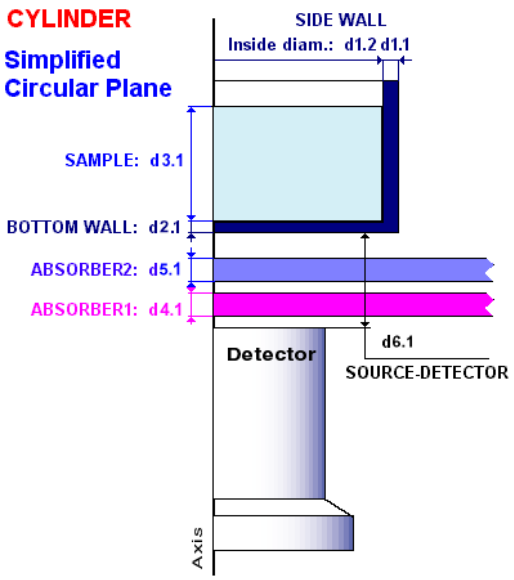

Geometry Composer Report

Date: Wednesday, December 10, 2014
Description: 226-Ra_HSlag13
Comment: Schlacke
File Name: C:\GENIE2K\isocs\data\GEOMETRY\Laboratory\CYLINDER_DISK_AND_POINT\226-ra_hslag13_pq_ptb.geo
Software: LabSOCS
Template: CYLINDER_DISK_AND_POINT, Version: cylinder
Detector: B94028
Environment: Temperature= 22 C, Pressure= 760 mmHg, Rel.Humidity= 30%
Integration: Convergence= 1.00%, MDRPN= 2^(4) CRPN= 2^(44)

#	Geometry Compon.	Dimensions (cm): d1	d2	d3	d4	d5	d6	Material	D(g/cm3)	R.Conc.
1	Side Walls	0.17	7.20					polyprop	0.90	
2	Bottom Wall	0.12						polyprop	0.90	
3	Sample	1.80						slag_new	2.18	
4	Absorber1	4.55						dryair	0.00	
5	Absorber2	0.20						plexigls	1.18	
6	Source-Detector	4.75								

List of energies for efficiency curve generation:

100.0 150.0 200.0 300.0 500.0 700.0 1000.0 1400.0 2000.0

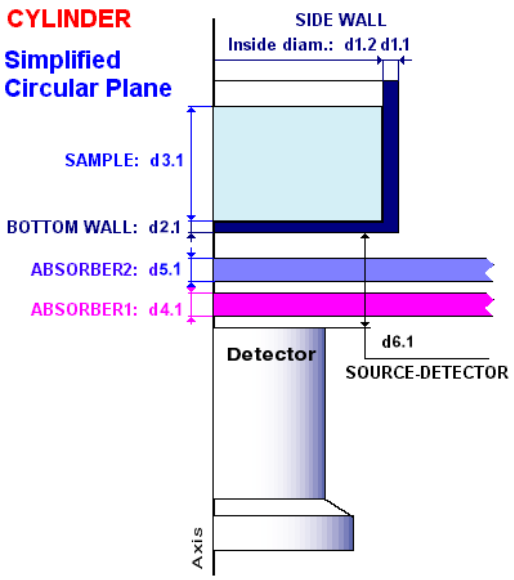

Geometry Composer Report

Date: Wednesday, December 10, 2014
Description: SK_hFD_ID03
Comment: Fume_Dust
File Name: C:\GENIE2K\isocs\data\GEOMETRY\Laboratory\CYLINDER_DISK_AND_POINT\getestet\Sk hFD ID03\Sk hFD ID03_1.geo
Software: LabSOCS
Template: CYLINDER_DISK_AND_POINT, Version: cylinder
Detector: B94028
Environment: Temperature= 22 C, Pressure= 760 mmHg, Rel.Humidity= 30%
Integration: Convergence= 1.00%, MDRPN= 2^(4) CRPN= 2^(44)

#	Geometry Compon.	Dimensions (cm): d1	d2	d3	d4	d5	d6	Material	D(g/cm3)	R.Conc.
1	Side Walls	0.10	6.95					polyprop	0.90	
2	Bottom Wall	0.10						polyprop	0.90	
3	Sample	1.87						fumedust	0.71	
4	Absorber1	4.45						dryair	0.00	
5	Absorber2	0.20						plexigls	1.18	
6	Source-Detector	4.65								

List of energies for efficiency curve generation:

100.0 150.0 200.0 300.0 500.0 700.0 1000.0 1400.0 2000.0